PhD degree in Systems Medicine (curriculum in Human Genetics)

European School of Molecular Medicine (SEMM),

University of Milan and University of Naples "Federico II"

Settore disciplinare: MED/03

THE OFD1 PROTEIN CONTROLS AUTOPHAGOSOME BIOGENESIS THROUGH SELECTIVE AUTOPHAGY

Simona Brillante

Tigem, Naples

Matricola n. R11745

Supervisor: Prof. Brunella Franco

Added Supervisor: Dr. Manuela Morleo

Anno accademico 2019-2020

Table of Contents

List of Abbreviations

AMPK AMP-activated protein kinase

Atg Autophagy related gene

ADPKD Autosomal dominant polycystic kidney disease

ARPKD Autosomal recessive polycystic kidney disease

Baf-A1 Bafilomycin

BNIP3L BCL2 Interacting Protein 3 Like

BECN1 Beclin1

Co-IP Co-immunoprecipitation

cAMP Cyclic adenosine monophosphate

CHX Cycloheximide

CS Centriolar satellites

ER Endoplasmic reticulum

FIP200 Focal adhesion kinase family interacting protein of 200 kDa

GABARAP Gamma-aminobutyric acid receptor-associated protein

GST Glutathione S-transferase

HBSS Hanks' Balanced Salt Solution

Hh Hedgehog

HK2 Human Kidney 2

IF Immunofluorescence

IFT Intra-flagellar transport

KO Knock Out

LC3 Microtubule-associated protein light chain 3

LIR LC3-Interacting Region

LisH LIS1 homology domain

MEF Mouse embryonic fibroblast

mTOR Mammalian target of rapamycin

mTORC1 mTOR complex 1

mTORC2 mTOR complex 2

MTOC Microtubule-organizing center

NBR1 Neighbour of BRCA1 gene 1

NDP52 The nuclear dot protein 52 kDa

OFD1 Oral facial digital 1 protein

OFDI Oral facial digital type I syndrome

PC1 Polycystin 1

PC2 Polycystin 2

PCD Primary ciliary dyskinesia

PCM Pericentriolar material

PCM1 Pericentriolar material 1 protein

PCP Planar-cell-polarity

PDGF Platelet-derived growth factor

PE Phosphatidylethanolamine

PI3K Phosphatidylinositol 3-kinase

PI3P Phosphatidylinositol-3-phosphate

PKD Polycystic kidney disease

RPE Retinal pigmented epithelium

S6K1 S6 kinase beta 1

SDM Site-Direct Mutagenesis

SEM Standard error mean

Shh Sonic Hedgehog

SQTM1 Sequestosome-1

TRAF6 TNF receptor associated factor 6

ULK1 Unc-51-like kinase 1

UVRAG UV irradiation resistance-associated gene

VPS34 Vacuolar protein sorting 34

WB Western blot

Wnt Wingless/Integrated

WT Wild type

Figures Index

Abstract

Cilia are cellular projections that serve a wide variety of essential functions in mammals. Defects in cilia structure or function have emerged as etiological mechanisms underpinning human diseases called ciliopathies. The *OFD1* gene, defective in a rare developmental ciliopathy known as Oral facial digital syndrome type I, encodes for a centrosomal/basal body protein required for cilia formation.

Recent data link ciliary structures to autophagy, the major intracellular degradation system, although the mechanisms and the main players underlying this connection are still to be determined.

Autophagy is an evolutionarily conserved and strictly regulated lysosomal pathway which plays a wide variety of physiological and pathophysiological roles in cellular homeostasis. Either too little or too much autophagy may contribute to pathological conditions.

In the past decade a great deal of progress has been made in the molecular dissection of stimulatory autophagy inputs. On the other hand, our understanding of the mechanisms that restrain autophagy is only partial and far from being complete.

Data obtained during my PhD program contribute to the description of a new negative feedback mechanism that inhibits autophagosome biogenesis through selective autophagy-mediated degradation of ATG13, a component of the ULK1 autophagy initiation complex. I demonstrate that the ciliary OFD1 protein is involved in selective autophagy and acts as autophagy receptor for ATG13 via direct interaction with the Atg8/LC3/GABARAP family of proteins. Preliminary data also indicate that excessive autophagy may contribute to the disease pathogenesis. My results add a new tile to the puzzle of the cilia/autophagy interconnection and will help shedding light on these complex biological processes.

Introduction

1. Cilia and centrosome: definition and function

1.1. Structure of primary cilia

In the past half century, novel insights have been obtained regarding the structure and function of primary cilia. Cilia are highly conserved microtubule-based organelles projecting from the surface of most eukaryotic cells (Satir and Christensen, 2007). These complex and dynamic structures are broadly classified into two main functional groups: motile and non-motile cilia (known as sensory or primary cilia). Motile and non-motile cilia are structurally related and have developed different functions (Keeling, Tsiokas and Maskey, 2016) (Fig.1).

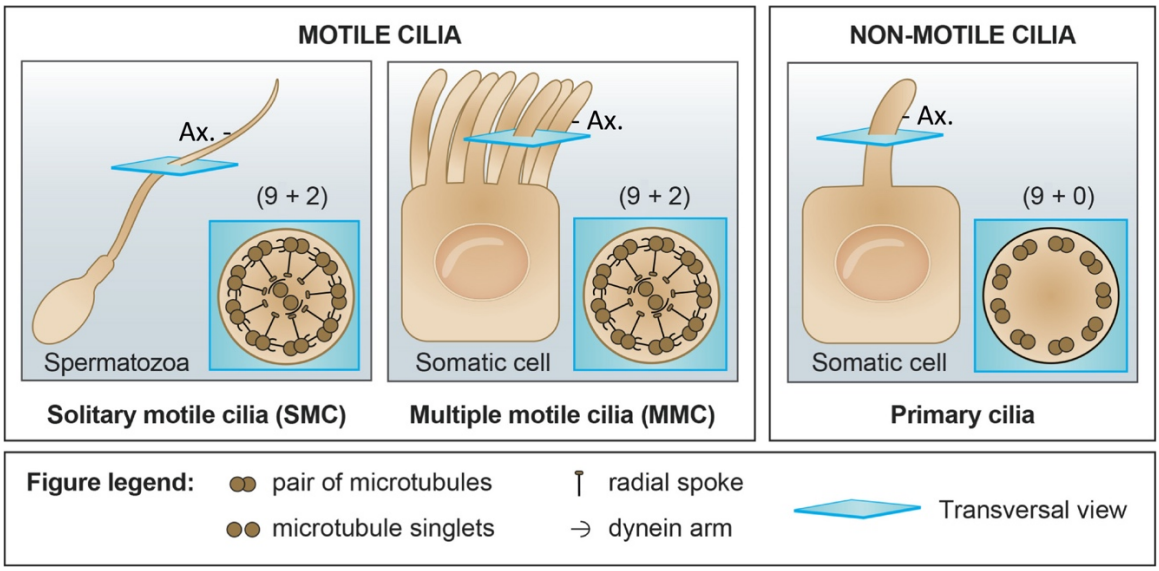

Figure 1. Types of cilia.
Cilia typically occur on cells surface and are classified into two main groups: motile and non-motile cilia. In motile cilia, axonemes (Ax.) consist of a 9+2 microtubular structure and contain motility-related structures (e.g., the central pair of microtubules and axonemal dynein). Cells like spermatozoa have a solitary motile cilium (SMC or flagellum); other cells present multiple motile cilia (MMC). Non-motile cilia (primary cilia) lack the axonemal central microtubules (9+0 structure), dynein arm, and radial spokes. Primary cilia occur as a single immotile organelle designated to sense and transduce signals into the cells (adapted from (Girardet *et al.*, 2019)).

Motile cilia occur as clusters of 100–300 on the apical epithelial cell surface, where they beat in a coordinated and polarized manner to drive directional fluid flow. These multi-ciliated cells are found, for example, in spinal cord and ventricles of adult brains, where they drive polarized fluid flow important for circulation of cerebrospinal fluid and neuronal migration (Sawamoto *et al.*, 2006); in the airway epithelium, where they allow protective mucus clearance (Wanner, Salathe and O'Riordan, 1996); and, in the oviduct/fallopian tubes where they determine oocytes movement (Lyons, Saridogan and Djahanbakhch, 2006) (Fig. 1).

In contrast, primary cilia are non-motile solitary organelles widespread in the organism (Satir and Christensen, 2007) (Figure 1). They line the surface of epithelial cells such as those found in kidney tubules, bile ducts, endocrine pancreas, thyroid and also of non-epithelial cells such as chondrocytes, fibroblasts, smooth muscle cells, neurons, and Schwann cells (Singla and Reiter, 2006). Primary cilia were long believed to be vestigial organelles without relevant biological functions. However, experimental evidence collected over the past 20 years revealed that primary cilia are essential sensory organelles functioning as cells' antenna in different instances: signal transduction (Brown and Witman, 2014); mouse embryo patterning (Huangfu *et al.*, 2003); chemosensing in olfactory neurons (e.g. for detecting odorants), photo-sensing in rods and cones (e.g. for receiving and transducing light stimuli to the retina), and as mechanosensors in renal epithelia (e.g. for sensing fluid flow) (Satir and Christensen, 2007).

Primary cilia consist of a single membrane protrusion containing a microtubule-based scaffold, termed the axoneme, which is nucleated upwards from the older (mother) centrioles in the centrosome, which is the major microtubule organizer (see above) (Satir and Christensen, 2007) (Fig. 2).

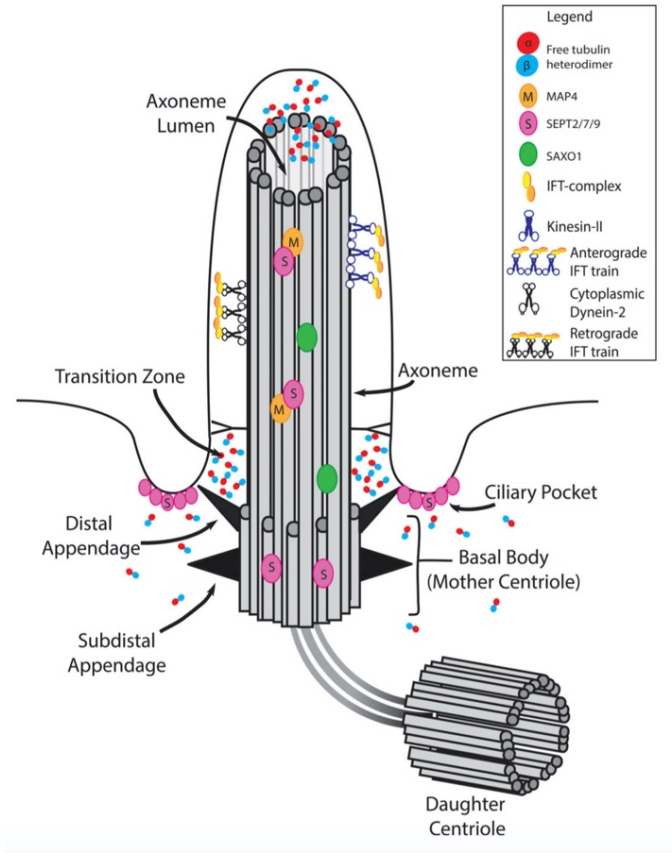

Figure 2. Primary cilium structure.
The primary cilium is made up of a microtubule-based core-skeleton, the axoneme, which is surrounded by a ciliary membrane, continuous with the plasma membrane. The basal body is attached to the ciliary membrane by the transition fibers. Between the basal body and the axoneme of the primary cilia there is a substructural zone, named transition zone (TZ). IFT is carried out by the anterograde IFT-A and retrograde IFT-B complexes powered by dynein-2 and kinesin-2 motors, respectively (adapted from (Mirvis, Stearns and Nelson, 2018)).

The ciliary membrane is continuous with the plasma membrane at the basal portion of the primary cilium but differs from it in the structure and composition of lipids and proteins. The ciliary membrane harbors a large variety of receptors for cell signaling, including those for soluble factors involved in cell growth, migration, development and differentiation, and G-protein-coupled receptors (Singla and Reiter, 2006). Particularly the ciliary tip, a specific portion of the ciliary membrane extending from the axoneme, shows important roles for signals transduction (Rohatgi and Snell, 2010) and in the constrain of the ciliary length (Liang *et al.*, 2016) (Fig. 2).

The core of cilia is the axoneme, which emanates from the basal portion of the cilium (the basal body). It consists of nine circumferentially arranged doublet microtubules

(9+0 pattern) and lacks key elements critical for motility such as the central pair of microtubules which are typical of motile cilia (9+2 pattern) (Fig. 1). An exception to this configuration is the kinocilium of the inner ear that retains a 9+2 configuration and cilia localized at the embryonic node (nodal cilia) that consist of motile organelles with a 9+0 arrangement. The absence of the central microtubule doublet and of the accessory motility machinery (e.g. dynein arms, radical spokes, central pair projections) makes primary cilia non-motile. The 9+0 pattern of the primary cilium is often lost towards the cilium tip, where doublet microtubules end or change position (Fig. 1). The microtubule subunits undergo post-translational modification for the establishment of functional microtubules (Janke and Kneussel, 2010), mainly acetylation (Piperno, LeDizet and Chang, 1987), detyrosination (Gundersen and Bulinski, 1986) or polyglutamylation (Lee *et al.*, 2012). These modifications are thought to be important for stability, motility, formation, and function of primary cilia (Janke and Kneussel, 2010; Konno, Setou and Ikegami, 2012).

The intraflagellar transport (IFT) machinery, a multiprotein complex responsible for transporting cargoes into the cilia (anterograde transport) and out of the cilia (retrograde transport) runs along axonemal microtubules. It mediates both the assembly and resorption of the cilium, and the trafficking of key intermediates of signaling cascades. The anterograde transport is regulated by the IFT-B complex and the kinesin2 motor, whereas the retrograde transport is mediated by the IFT-A complex and the dynein motor (Scholey, 2008). Perturbation of ciliary trafficking by disruption of the IFT transport results in short or absent cilia (Lechtreck, 2015).

At the base of the axoneme, under the cell surface, is located the basal body (Fig. 2). This structure derived from the mother centriole, anchors microtubules, and connects the axoneme to the rest of the cell (Dirksen, 1991). The basal body contains a ring of nine microtubule triplets which represent the nucleation site for

cilia growth. Another specialized ciliary subdomain is represented by the transition zone (TZ), that appears as a Y-shaped structure that links the ciliary membrane to the axoneme. The TZ controls protein trafficking acting as a physical gate that prevents free mixing of proteins between plasma and ciliary membranes. Protein complexes, responsible for cilia formation as well as for selectively loading of ciliary proteins to IFT cargoes, localize at the TZ (Gonçalves and Pelletier, 2017) (Fig. 2).

1.2. Primary cilia biogenesis

The formation of primary cilia is a process tightly linked to the cell cycle. Indeed, the primary cilium assembles only when cells exit the cell cycle from mitosis and, it is thus defined as an organelle of cells in quiescent or differentiated state. Therefore, when cells re-enter the cell cycle, cilium resorption occurs (Quarmby and Parker, 2005). Biogenesis of the cilium, or ciliogenesis, is a well-orchestrated and highly regulated process that involves many factors and signaling pathways. In quiescent cells, the mother centriole, equipped with distal and subdistal appendages, migrates to the apical surface of the cell, connects to the membranes destined to become the ciliary membrane and matures into the basal body. Once the basal body docks at the plasma membrane, the extension of the axoneme from the distal end into the extracellular space occurs. During this time, ciliary building blocks (tubulin) and resident proteins accumulate at the developing cilium (SOROKIN, 1962; Sorokin, 1968). Two main pathways have been proposed for primary cilia biogenesis (intracellular and extracellular/alternative pathways) (Fig. 3A-B).

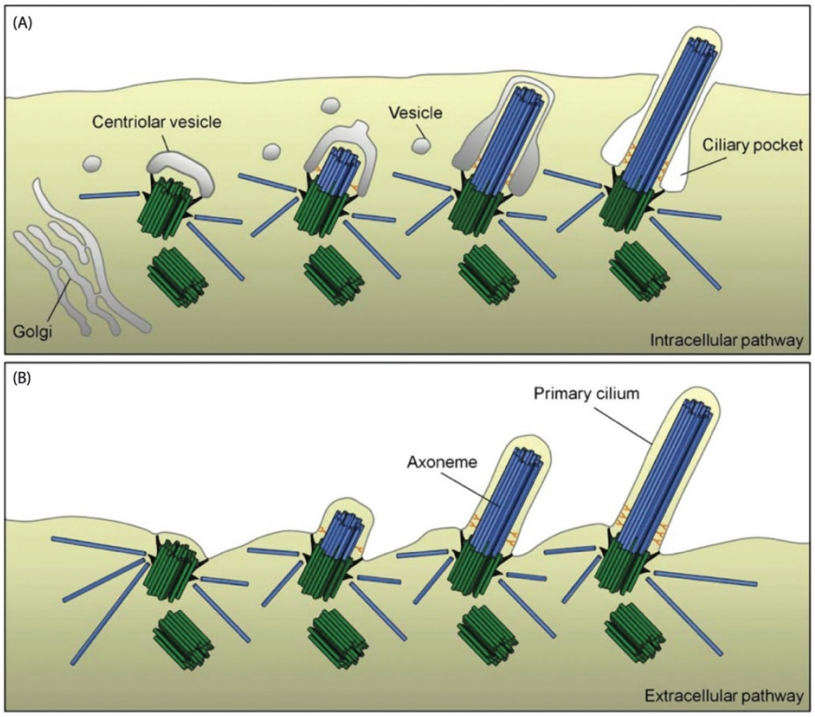

Figure 3. Primary cilia assembly.
There are two main pathways for ciliogenesis: the intracellular route, in which the basal body associates with distal appendages vesicles (DAVs) originated from the Golgi and likely to start axoneme elongation in the cytosol (A) and the extracellular pathway, in which the mother centriole docks directly to the plasma membrane and, the cilium, then protrudes into the extracellular space where it elongates (B) (adapted from (Pedersen *et al.*, 2012)).

In the intracellular route, ciliogenesis initiates with the formation of a large ciliary vesicle (CV) at the distal end of the appendages of the mother centriole by fusion of smaller distal appendages vesicles (DAVs). These structures originate from the Golgi and associate with the basal body of cilia. The axoneme elongates within the vesicles and, as it grows, deforms the CV and establishes an inner membrane (shaft) and an outer membrane (sheath). The outer membrane eventually touches and fuses with the plasma membrane, and the cilium becomes exposed in the plasma membrane (SOROKIN, 1962; Bernabé-Rubio and Alonso, 2017) (Fig. 3A). Conversely, in the extracellular route, the basal body fuses with the apical membrane prior to axoneme growth and the cilium protrudes directly into the extracellular space where it elongates (Kobayashi and Dynlacht, 2011) (Fig.3B).

The use of a pathway rather than the other depends on the cell type and the position of the centrosome in the cell (Bernabe-Rubio and Alonso 2017). In non-polarized cells of connective tissues, as in the case of fibroblasts, where the centrosome is near the nucleus, ciliogenesis starts intracellularly and finishes at the plasma membrane, generating an invagination, known as the ciliary pocket; whereas, in polarized epithelial cells, the centrosome is close to the plasma membrane and the process takes place entirely at the plasma membrane and no ciliary pocket appears (Bernabé-Rubio and Alonso, 2017).

The formation of the primary cilium is also induced by other conditions, such as starvation by using serum-free media and by cell confluency, which forces the cell into a non-mitotic state. Other stimuli are fluid flow and cell spreading (Plotnikova, Pugacheva and Golemis, 2009; Orhon *et al.*, 2016).

1.3. Cilia-mediated pathways

Cilia act as complex sensory machines involved in transducing extracellular stimuli into cellular responses as they sense extracellular signals and transmit them from the cilium to the cytoplasm and nucleus in order to control gene expression and cell behavior, thereby playing several important roles in cell and developmental biology (Satir, Pedersen and Christensen, 2010) (Fig. 4). A variety of receptors, ion channels and transporter proteins localize to cilia and allow the cell to sense and to respond to various external stimuli which include chemical signals, mechanical stress (Nauli *et al.*, 2003), light and temperature (Prodromou *et al.*, 2012).

Primary cilia coordinate a variety of cellular processes, such as maintenance of tissue homeostasis, cell fate determination, cellular proliferation and cell survival, and migration (Clement *et al.*, 2009; Christensen *et al.*, 2013). Examples of signaling

pathways that need intact cilia to properly transduce their signals include: the Sonic Hedgehog (Hh) pathway (Bangs and Anderson, 2017); the Platelet-derived growth factor (PDGF) signaling (Clement *et al.*, 2013); the Wingless/Integrated (Wnt) pathway (Jackson, 2018), the Ca2+ signaling cascade (Lee *et al.*, 2015), the cyclic adenosine monophosphate (cAMP) signaling (Ye *et al.*, 2017) and the mammalian target of rapamycin (mTOR) pathway (Boehlke *et al.*, 2010) (Fig. 4).

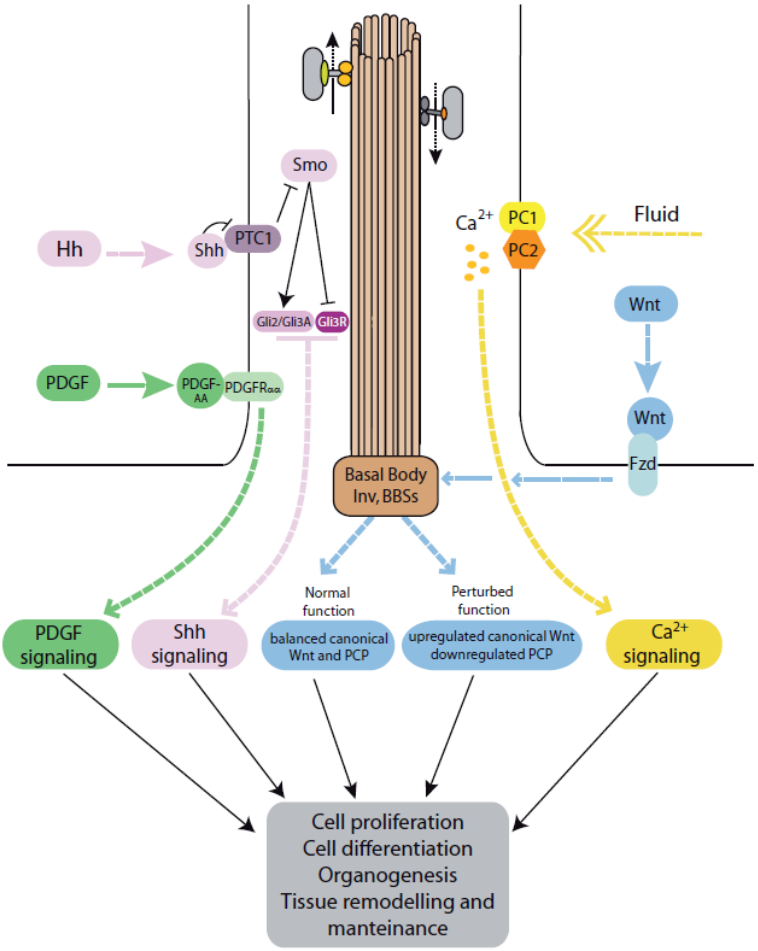

Figure 4. Ciliary signaling pathways.
The primary cilium is a sensory organelle which acts as an antenna to capture external inputs and transduce them into the cell, involving several cellular pathways. Indeed, the cilium regulates key developmental pathways such as Sonic Hedgehog (Shh) and Wnt (planar cell polarity (PCP). Cilia participate also to the regulation of intracellular Ca2+ level, through its mechano-sensation capacity (adapted from (Irigoin and L. Badano, 2011)).

1.4. The centrosome

As mentioned before, the basal body is a protein structure which functions as an organizing center for cytoskeletal components. It derives from the mother centriole and comprises several accessory proteins. Indeed, in mammalian cells the centrosome consists of an amorphous spherical mass of centrosomal proteins known as the pericentriolar material or PCM surrounding a pair of centrioles arranged in orthogonal configuration at its center (Nigg and Stearns, 2011) (Fig. 5).

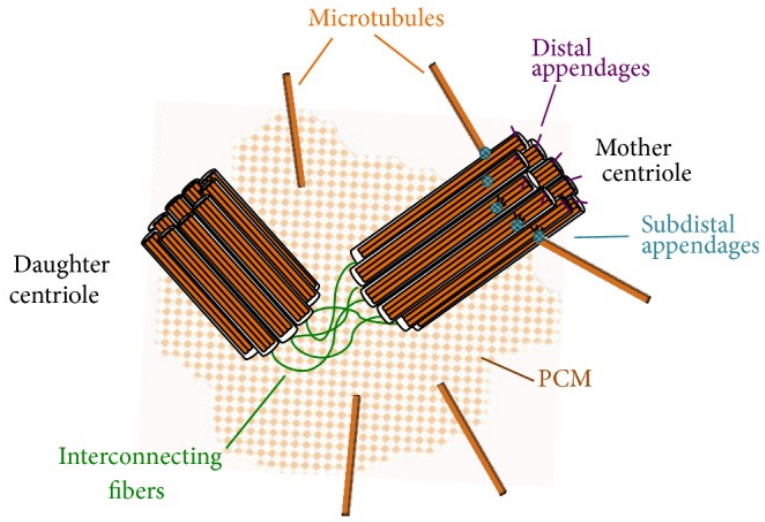

Figure 5. Centrosome structure.
Centrosomes are made up of two perpendicular centrioles (orange cylinders), defined as mother and daughter centrioles, which are linked together by interconnecting fibers (in green). The pericentriolar material (PCM), an amorphous matrix (dotted orange background) surrounds the centrioles and contributes to nucleation and anchoring of cytoplasmic microtubules. Only the mother centriole possesses the distal (purple) and subdistal (blue) appendages necessary for cilia assembly and microtubule anchoring, respectively (adapted from (Barbelanne and Tsang, 2014)).

The PCM is a scaffold for anchoring of numerous proteins required for microtubule nucleation, primary cilia formation and other cellular processes (Lopes *et al.*, 2011). In addition to these structures, some electron-dense spherical granules termed centriolar satellites have been identified around the centrosome. They function as shuttle that transport components from the cytoplasm to the centrosome and vice versa (Lopes *et al.*, 2011).

Centrosome duplication is strictly coupled with cell cycle; indeed, during mitosis, a new centriole grows at the proximal end of both centrioles and each daughter cell inherits two centrioles: one centriole derives from the mother cell and the other is replicated from the mother centriole during the cell cycle. It has been demonstrated that dysfunctional regulation of centrosomes induce carcinogenesis through enhancement of chromosome instability and metastatic potency (Sankaran, Stemm-Wolf and Pearson, 2019). The major functions of the centrosome are to regulate the intracellular organization of the microtubule and to integrate signals from different pathways which regulate cell cycle progression, mitosis, cell polarity and migration (Arquint, Gabryjonczyk and Nigg, 2014).

2. Disorder affecting cilia

2.1. Ciliopathies

The biomedical interest in cilia is driven by the identification of a growing number of inherited diseases called ciliopathies caused by mutations in genes encoding proteins with a role in cilia assembly and / or function and localizing to different ciliary structures. Ciliopathies represent an important and rapidly expanding disease category (D'Angelo and Franco, 2009; Reiter and Leroux, 2017). They are multisystem disorders characterized by extensive genetic heterogeneity and clinical variability. These disorders show a broad spectrum of shared and overlapping phenotypes, involving various organ systems, such as retinal degeneration, renal, hepatic and pancreatic cysts, skeletal defects, situs inversus, obesity, ciliary dyskinesia, mental retardation, and Central Nervous System (CNS) malformations (Cardenas-Rodriguez and Badano, 2009) (Fig. 6).

Ciliopathies can be caused by dysfunction of ciliary proteins involved in the assembling and functioning of motile cilia (motile ciliopathies) and disorders due to disruption of proteins with a role in immotile cilia assembly and/or function (sensory ciliopathies). In addition, non-ciliary proteins can also contribute to ciliopathies influencing ciliary functions, and ciliary proteins can have extra-ciliary roles causing phenotypes that are unrelated to ciliopathies when they are impaired (Reiter and Leroux, 2017).

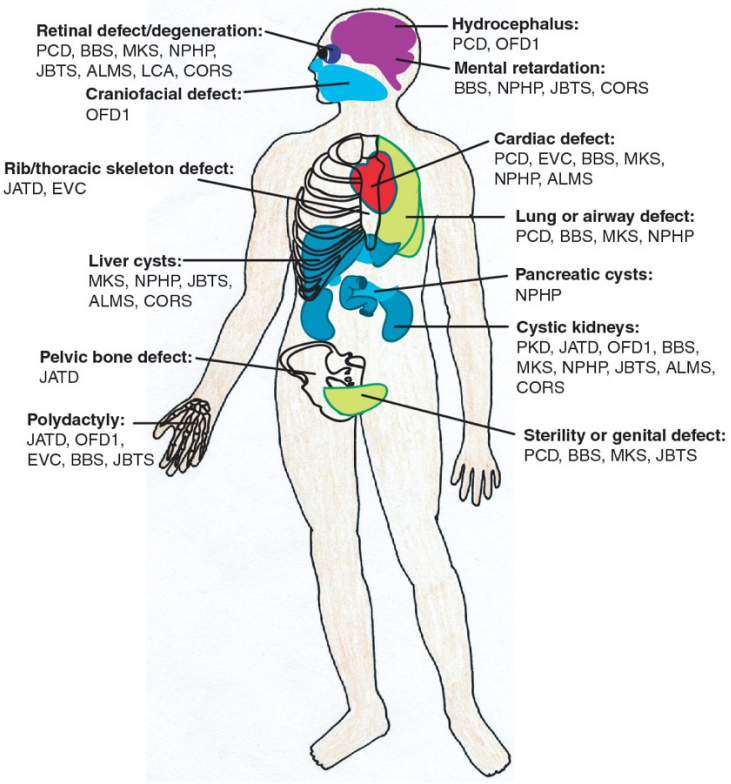

Figure 6. Ciliopathies affect multiple organs and show overlapping clinical features. Ciliopathies are inherited human disorders caused by dysfunction in both motile and non-motile cilia. Almost every organ in the body can be involved. Indeed, most ciliopathies have overlapping phenotypes. ALMS, Alström syndrome; BBS, Bardet-Biedl syndrome; CORS, cerebello-oculo-renal syndrome; EVC, Ellis-van Creveld syndrome; JATD, Jeune asphyxiating thoracic dystrophy; JBTS, Joubert syndrome; LCA, Leber congenital amaurosis; MKS, Meckel syndrome; NPHP, nephronophthisis; OFD1, oral-facial-digital syndrome type 1; PCD, primary ciliary dyskinesia; PKD, polycystic kidney disease.(adapted from (Lee and Gleeson, 2011)).

Motile ciliopathies are characterized by dysfunction of tissues and organs which need effective ciliary and flagella machineries for generating fluid flow or movement within fluids. Failure of these mechanisms, due to altered formation or function of

motile cilia, compromises mucus clearance, causing chronic airway diseases which are associated with defects of laterality, fertility, and brain development. The most common disease affecting motile cilia is known as *Primary Ciliary Dyskinesia (PCD)* (Horani and Ferkol, 2016) (Fig. 6).

Sensory ciliopathies result specifically from defects in the sensory and/or signaling functions of cilia and are primarily caused by defects in non-motile cilia.

Examples of ciliopathies caused by mutation in proteins affecting primary cilia include: *Bardet-Biedl Syndrome (BBS)*, a multisystemic disorder involving developmental abnormalities and degenerative phenotypes (Tsang, Aycinena and Sharma, 2018); *Leber Congenital Amaurosis (LCA)*, that results in early vision loss (Koenekoop, 2004); *Oral-Facial-Digital type 1 syndrome (OFDI)*, an X-linked dominant male lethal developmental disorder (Franco and Thauvin-Robinet, 2016). In this condition, female patients present malformations of the oral cavity, face, digits, renal cysts, and CNS malformations (see also next section) (Fig. 6).

Other ciliopathies include *autosomal dominant (ADPKD) or recessive (ARPKD) polycystic kidney disease* characterized by the development of cysts in the kidney, gradually leading to renal failure (Ward *et al.*, 2003; Cornec-Le Gall, Alam and Perrone, 2019); *Joubert Syndrome (JBTS)* (Doherty, 2009); *Nephronophthisis (NPHP)* (Hildebrandt, Attanasio and Otto, 2009); *Meckel Grouber Syndrome (MKS)* (Barker, Thomas and Dawe, 2014) (Fig. 6).

Some of these conditions such as most of the syndromic conditions (e.g. OFDI, BBS, JBTS, NPHP, MKS) are rare, others, such as ADPKD are more common.

Primary cilia have evolved several modes for sensing environmental and intercellular stimuli with respect to motile cilia. Therefore, it is expected that defects in sensory cilia functions cause more varied sensory, physiological, and developmental abnormalities. Sensory ciliopathies have multiple possible molecular

etiologies, including impaired cilium formation or maintenance, abrogation of ciliary signaling pathway components, or trafficking defects that prevent the signaling machinery from being localized to, or removed from, cilia (Reiter and Leroux, 2017).

2.2. Oral-facial-digital type I syndrome (OFDI)

2.2.1. Clinical features and the *OFD1* gene

Oral-facial-digital syndromes (OFDs) are a heterogeneous group of developmental disorders identified by distinctive features: malformations of the face, oral cavity, and digits. Other organ systems can also be involved, helping to define several different forms of OFDs; indeed, the current classification includes up to 13 different types of OFDs (Franco and Thauvin-Robinet, 2016; Bruel *et al.*, 2017).

Oral-facial-digital syndrome type I (OFDI, MIM #311200) is the most frequent type, occurs in 1:50000-1:250000 live births, and is inherited as a X-linked dominant male lethal trait. OFDI can be easily recognized in familiar cases for the peculiar pattern of inheritance and for the male lethality, even though few live males with mutations in the causative gene *OFD1* have been reported (Thauvin-Robinet *et al.*, 2013). As stated above OFD type I is caused by mutation of the *OFD1* gene (MIM #300170) previously known as CXORF5 (De Conciliis *et al.*, 1998), located on the chromosome Xp22.2-Xp22.3 region (Ferrante *et al.*, 2001). About 75% of affected females have no family history of OFDI, therefore represent *de novo* mutations (Prattichizzo *et al.*, 2008). Mutations in the OFD1 gene are also responsible for recessive X-linked phenotypes: X-linked recessive form of Joubert syndrome (MIM #300804), Intellectual disability, Simpson-Golabi-Behmel syndrome type 2 (MIM #300209), Retinitis Pigmentosa (MIM #300424) and Primary Cilia Dyskinesia (MIM #244400).

Predominant clinical features in OFD type I syndrome include craniofacial abnormalities (facial asymmetry, hypertelorism, frontal bossing, cleft palate, multi-lobulated tongue with nodules, and abnormal dentition), and digital abnormalities (which affect the hands more often than the feet) including brachydactyly, syndactyly, clinodactyly, and more rarely polydactyly (Marina and Franco, 2009) (Fig. 7).

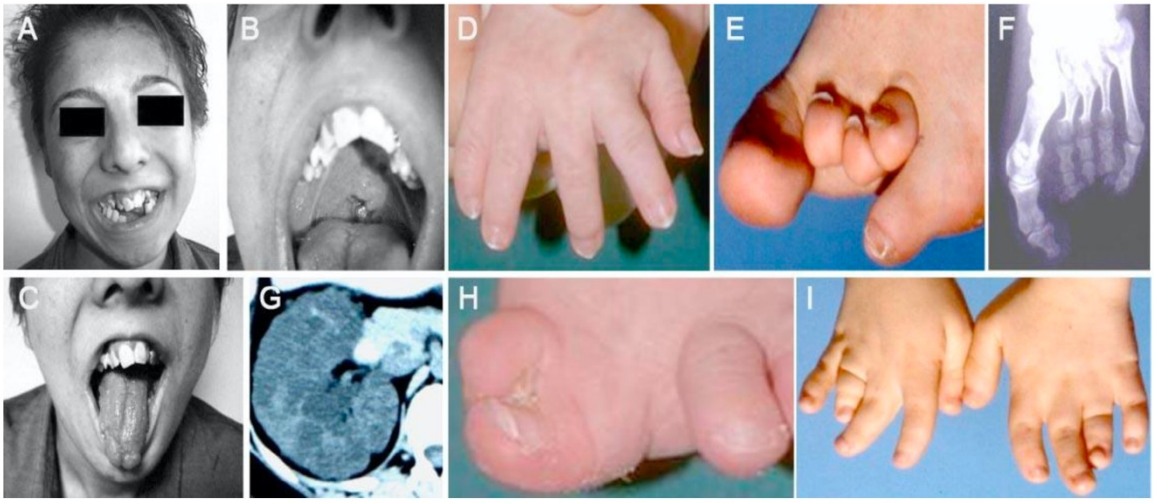

Figure 7. Clinical features of OFD type I syndrome.
(A) Peculiar face of the patient and tooth abnormalities, (B) cleft palate, (C) lobulated tongue, (D) clinodactyly, (E and F) Brachydactyly, (G) Cystic kidney, (H) Hallux duplication, (I) Brachydactyly and syndactyly. (modified from (Toprak *et al.*, 2006; Marina and Franco, 2009)

The phenotype of patients with OFDI also includes CNS involvement with brain structural abnormalities, developmental delay, and intellectual disabilities (Del Giudice *et al.*, 2014), and renal cystic disease (Ferrante *et al.*, 2001; Prattichizzo *et al.*, 2008; Marina and Franco, 2009). In addition, about 5% of OFD-I affected females develop pancreatic, hepatic, and/or ovarian cysts (Ferrante *et al.*, 2001; Macca and Franco, 2009). Interestingly, the OFD1 gene escapes X-inactivation in humans while the murine counterpart is subjected to X-inactivation (Ferrante *et al.*, 2003). Therefore, it has been proposed that X-inactivation may play a role in the extensive intrafamilial and interfamilial clinical variability observed in this disorder (Franco and Ballabio, 2006; Morleo and Franco, 2008).

OFD1 contains an open reading frame of 3033 base pairs (bp) spanning over 24 coding exons and generates three main splice variants, *OFD1* isoform 1, also known as *OFD1a* (NP_003602.1), *OFD1* isoform 2, alternatively named as *OFD1b* (NP_001317138.1), *OFD1* isoform 3 (NM_001330210). *OFD1b* (exons 1-11) codifies for an unstudied putative protein of 367 amino acids (aa), while *OFD1a* encodes for a 1012-amino acid protein (hereafter called OFD1) evolutionarily conserved among vertebrates (De Conciliis *et al.*, 1998; Ferrante *et al.*, 2001). This huge protein contains a Lis1 homology (LisH) motif in its N-terminal region, and six predicted coiled-coil (CC) domains distributed along the C-terminal region (De Conciliis *et al.*, 1998; Lopes *et al.*, 2011).

To date, over 100 different mutations affecting the *OFD1* gene have been identified, the majority of these consists in small insertions or deletions resulting in frameshifts, with missense and nonsense mutations accounting for about 20% of cases (Marina and Franco, 2009). Most mutations affect the first part of *OFD1* gene and, interestingly, no mutations were identified beyond exon 17, highlighting the functional importance of the N-terminal region of the protein (Prattichizzo *et al.*, 2008; Marina and Franco, 2009) (see below).

The OFD1 transcript is expressed in humans, in all tissues affected by the disorder from early stages of development to adulthood. In particular, it is highly expressed during human organogenesis in the metanephros, gonads, brain, tongue, and limbs, and at lower levels in pancreas, kidneys, skeletal muscle, liver, lung, placenta, brain, and heart (De Conciliis *et al.*, 1998; Ferrante *et al.*, 2001).

2.2.2. The OFD1 protein: subcellular localization and functional studies

OFD1 is a centrosome-associated protein (Romio *et al.*, 2004; Giorgio *et al.*, 2007) and in post-mitotic cells, when the mother centriole forms the basal body to allow nucleation of the ciliary axoneme, OFD1 localizes at the basal body of primary cilia (Romio *et al.*, 2004; Giorgio *et al.*, 2007) (Fig. 8).

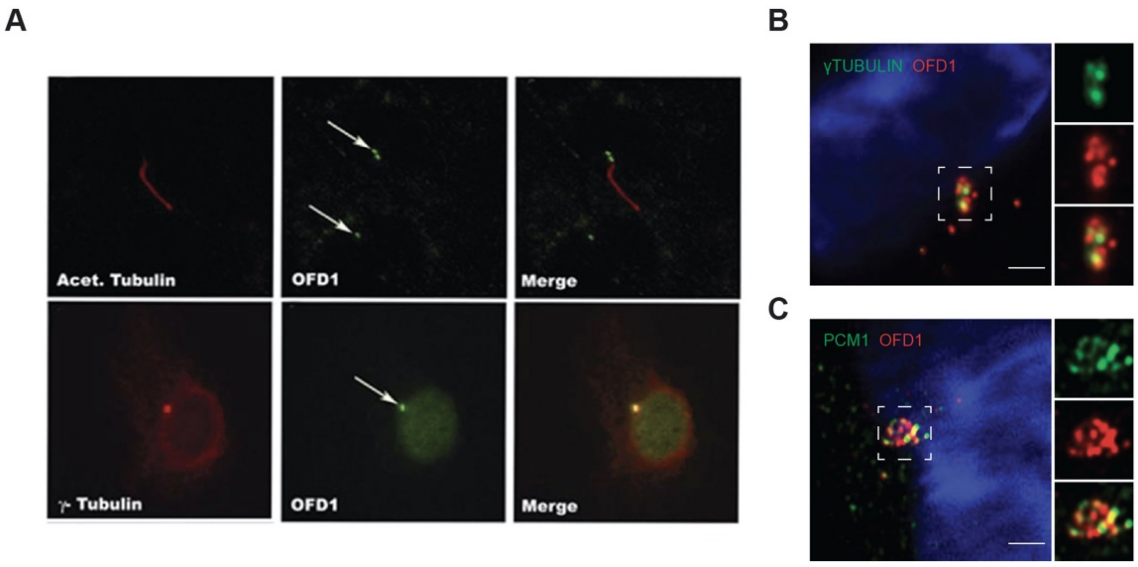

Figure 8. Subcellular localization of the endogenous OFD1 protein.
A. OFD1 (green) is located at the base of primary cilia marked by Acetylated tubulin (red, top) and colocalizes with γ-Tubulin (red, bottom) used to detect centrosomes (adapted from (Giorgio *et al.*, 2007)). B. Staining with OFD1 (red) and γ-Tubulin (green, top) to detect centrosomes and PCM1 (green) to detect pericentriolar material (bottom).

More specifically, OFD1 localizes at the distal ends of centrioles (Singla *et al.*, 2010) and is an important component of centriolar satellites, the PCM particles surrounding centrosomes and basal bodies (Lopes *et al.*, 2011). Indeed, the localization of OFD1 to centriolar satellites, together with CEP290 (a protein mutated in Joubert syndrome and NPHP), PCM1 (pericentriolar material-1) and BBS4 (Bardet-Biedl syndrome protein 4) has been shown to be necessary to maintain satellites integrity (Lopes *et al.*, 2011). OFD1 appears to be important in

the control of centriole length, centriole distal appendage formation, and centriolar recruitment of the Intraflagellar transport protein 88 (Ift88) (Singla *et al.*, 2010).

Based on SMART analysis prediction (http://smart.embl-heidelberg.de/), the OFD1 protein is structurally composed by a LisH motif and six putative coiled-coil domains (CC). The function of the LisH motif has not been completely understood. It has been reported to be involved in microtubule dynamics, chromosome segregation and cell migration but is not required for centrosomal localization (Emes, 2001; Romio *et al.*, 2004). Mutations in OFD1 localized in the LisH region have been shown to decrease OFD1 ability to restrain centrioles elongation, resulting in abnormally long centrioles and impaired Ift88 recruitment (Singla *et al.*, 2010).

CC domains are structural motifs made by two or more alpha-helices connected to form a supercoil, which functions as scaffold region for oligomerization and protein-protein interaction. Indeed, the OFD1 protein binds centrosome structures through its CC domain and mutations within these regions are able to influence OFD1 localization and distribution (Romio *et al.*, 2004). CC domains are also responsible for OFD1 binding to PCM1; indeed, OFD1, BBS4 and CEP290 localize at centriolar satellites thanks to the interaction with PCM1, which acts as the core structural element of satellites (Lopes et al., 2011). Stability of the interaction between OFD1 and satellites seems to be regulated also by TRAPPCIII complex components in human renal retinal epithelial (hTERT-1 RPE1) cells, which mediate association and trafficking of OFD1 from cytosol to centriolar satellites, without affecting the pool settled at centrosomes (Zhang et al., 2020). Recently, it has been discovered that the OFD1 pool at centriolar satellites exerts a negative action on cilia formation and it needs to be removed to properly induce ciliogenesis (Tang et al., 2013).

OFD1 is also found in the nucleus where directly interacts with RuvBl1. Indeed, through its CC domains, OFD1 is able to self-associate and co-immunoprecipitates

with subunits of TIP60 histone acetyltransferase (HAT) multi-subunit complex which is involved in cell-cycle progression and transcriptional regulation of genes active in DNA repair and apoptosis (Doyon and Côté, 2004; Giorgio et al., 2007). Moreover, reduced level of OFD1 protein expression has been linked to TIP60 mislocalization, as well as impairment of double-strand-break (DBS)-induced histone modification (Abramowicz et al., 2017).

Studies on ciliary signaling, have identified a peculiar ciliary complex shared by epithelial cells of kidney tubules and oral cavity. This complex is formed by ciliary proteins Polycystins (PC1 and PC2) and OFD1, and membrane proteins epidermal growth factor receptor (EGFR) and flotillins and actually defines a primary cilia microdomain. Indeed, mutations in one of the complex components lead to dysfunctions of the ciliary signaling route and affect other component stability and activity (Jerman et al., 2014).

Finally, analysis of the OFD1 interactome reveals other appealing potential interactors, not necessarily associated with expected ciliary functions and structures. An example is represented by protein synthesis as experimental evidence demonstrated interaction of the OFD1 protein with components of the Preinitiation complex of translation and of the eukaryotic Initiation Factor (eIF)4F complex (Iaconis et al., 2017).

3. Autophagy: general features

3.1. What is autophagy?

Autophagy (also known as macroautophagy or autophagocytosis) is an evolutionarily conserved cellular catabolic process which degrades in response to nutrient stress intracellular components, such as soluble proteins, cellular

aggregates, organelles, macromolecular complexes, and infectious agents. The term “autophagy” comes from the Ancient Greek word “autóphagos” which just means “eating of self” (Mizushima, 2007). The key element of autophagy consists in a large double-membrane vesicle named autophagosome which collects the materials targeted for degradation delivering its cargoes to lysosomes. Once reached its destination, the outer membrane of the autophagosome fuses with the lysosome membrane and, then, the acidic environment of this organelle dissolves the inner membrane of autophagosomes and degrade the cargoes (Xie and Klionsky, 2007) (Fig. 9).

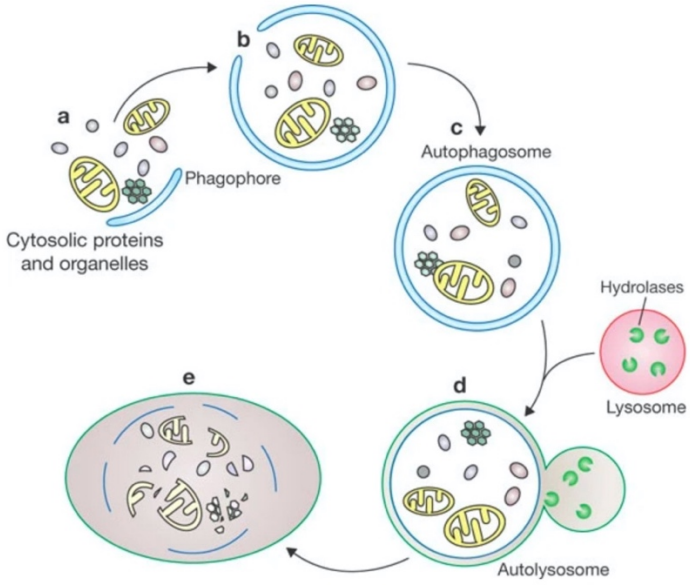

Figure 9. Autophagosomes biogenesis.
(a, b) Cytosolic proteins and organelles are first sequestered within expanding phagophores, (c) resulting in the formation of a double-membrane vesicle called autophagosome; (d) the outer membrane of the autophagosome subsequently fuses with a lysosome, exposing the inner single membrane to lysosomal hydrolases; (d) the cargo-containing membrane compartment is then lysed, and the contents are degraded (adapted from (Xie and Klionsky, 2007))

A large and heterogeneous group of molecules orchestrates the autophagic process; indeed, every step is regulated by definite complexes of proteins which were initially isolated and characterized by mutants screening in yeast and, subsequently, identified in more complex systems, like mammals. The so-called

autophagy-related gene (Atg/ATG in yeast and in mammals, respectively) proteins represent, therefore, the molecular machinery ruling and regulating autophagy (Wesselborg and Stork, 2015) (see below and Fig. 10).

The main function of autophagy is to enable cells to survive to environmental stress like nutrient and growth factor deprivation and also allows them to withstand to intracellular injury removing damaged organelles, misfolded proteins and infective organisms invasion (Moreau, Luo and Rubinsztein, 2010). Cells, through autophagy, degrade macromolecules into their building blocks, which can be used for protein synthesis and ATP energy production. These pro-survival functions are highly conserved from yeast to humans and generally the lack of any type of essential nutrient is able to induce autophagy. For example, nitrogen starvation can widely induce autophagy in yeast; nitrogen or carbon deprivation also triggers autophagy in plant cells. In mammalian cells, autophagy is under the control of multiple signaling pathways, therefore its regulation appears more complicated. It is known that depletion of total amino acids strongly induces autophagy in many cultured cell types; the endocrine system, particularly insulin, manages autophagy regulation *in vivo*; it is also demonstrated that starvation by serum is a strong stimulus of autophagy. Other growth factors and hormones such as interlukin-3 (IL-3) which acts as a autophagy suppressor mediating nutrient availability (Mizushima, 2007) are able to control autophagy.

However, different studies have clearly demonstrated that the role of autophagy is not restricted to starvation response. Indeed, autophagy occurs constitutively at low levels even under normal growth conditions acting as quality control of turnover of cell compartments (*basal autophagy*) (Moreau, Luo and Rubinsztein, 2010). Autophagy-deficient cells undergo abnormal accumulation of aggregates and damaged organelles (Komatsu *et al.*, 2005); autophagic induction by Atg7

is sufficient to reduce misfolded proteins and aggregates content in protein misfolding-stressed cardiomyocytes (Pattison, Osinska and Robbins, 2011).

Any organelle such as peroxisomes, endoplasmic reticulum and ribosomes can be selectively degraded by autophagy to maintain cellular homeostasis. Damaged and dysfunctional mitochondria are removed by autophagy to protect cells from radical oxygen species. This selective mitochondrial degradation is called mitophagy and is the major route for mitochondrial turnover. The molecular mechanisms for mitochondria's recognition by autophagy (either selective, random or both) remain to be clarified in mammalian systems (Ding and Yin, 2012). Mitochondrial homeostasis has been linked to many physiological and pathophysiological conditions and diseases. In particular, mitophagy plays an essential role in erythrocyte differentiation and maturation. In most mammals, mature red blood cells lack mitochondria, and this is achieved by mitophagy during maturation of immature red blood cells. In several neurodegenerative disorders, such as Parkinson, Alzheimer and Huntington, in which the accumulation of aggregated/misfolded proteins and the dysfunction of mitochondria are the major defects, mitophagy appears to be cytoprotective, preventing cell death in neuronal tissues (Ravikumar, 2002). Moreover, several genes causative of neurodegenerative diseases have been implicated at specific stages of autophagic regulation. Examples include huntingtin (Htt), the protein mutated in Huntington disease, which functions as a scaffold protein to promote autophagic protein-protein interaction, cargo recognition and autophagosome initiation (Rui *et al.*, 2015); the kinase PINK1 and the cytosolic E3 ubiquitin ligase parkin, both mutated in inherited forms of Parkinson's disease, physiologically contribute to mitochondria clearance and are widely and strongly connected to mitophagy (Cookson, 2012).

The same autophagic mechanism used to selectively capture intracellular organelles is also used for the selective delivery of microorganisms to lysosomes in a process termed xenophagy. Indeed, it has been demonstrated that autophagy actively participates in the initialization of innate and adaptive immune response (Mizushima *et al.*, 2008).

Finally, autophagy has a controversial role also in cancer. Indeed, autophagy induction may act as suppressor of tumorigenesis by inhibiting cancer-cell survival and inducing cell death, but it may also facilitate tumor progression by promoting cancer-cells proliferation and tumor growth (Mathew, Karantza-Wadsworth and White, 2007). It has been reported that Beclin1 (BECN1), a key player in autophagy, is frequently mutated in human breast, ovarian and prostate cancers (Gong *et al.*, 2013). In addition, autophagy can also influence the dynamics of DNA repair by recycling key proteins involved in the processing of cancerous lesions and mitigate DNA damage by controlling ROS production (Karantza-Wadsworth *et al.*, 2007). On the other side excessive activation of autophagy has also been observed concomitantly in cells undergoing cell death in a pathway distinct from apoptosis or necroptosis, named autosis (Liu and Levine, 2015). Autophagic cell death is identified by the presence of autophagic vacuoles in the dying cell. The excessive activation of autophagy may increase the amount of cargo randomly sequestered by autophagosomes and the loss of selectivity leads to a complete self-digestion of the cell (Wong and Cuervo, 2010).

From this perspective, either too little or too much autophagy could be deleterious, a complexity seen in its dual role in cytoprotection and cell death.

3.2. The autophagic machinery

In the past decade the identification of components of the autophagic machinery has quickly progressed mainly through extensive studies in yeast. Most of these autophagy related genes (ATG) have orthologs in mammals with similar functions, revealing conservation of the autophagic machinery across species. Up to date, over 30 ATG genes have been identified as necessary for various types of autophagy in yeast. Among them, 18 ATG genes are essential for autophagosome formation upon starvation.

Membrane dynamics during autophagy is a peculiar feature of this catabolic process and is also highly conserved from yeast to humans. The cargo must be segregated from the cytoplasm, often in a directed or selective manner, and moved from the intracellular space into the lysosome lumen. Bulk sequestration involves the formation of an essential double-membrane intermediate, called phagophore that will later become the autophagosome. The phagophore or isolation membrane, the counterpart of the pre-autophagosome structure (PAS) in yeast, is a cup-shaped double-membrane whose edges extend and fuse, trapping the engulfed cytosolic material as autophagic cargo (Mizushima, 2007; Tanida, 2011). Phagophores nucleate from a specific compartment of the endoplasmic reticulum (ER) membrane termed “omegasome” because of its morphology resembling the Greek capital letter omega (Ω) (Karanasios *et al.*, 2013).

Omegasomes formation requires type III phosphatidylinositol-3 kinase (PI3K) activity. As a consequence, these structures are labelled by proteins capable to bind phosphatidylinositol-3 phosphatase (PI(3)P) *in vitro* (Axe *et al.*, 2008). The double FYVE-containing protein 1 (DFCP1) localizes to ER and migrates to omegasomes upon PI(3)P production, a process that depends on its ER localization and PI(3)P-binding FYVE domains (Axe *et al.*, 2008). Although DFCP1 marks omegasomes, its

knockdown has no clear autophagy impairment (Axe *et al.*, 2008). PI(3)P production then promotes the recruitment of other effectors, the WD-repeat PI(3)P (WIPI) protein family. Among them, WIPI2b has been shown to interact with ATG16L1, a key player in autophagy (see below), thus favoring its recruitment to PI(3)P-positive structures (Dooley *et al.*, 2014) (Fig. 10).

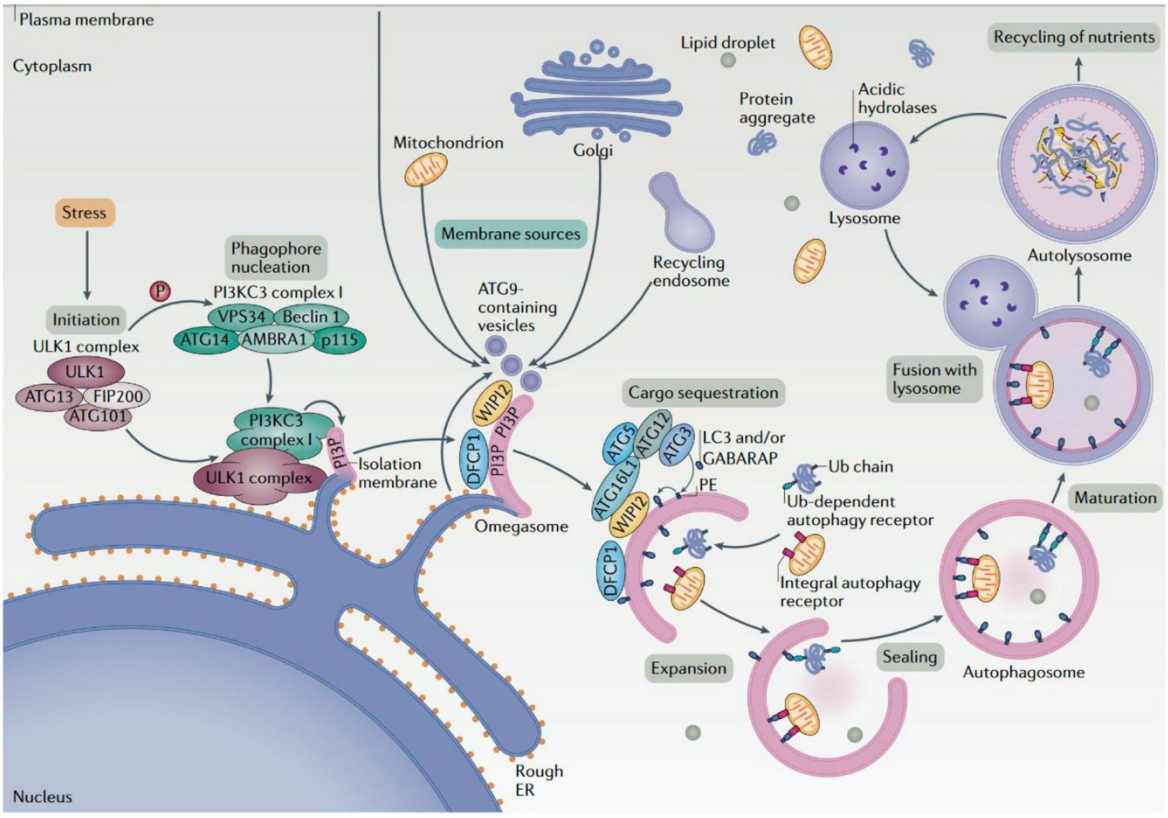

Figure 10. Autophagosome formation and main complexes.
Autophagosome formation involves many factors and protein complexes. The first to be activated is represented by the ULK1 complex which mediates the phosphorylation of components of the PI3K class III complex which in turn produces local PI3Ps at omegasomes. Consequently, PI3P recruits the PI3P-binding proteins WIPI2 and DFCP1 at rising membranous structures. Expansion and closure of the autophagosomal membrane are dependent on the ATG5-ATG12-ATG16L complex and on the mammalian homologs of Atg8, which are LC3 and GABARAP. Cellular membranes, delivered by ATG9-containing vesicles, contribute to elongation of the autophagosomal double membrane. Finally, phagophore closure allows autophagosomes to fuse with lysosomes, generating autolysosomes in which enclosed cargoes are degraded (adapted from (Dikic and Elazar, 2018)).

An essential role in the control of intracellular vesicular trafficking is shared by protein kinases able to phosphorylate phosphoinositides at the 3' position of the inositol ring. In particular, the vacuolar protein sorting 34 (VPS34) PI(3)K, is the main

producer of PI(3)P and plays an essential role in the biogenesis of the autophagosomes. VPS34 was identified initially in yeast, thanks to a screen for genes involved in protein sorting and was demonstrated to regulate membrane trafficking by the recruitment of downstream effectors containing PI(3)P binding domains (Jaber and Zong, 2013). In mammalian cells, VPS34 is part of two heterotetrameric core complexes known as complexes I and II. VPS34, VPS15 (p150), Beclin1 (BECN1; Atg6 in yeast) and ATG14L (Vps30/Atg14 in yeast) are part of complex I, whereas UV irradiation resistance-associated gene (UVRAG; Vps30/Vps38 in yeast) substitutes ATG14L in complex II. Structurally, VPS34/VPS15 form the catalytic core and BECN 1/ATG14L or BECN1/UVRAG the regulatory one (Itakura *et al.*, 2008; Ohashi, Tremel and Williams, 2019). Although both human ATG14 and UVRAG interact with BECN1, they act at different levels. In particular, ATG14L is present on autophagic isolation membranes recruiting PI(3)K class III protein and helps in the nucleation step (Matsunaga *et al.*, 2010); conversely, UVRAG associates with endosomes and is involved in autophagosome maturation and in recycling of membranes (Y. M. Kim *et al.*, 2015) (Fig. 10).

As stated above, PI(3)P production induces a cascade of events resulting in the recruitment of macromolecular complexes on specific sites of ER membrane that lead to the nucleation of phagophores. At this point, autophagy requires the activity of two conjugation systems involving ubiquitin-like (UBL) proteins which contribute to expansion of the phagophore (Nakatogawa, 2013). First, the E1 enzyme ATG7 and the E2 enzyme ATG10 conjugate ATG12 to the lysine residue in ATG5, and the resulting ATG12-ATG5 complex conjugate non-covalently with ATG16L which eventually associates with the extending phagophore (Ohsumi and Mizushima, 2004). Once the autophagosome is formed, the ATG5-ATG12-ATG16L complex dissociates from the membrane. The second UBL protein conjugation system

causes specific modification of a class of proteins represented by autophagosomal orthologs of yeast Atg8, the microtubule-associated protein light chain 3 (MAP1LC3 or simply LC3) and the gamma-aminobutyric acid receptor-associated (GABARAP) protein families. Nascent Atg8/LC3 (proLC3) is cleaved by cysteine protease ATG4 into LC3-I immediately after synthesis and then conjugated with phospholipid phosphatidylethanolamine (PE) by ATG7 and ATG3, a second E2-like enzyme (Ichimura *et al.*, 2000) (Fig. 10). Therefore, LC3 is detected in a double form, LC3-I represents the cytosolic part, and the lipidated LC3-II associates with newly forming autophagosome membranes and remains on mature autophagosomes until its fusion with lysosomes. Atg8-family proteins are the best-studied proteins of the core autophagic machinery. The cellular localization of Atg8/LC3 in the autophagosome has been associated with closure, hemi-fusion, or transport of the autophagosome during its maturation. LC3 is actively involved in sequestration of material in the growing phagophore and can itself be degraded by autophagy indicating that it is an autophagic substrate. LC3 is attached to both outer and inner membranes of autophagosomes and is widely used to monitor the number of autophagosomes as well as autophagic activity (Lee and Lee, 2016). The most recent features discovered for this essential protein, include the activity as adaptor protein to transport selective cargoes to autophagosomes via direct interaction with cargo receptors during selective autophagy (see below).

Another protein involved in phagophores expansion is ATG9, the unique transmembrane protein in the autophagy core machinery. ATG9-containing structures have been predicted to be a source of autophagosomal membranes (Yamamoto *et al.*, 2012; Feng and Klionsky, 2017). However, direct experimental evidence regarding the role of ATG9 in membrane movement are not available yet. Once the autophagosome has formed, it fuses with lysosomes and delivers its

contents for degradation. The resulting structures are called “autolysosomes” or “autophagolysosomes” (Mizushima, 2007). Phagophore membrane closure is a critical step for proper maturation of autophagosomal structures, double-membrane vesicles scission and consequent fusion with lysosomes. Recently, the endosomal sorting complexes required for transport (ESCRT) machinery, usually involved in repairing of membrane ruptures, has been proposed to function also in autophagosome closure (Takahashi *et al.*, 2018). Indeed, ESCRT defects lead to accumulation of immature autophagosomal structures both in C.elegans and in mammals, supporting its involvement in phagophore membrane closure (Takahashi *et al.*, 2018).

Although the endoplasmic reticulum exit sites (ERES) is the best characterized site for autophagosome biogenesis and maturation (Hamasaki *et al.*, 2013), also mitochondria, ER-mitochondria contact sites, ER-Golgi intermediate compartment (ERGIC), Golgi apparatus, and plasma membranes (PM) have been suggested to supply lipids to the growing isolation membrane in mammalian cells, but the exact mechanism/s mediating this process remain/s not fully elucidated.

3.3. Mechanisms and signaling pathways in the control of autophagy

As mentioned above, autophagy occurs at basal level in most tissues in a low rate, contributing to the routine turnover of cellular unwanted material. Therefore, an efficient mechanism of induction is crucial to mediate adequate response to stress and a rapid adaptation of cells to adverse growth conditions. In mammals, the very first autophagy-specific complex that comes into play is the unc-51-like kinase 1 (ULK1) complex, consisting of ULK1 itself, ATG13, FIP200 (focal adhesion kinase family interacting protein of 200 kDa), and ATG101 (Mizushima, 2010; Zachari and

Ganley, 2017) (Fig. 10). ULK1 is a serine/threonine kinase, orthologue of Atg1 in yeast and, together with its homolog ULK2, is one of the main players of autophagy. Although it has been shown in most cell types that loss of ULK1 is sufficient to disrupt autophagy, the redundant action of ULK2 has been demonstrated. On the other side, only the mouse model lacking both ULK1 and ULK2 shows the same neonatal lethality observed in other mice model knockout for other essential autophagy genes such as ATG5 or ATG7 (Lee and Tournier, 2011).

As opposed to yeast, in mammals ULK1 is constitutively in complex with the other proteins, namely ATG13, FIP200 and ATG101, independently from nutritional status conditions, suggesting that autophagy induction does not appear to be regulated at the level of assembly of the complex. Both FIP200 and ATG13 contribute to increase ULK1 activity and stability; indeed, mice knockout for FIP200 or ATG13 show embryonic lethality, and MEFs derived from these mice fail to initiate and complete autophagy (Gan *et al.*, 2006; Kaizuka and Mizushima, 2016). Regarding the third complex member, ATG101 has been demonstrated to form an heterodimer with ATG13 which mediates the interaction between FIP200 and ULK1 but no additional information are available for this molecule (Hosokawa, Sasaki, *et al.*, 2009).

The kinase activity of ULK1 represents the starting point of the autophagic machinery assembling. Good evidence of this can be found in ULK1 kinase-dead mutants, as well as in the chemical inhibition of kinase activity, which strongly blocks the autophagic response to starvation (Egan *et al.*, 2011). ULK1 phosphorylates the initiation complex members ATG13, FIP200 and ATG101, including ULK1 (autophosphorylation) (Hosokawa, Hara, *et al.*, 2009) and also phosphorylates components of the VPS34 complex such as BECN1 and ATG14L, enhancing VPS34 activity and PI3P production (Russell *et al.*, 2013). ULK1 controls VPS34 complex also through the phosphorylation of AMBRA1, a BECN1 interactor, which

results in translocation of the VPS34 complex to phagophore assembly sites (Di Bartolomeo *et al.*, 2010) (Fig. 10).

Several pathways work upstream to regulate autophagy promoting its activation/inhibition, mainly by ULK1 post-translational modifications. The well-known master regulator of autophagy is represented by the mammalian target of rapamycin (mTOR) protein, which senses fluctuations in nutrient status to modulate cell growth, metabolism and survival (Jung *et al.*, 2009). mTOR is a serine/threonine protein kinase and the catalytic subunit is shared by two structurally distinct complexes: mTOR complex 1 (mTORC1) and mTOR complex 2 (mTORC2) which can be distinguished on the basis of their sensitivity to rapamycin which is able to specifically inhibit only mTORC1. Different stimuli activate these two complexes as well as different downstream responses they produce. In particular, mTORC2 regulates cytoskeleton organization and cell survival, while the major role of mTORC1 is the control of cell growth playing as energy-sensor. In nutrients-rich conditions, the active mTORC1 promotes anabolic processes, phosphorylating its downstream effectors, ULK1 and ATG13 thus leading to the inhibition of autophagy. In particular the phosphorylation of ULK1 takes place at a serine in position 757. Conversely, upon stress conditions, such as amino acid deprivation or rapamycin treatment, mTORC1 kinase activity is suppressed, both ULK1 and ATG13 are rapidly dephosphorylated, resulting in activation of autophagic processes (Hosokawa, Hara, *et al.*, 2009).

The AMP-activated protein kinase (AMPK) also participate in this nutrient-sensing pathway responding inversely to mTORC1. When energy intake falls and ATP consumption produces large amounts of cytosolic AMP (cAMP), AMPK is phosphorylated and activated. In turn, AMPK inactivates mTORC1 through the phosphorylation of the regulatory-associated protein of mTOR (RAPTOR), thus

indirectly activating ULK1 activity (Kim *et al.*, 2011). However, AMPK can also directly phosphorylate and activate ULK1 at multiple serine residues in a nutrient dependent manner, thus leading to autophagy induction (Egan *et al.*, 2011).

Autophagy can also be regulated by the ubiquitination system through the control of ULK1 levels. It has been shown that both AMBRA1 and the E3-ligase TNF receptor associated factor 6 (TRAF6) can promote ULK1 ubiquitination and its subsequent stabilization thus enhancing ULK1 activity (Nazio *et al.*, 2013). Conversely, the ubiquitination of ULK1 by the Cullin E3 ligase complex, composed of the E3 ligase Cullin-3 (Cul3) and the adaptor kelch-like family member 20 (KLHL20) has been shown to promote ULK1 degradation in a proteasome-dependent manner (C. C. Liu *et al.*, 2016). These mechanisms of regulation control and regulate the restrain of the amplitude and duration of autophagy (C. C. Liu *et al.*, 2016).

3.4. Selective regulation of autophagy

Three morphologically and mechanistically distinct types of autophagy have been described in cells: microautophagy, macroautophagy and chaperone-mediated autophagy. In microautophagy, the cytosolic components are directly taken up by the lysosome itself through the lysosomal membrane, while, in chaperone-mediated autophagy, the targeted proteins are translocated across the lysosomal membrane in a complex together with specific chaperone proteins. All types of autophagy have been initially described as non-selective recycling processes. Conversely, in the last decade, it has been clearly demonstrated, how autophagy may be employed for selective degradation of specific cargo. This highly regulated mechanism is named selective autophagy (Zaffagnini and Martens, 2016) (Fig. 11).

Few principles, not necessarily stepwise or all required, characterize selective autophagy: a) the presence of a degradation cue; b) cargo recognition via a selective autophagy receptor protein, which can be itself engulfed and degraded into autophagosomes; c) the specialized recruitment of autophagosome machinery/membranes for delivery to lysosomes for degradation. The molecular basis of selective autophagy receptors action is based on their ability to link their bound cargo to nascent autophagosomes by interacting with the lipidated form of LC3/GABARAP attached to the isolation membrane. Many LC3/GABARAP associated-proteins contain short tag sequences, called **L**C3-**I**nteracting **R**egion, or simply *LIR motif,* that mediate the direct bind with LC3/GABARAP-family proteins (Birgisdottir, Lamark and Johansen, 2013). The LIR motif is defined by a characteristic consensus sequence which corresponds to the shortest sequence required for interaction with LC3/GABARAP-family members. The canonical sequence typically contains **W/F/Y**-X-X-ψ core (ψ, hydrophobic residue: **L/I/V**, X is any residue); where the aromatic residue in positions 3 and the hydrophobic residue in position 6 (marked in bold) mark the amino acids crucial for the interaction. This core motif is often preceded or followed by acidic residues or phosphorylation sites, responsible for binding modulation (Jacomin *et al.*, 2016). Non-canonical LIR sequences have also been described, suggesting that further molecular determinants of ATG8 interacting proteins may yet be uncovered (von Muhlinen *et al.*, 2012).

The first ever selective autophagy receptor to be identified was sequestosome 1 (SQSTM1; better known as p62), which mediates the autophagic degradation of polyubiquitinated cargo material through the LIR-mediated interaction with LC3 (W. J. Liu *et al.*, 2016). Since p62 accumulates when autophagy is inhibited, and

decreased levels can be observed when autophagy is induced, p62 has been frequently used as a marker to study the autophagic flux.

Following the discovery of p62 and the identification of the LIR consensus sequence, several selective autophagy receptors have been identified and increasingly associated with specific subtypes of autophagy.

An example is represented by the related neighbor of BRCA1 gene 1 (NBR1), which, similar to p62, contains both a LIR and an ubiquitin-binding domain and was found to act as an aggrephagy receptor (Kirkin *et al.*, 2009). Other selective autophagy receptors are: the nuclear dot protein 52 kDa (NDP52) which functions as xenophagy receptor (Von Muhlinen *et al.*, 2010), the BCL2 Interacting Protein 3 Like (BNIP3L) and optineurin, involved in mitochondria clearance and mitophagy (Birgisdottir, Lamark and Johansen, 2013).

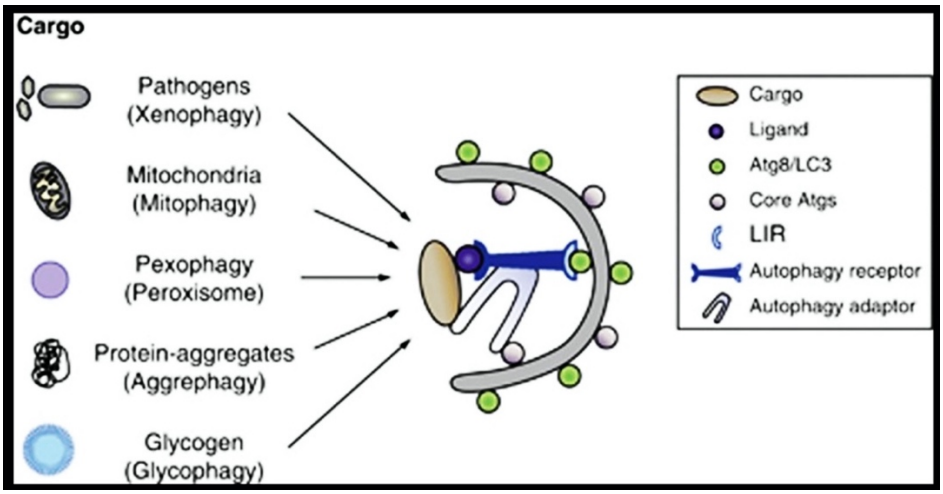

Figure 11. Selective autophagy.
Selectivity in autophagy is conferred by cargo receptor or adaptor proteins which deliver cytosolic materials into the autophagosome, binding simultaneously both the cargo and autophagosomal membrane. Autophagy receptors have a specific ligand-binding domain well-known as LIR which mediates its interaction with Atg8/LC3 family proteins. An adaptor protein further facilitates sequestration of the specific cargo by linking the cargo-receptor complex to the core of Atg proteins. Various types of selective autophagy are known, like xenophagy (invasive pathogens), mitophagy (mitochondria), pexophagy (peroxisomes), aggrephagy (aberrant protein aggregates and disease-related inclusions) and glycophagy (glycogen particles) (adapted from (Isakson, Holland and Simonsen, 2013)).

Lastly, LIR motifs are not restricted to autophagy receptors but can be considered as a general surface for interaction with LC3/GABARAP family proteins. Indeed, functional LIR motifs have been identified in many core ATG proteins. ULK1 contains a canonical LIR motif, required for its starvation-induced association with autophagosomes but not for its degradation (Alemu *et al.*, 2012). Functional LIR motifs have been also identified in adaptor proteins regulating the movement of autophagosomes along microtubules and autophagosome maturation (Birgisdottir, Lamark and Johansen, 2013). Moreover, several signaling proteins, such as Dishevelled 2, have a functional LIR which is necessary for their autophagic degradation (Gao *et al.*, 2010).

However, the mechanism of binding described so far, is evolutionarily conserved, since several proteins from yeast up to mammals, retain classical Atg8/LC3-interacting regions (AIMs/LIRs). Recently, it has been proposed a new type of binding sequence called GABARAP-interacting motif (GIM), which specifically designates enhanced attitude to bond with GABARAP versus LC3 family members (Rogov *et al.*, 2017). The improvement of current knowledge about the features characterizing Atg8/LC3/GABARAP binding sites will contribute expanding the recognized set of autophagy receptors and adaptor proteins and their functions.

4. The autophagy-cilia axis

4.1. Cilia as new site of the autophagic machinery assembling

As sensory organelles, primary cilia are equipped to feel extracellular fluctuations and transduce signals into the cell influencing its fate; in the same way, autophagy could act as a specific mechanism of control for cilia assembling. As evidence of that, recent studies have revealed a bidirectional relationship between cilia and

autophagy. Primary cilia and related ciliary signaling and proteins seem to be able to control autophagy; conversely, autophagy appears to be one of the main players in ciliogenesis regulation (Pampliega and Cuervo, 2016).

A first evidence comes from the observation that ATG proteins localize at cilia or periciliary structures. Upon serum starvation, both LC3 and GABARAP, markers of mature autophagosomes, and VPS15, ATG16L1 and AMBRA1, acting in the phagophore nucleation step, form discrete puncta at the level of basal bodies and cilia axonemes. In addition, VPS34, Atg14, and other proteins of the elongation complex (i.e. Atg7 and Atg5) associate with basal bodies, while ULK1 and Beclin1 are not found at ciliary regions (Pampliega *et al.*, 2013; Orhon *et al.*, 2015) (Fig. 12A-B).

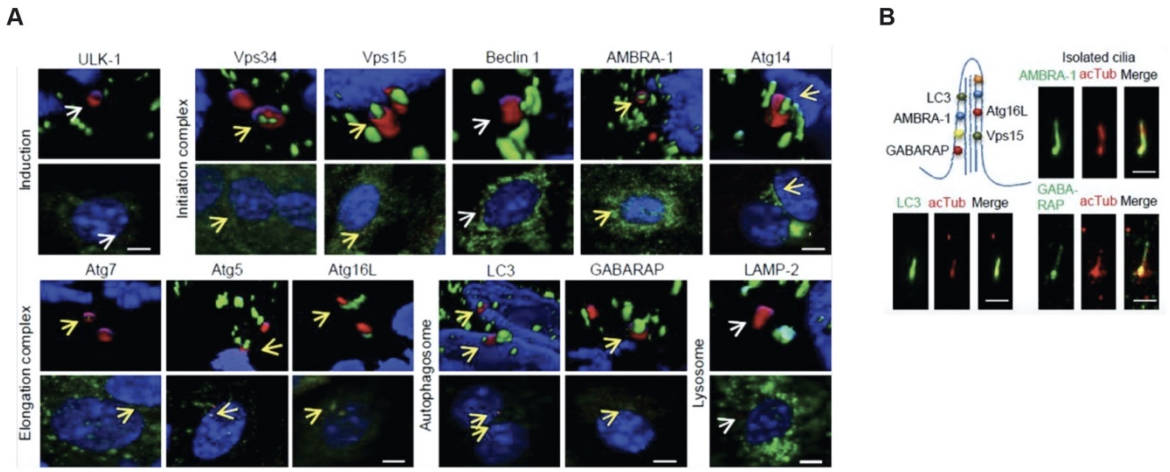

Figure 12. Autophagy-related proteins associate with ciliary structures.
Some ATG proteins are found to associate with ciliary structures, as the basal body and the ciliary axoneme. A. Co-immunostaining (bottom) and 3D reconstruction (top) for the indicated autophagy-related proteins (green) and gamma tubulin (red), which marks basal body of cilium, in KECs after 24 hours of serum- starvation. Yellow arrows indicate colocalization; white arrows no colocalization. B. ATGs protein (green) localize at ciliary axoneme (marked by acetylated tubulin, red) (adapted from (Pampliega *et al.*, 2013)).

The presence of key regulators of autophagy at cilia, led researchers to suggest that the ciliary membrane could represent a new nucleation site for autophagosome assembly and the plasma membrane a source of new autophagosomes, despite the

favored sites for the majority of autophagic processes are still the endoplasmic reticulum and the outer mitochondrial membranes. On the other hand, some of the key players of autophagy, such as ULK1 and Beclin-1, are not found to associate with ciliary structures, suggesting the involvement of undiscovered complexes and mechanisms in the regulation of the main steps of autophagy (Pampliega *et al.*, 2013). Cilia sensorial ability may be useful to ensure fast activation of autophagy in response to different stimuli, and cilia formation and elongation can benefit from selective autophagic removal of positive and/or negative regulators of ciliogenesis.

4.2. Autophagy controls cilia-related processes

As stated above, the assembly of the primary cilium usually occurs during the G1/G0 phase of cell-cycle when cells enter quiescence. Serum deprivation is known to be a strong stimulus of ciliogenesis induction and, interestingly, it is also able to activate an acute autophagic response. Recent evidence suggests that, these two cellular processes not only share induction stimuli, but are also connected to each other.

An evidence of this connection comes from Tang and colleagues, which demonstrated that autophagy can actively affect cilia and cilia related processes. Indeed, selective degradation by autophagy of the protein encoded by the gene responsible for OFD type I syndrome, OFD1, improves ciliogenesis (Tang *et al.*, 2013). OFD1, as mentioned before, is a ciliopathy protein localizing to basal body of cilia and to centriolar satellites (CS) surrounding the centrosome, where the pool of OFD1 act as suppressor of ciliogenesis. Tang et al. demonstrated that in mouse embryonic fibroblast (MEFs) and in retinal pigmented epithelial (RPE) cells, OFD1 is selectively removed from satellites by autophagy to promote cilia formation; conversely the basal body pool of the OFD1 protein is not affected by degradation

and remains unchanged. In addition, tandem affinity purification experiments of the autophagosome marker LC3 identified several centriolar satellites proteins as putative interactors (i.e. PCM1, OFD1 and CEP131), but among them, only OFD1 seems to be specifically targeted by LC3 for degradation (Tang *et al.*, 2013) (Fig. 13A-C). It has also been demonstrated that OFD1 accumulates in autophagy-defective system (Tang *et al.*, 2013; Holdgaard *et al.*, 2019) and it has been proposed as an autophagy substrate together with other component of CS targeted by a novel type of selective autophagy, identified as doryphagy (from the Greek word *doryfóros* meaning satellite) (Holdgaard *et al.*, 2019).

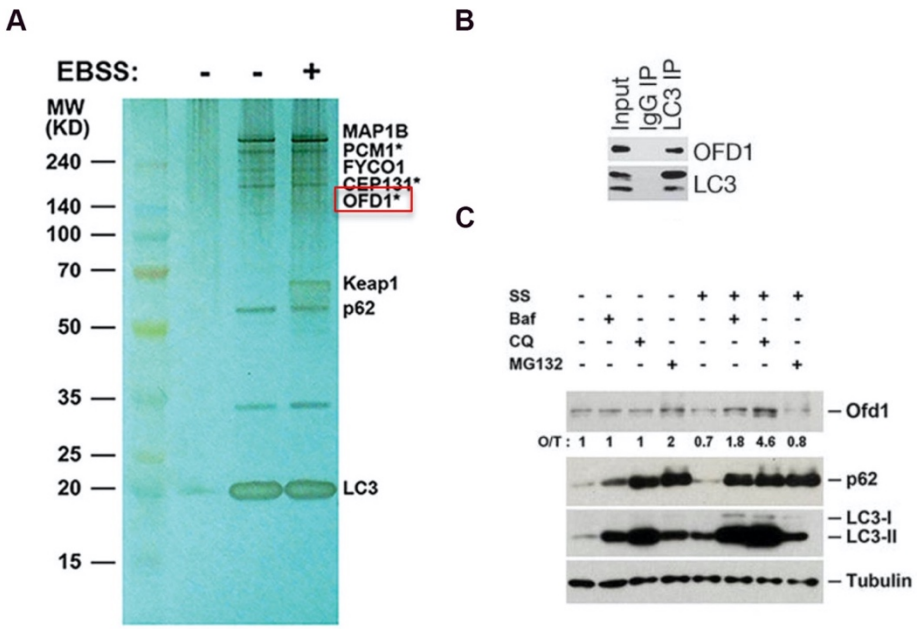

Figure 13. OFD1 interacts with LC3 and is an autophagy substrate.
A. Silver staining of LC3 complexes purified from U_2OS cells expressing ZZ-Flag-LC3. *, centriolar satellites proteins. B. Co-IP of OFD1 with LC3 in HEK293T cells. C. WB analysis of Ofd1, p62 and LC3 in MEFs in normal medium or subjected to 24-hour serum starvation (SS), 50 nM bafilomycin A1 (Baf), 20 μM chloroquine (CQ), or 1 μM MG132. Quantified Ofd1 level was normalized with β-tubulin (adapted from (Tang *et al.*, 2013)).

On the other hand, Pampliega et al. reported that in non-ciliated cycling MEFs, basal autophagy governs ciliogenesis acting as a negative regulator of cilia assembly. Indeed, the authors reported that in a status of regular supply of nutrients,

autophagy controls cilia assembling promoting the degradation of IFT20, known to be a positive modulator of ciliogenesis (Pampliega *et al.*, 2013).

Other studies support the involvement of autophagy in the control of cilia formation and cilia length: in MEFs autophagy-mediated decrease in expression of cilia-associated proteins (IFT88, KIF3a and Ac-tubulin) negatively regulates primary cilia length (Xu *et al.*, 2016); chemical induction of autophagy through sertraline, an antidepressant of a selective serotonin reuptake inhibitor class, and thioridazine an antipsychotic, lead to improvement of ciliogenesis in RPE cells and lung cancer A549 cells, respectively (Kim *et al.*, 2015; Bao and Huang, 2017); transcriptional regulation of autophagy also regulates cilia formation in several cell types, such as RPE, MEFs and human kidney-2 (HK2) cells, as described for PPARA and NR1H4, two nutrient-sensing receptors. In particular, PPARA is known to induce ciliogenesis in fasting condition, while NR1H4 negatively regulates cilia formation under nutrients (Liu and Levine, 2015).

However, other studies showed opposite findings regarding the role of autophagy in cilia biology. An example is given by Pampliega et al. who found that serum starvation induces the assembly of longer cilia in autophagy-deficient cells ($Atg5^{-/-}$ MEFs) compared to controls, demonstrating that in this model, autophagy is not required for cilia formation (Pampliega *et al.*, 2013).

Autophagy is also involved in the control of centrosome-related processes. Indeed, autophagy contributes to regulate proper centrosome number promoting degradation of the centrosomal protein of 63 kDa (CEP63) (Watanabe *et al.*, 2016). In the same way, inhibition of autophagy leads to supernumerary centrosome and, consequently, to mis-segregation of chromosome and genomic instability (Arquint, Gabryjonczyk and Nigg, 2014).

However, compelling experimental evidence suggest that differences in cell confluency and/or culturing conditions, can be crucial to explain what appears to be divergent findings. The regulation of autophagy-mediated ciliogenesis could also be related to the cell type and thus be cell context specific.

It is clear that the autophagy-cilia axis is emerging as an intriguing new field of studies, but further investigation will be necessary to better characterize the mechanisms underline this interplay. The influence exerted by autophagy on ciliogenesis indicates a new feedback mechanism of proper cilia formation committed to control, possibly in turn, autophagy itself. From this perspective, defective autophagy could underline some of the clinical manifestations observed in ciliopathies and, cilia could have a role in autophagy-associated diseases. This is, however, pure speculation at this point.

4.3. The primary cilium influences autophagy

Autophagy has also been demonstrated to control cilia formation and cilia length thus the hypothesis emerged of a dual crosstalk in which cilia and autophagy mutually influence each other (Morleo and Franco, 2019). Data favoring the involvement of primary cilia in autophagy regulation comes from Pampliega et al. which demonstrated that fully functional primary cilia are required for autophagy activation. Indeed, IFT20- and IFT88-inactivated cells (MEFs and KECs) show impairment in ciliogenesis as well as decreased autophagy induction upon serum removal. Moreover, under serum deprivation, the increase in autophagosome biogenesis is directly dependent on activation and expression of Hedgehog (HH) signaling target genes (Pampliega et al., 2013).

Other studies on the cilia/autophagy interplay, involve the mTOR pathway. In particular, it has been reported that autophagy is repressed in cells showing shorter cilia due to increase in mTOR negative regulation, as described for IFT88-inactivated HK2 cells that display shorter cilia, and wild-type renal epithelial cells selected for the presence of shorter cilia (Wang *et al.*, 2015). In these cells, treatment with the mTOR inhibitor rapamycin is able to restore autophagy (Wang *et al.*, 2015). The involvement of mTOR in cilia-mediated autophagy has been shown also in Rpgrip1-like (Rpgrip1l)-deficient MEFs. The Rpgrip1l protein localizes at the ciliary transition zone and is mutated in patients affected by Meckel-Gruber and Joubert syndrome. MEFs defective for Rpgrip1l show ciliary dysfunctions with longer cilia and reduced autophagy due to excessive MTORC1 activity, as demonstrated by rapamycin treatment which rescued dysregulated MTORC1, autophagic activity and cilia length (Struchtrup *et al.*, 2018).

Control of autophagy exerted by primary cilia has also been demonstrated to influence neuroectoderm (NE) lineage specification. Indeed, in human embryonic stem cells (hESC), serum starvation induces cilia-mediated autophagy reducing the abundance of several essential repressor of NE differentiation (i.e. Nrf2, OCT4 and NANOG) and promoting early NE markers expression (Jang *et al.*, 2016).

A properly working primary cilium is also essential to modulate autophagy in the control of proper cell size and volume in models of renal function. Indeed, Orhon and colleagues demonstrated that cilia sense fluid flow inducing autophagy which, in turn, regulates cell-volume of KEC cells. Conversely, defective ciliogenesis, due to IFT88 inactivation, impairs flow-induced autophagy and consequently the regulation of cell volume (Orhon *et al.*, 2016). Indeed, in kidney proximal tubules, primary cilia actually works as flow antenna transducing specific signals to the LKB1–AMPK–mTOR axis to activate autophagy (Orhon *et al.*, 2016).

Acting as a sensory platform, the primary cilium is able to receive and orchestrate many different types of stimuli and because of that, it is not surprising the emerging role of primary cilia in autophagy. Therefore, primary cilia may represent a sort of checkpoint for the cell, taking part in the physiological mechanism of adaptation to stress and in the maintenance of tissue homeostasis.

4.4. Functional crosstalk between ciliary and autophagic proteins

There are several examples of well-known ciliary proteins found to be novel players of autophagy (Fig. 14) although it is not always clear whether the role in autophagy is mediated by cilia.

The protein IFT20 represents the first example described of a ciliary protein directly involved in the regulation of starvation-induced autophagy. IFT20 is a highly dynamic IFT protein which moves from the Golgi complex to the cilium as well as along ciliary axonemes (Follit et al., 2006). IFT20 subunits have been found to colocalize with the autophagic protein ATG16L1 promoting its relocation from Golgi to cilia upon serum starvation through a IFT88-dependent mechanism (Pampliega et al., 2013).

Another cilia-related protein, PCM1, has been showed to influence autophagy through a different mechanism. PCM1, a protein of centriolar satellites, directly binds a pool of GABARAP residing at the centrosome and pericentriolar region (Joachim *et al.*, 2017). This interaction is mediated by a canonical LIR motif allowing PCM1 to control GABARAP localization at peripheral centriolar satellites and to promote its degradation. Indeed, PCM1 depletion results in more GABARAP-positive autophagosomes because of reduced GABARAP proteasomal degradation but has no effect on LC3-positive autophagosome formation. Furthermore, PCM1-

GABARAP-positive centriolar satellites colocalize with forming autophagosomes. In this study the authors hypothesized that PCM1 action on GABARAP-mediated autophagy is independent from cilia, since all experiments were performed in non-ciliated conditions (Joachim *et al.*, 2017).

Inositol 5-phosphatase (INPP5E), which is mutated Joubert syndrome has been involved in positive regulation of autophagy. In non-ciliated neuronal cells, INPP5E localizes at lysosomes where it is required for proper autophagosome-lysosome fusion in a cilia-independent mechanism. Moreover, authors showed that loss of INPP5E phosphatase activity impaired autophagy (Hasegawa *et al.*, 2016).

De Leo et al. demonstrated that OCRL1, another inositol 5-phosphatase (PI(4,5)P2 5-phosphatase), is recruited by lysosomes and, as INPP5E, is required for autophagosome-lysosome fusion. OCRL1 is mutated in the X-linked Lowe syndrome; in cells isolated from Lowe syndrome patients, the loss of enzymatic activity of OCRL1 leads to autophagosomes accumulation and lysosome anomalies (De Leo *et al.*, 2016).

Folliculin (FLCN) is another example of ciliary protein also localizing at the lysosomal compartment where FLCN colocalizes with RagC/D GTPase. In this compartment FLCN modulates nutrient sensing acting as a GTPase activating protein (GAP) specifically for RagC/D (Tsun *et al.*, 2013). Moreover, FLCN physically interacts with ULK1 kinase and GABARAP and plays a positive role in autophagy (Dunlop *et al.*, 2014).

As FLCN, also Huntingtin (HTT) interacts with components of the autophagic machinery by binding p62 and ULK1. HTT functions as a scaffold protein promoting p62-cargo association with LC3 on autophagosomes and ULK1 kinase activation favoring selective autophagic processes (Rui *et al.*, 2015). HTT is known to be mutated in Huntington disease and it has been found to localize at centrosomes

where mediates the movement of PCM1 from cytoplasm to the pericentriolar region (Kaliszewski, Knott and Bossy-Wetzel, 2015).

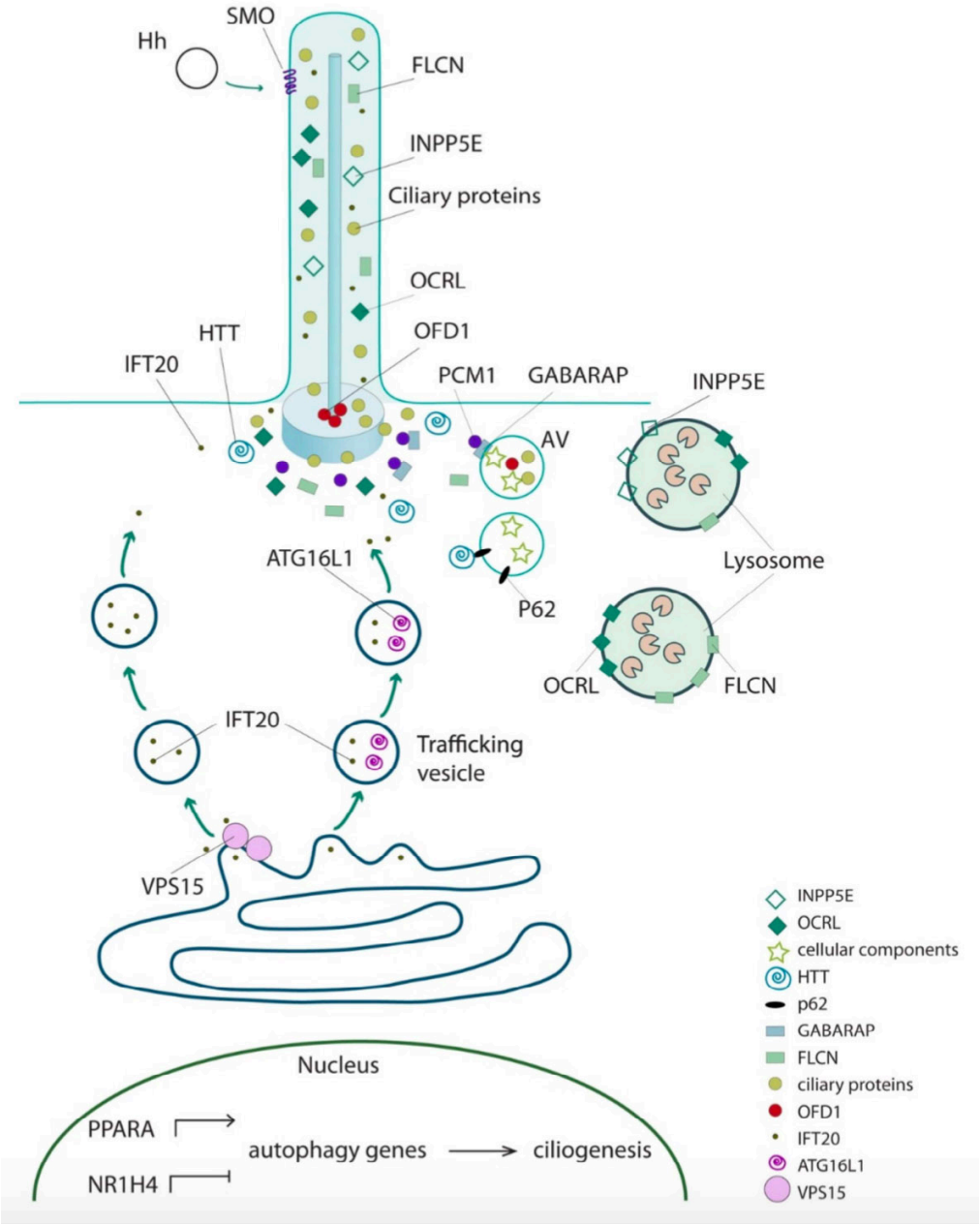

Figure 14. The autophagy-cilia axis.
The cartoon shows a schematic representation of proteins involved in the control of both ciliogenesis and autophagy. AV: autophagic vacuoles. (adapted from (Morleo and Franco, 2019)).

Finally, contrary to what described so far, VPS15 represents an example of autophagic protein involved in cilia biology. As mentioned before, VPS15 is a serine/threonine kinase which complexes with VPS34 and is required for membrane

trafficking and autophagy. VPS15 also localizes at basal bodies of cilia and along the axoneme and in human fibroblasts regulates primary cilium length. In fibroblasts carrying mutations in VPS15, IFT20-positive vesicles targeted at cilia, fail to be released from Golgi (Stoetzel *et al.*, 2016).

As described so far, there are many examples of ciliary proteins with a direct functional role in autophagy apparently separated from their involvement in cilia biology and other cilioproteins are expected to be implicated in distinct stages of autophagy. Furthermore, we can reasonably hypothesize that, as VPS15, other proteins typically associated to autophagy, could exert their functions also in other cellular processes, like ciliogenesis. Further studies addressing the intertwined functions between autophagy and cilia will be necessary to better understand the molecular mechanisms underlying this intriguing crosstalk and the possible implication for autophagy and cilia-related diseases.

Results

1. Components of ULK1 complex localize at centrosome

The limited knowledge about the link between autophagy and cilia/centrosome, makes the investigation of these two pathways extremely intriguing. Given our interest in the study of the ciliopathy protein OFD1 we focused our attention to inquire into a putative involvement of OFD1 in autophagy, assuming a counter-reaction mechanism in the balancing of autophagy and ciliogenesis.

Previously in the lab, a tandem mass spectrometry approach using tagged OFD1 as bait, pointed out as putative interactor FIP200, a component of ULK1 complex (Iaconis *et al.*, 2017). I thus set up experiments aimed at addressing the possible involvement of the OFD1 protein in this leading autophagic complex. I chose human kidney 2 (HK2) cells as principal cellular model for the *in vitro* analysis as renal cystic disease is one of the typical manifestations of OFD type I and I was looking for a disease-relevant in vitro model. HK2 cells are immortalized proximal tubular cells derived from adult normal kidney (Ryan *et al.*, 1994). These human renal cells are able to properly form cilia which elongate up to 24 hours of serum deprivation (see Fig. 19C). Before starting with the description of the results I would like to emphasize that all the experiments were performed in subconfluent condition, to avoid cilia assembling and, thus in order to analyze OFD1 function independently from its involvement in ciliogenesis.

Co-immunoprecipitation (co-IP) experiments established the interaction between endogenous FIP200 and OFD1 proteins (Fig. 15A). Given the close connection among these proteins, I also tested for the interaction with all the other components of ULK1 complex and interestingly, co-IP experiments revealed ATG13 the essential adaptive subunit of ULK1 conglomerate as interacting protein. The other proteins of

the complex do not seem to associate with the OFD1 protein (Fig. 15A). The OFD1-ATG13 interaction was also validate by reverse immunoprecipitation of endogenous ATG13 (Fig. 15B).

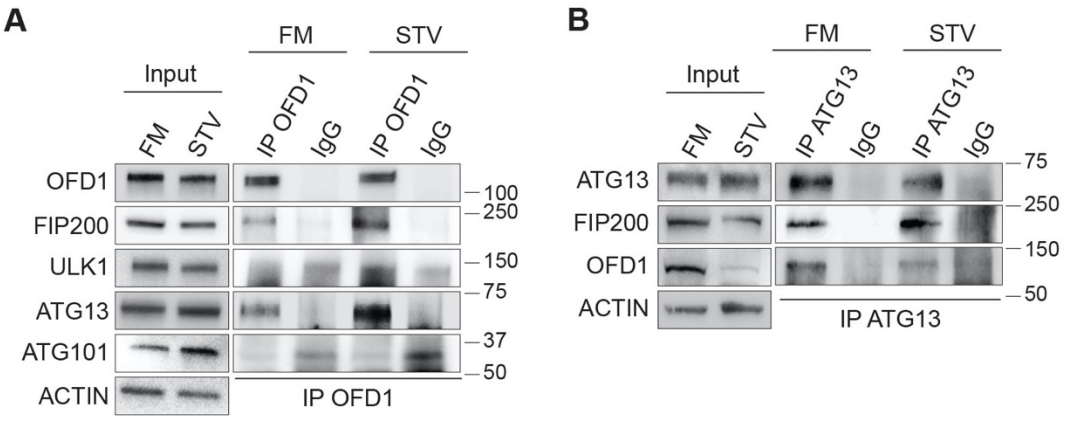

Figure 15. OFD1 interacts with components of the ULK1 complex.
HK2 cells were cultured in FM or STV in HBSS for 2h and lysates were immunoprecipitated with anti-OFD1 (A) and anti-ATG13 (B) antibodies or IgG as indicated and analyzed by WB; ACTIN as used as loading control. n=3 independent experiments. IP=immunoprecipitation, FM=full medium, STV=starvation.

The co-IP analysis was performed both in full medium condition and in nutrient deprivation after treatment with Hank's Balanced Salt Solution (HBSS), to test if the interactions occur both in basal condition and/or consequently to autophagy induction. As clearly shown in Fig. 15, OFD1 is able to associate with FIP200 and ATG13 in both conditions, suggesting that the interaction is not strictly dependent on activation of autophagy.

Since OFD1 is a centrosomal protein and its localization is predominant in that region and in surrounding satellites (see Fig. 8), I wondered whether the interactions revealed by co-IP experiments took place in the centrosome. In HK2 cells, treatment with HBSS is able to induce assembling of endogenous ATG13 and FIP200 to form discrete puncta. I evaluated the colocalization of these puncta with OFD1 and widely

used markers of centrosome, such as γ-Tubulin and centriolar satellites, like PCM1, through immunofluorescence (IF) experiments.

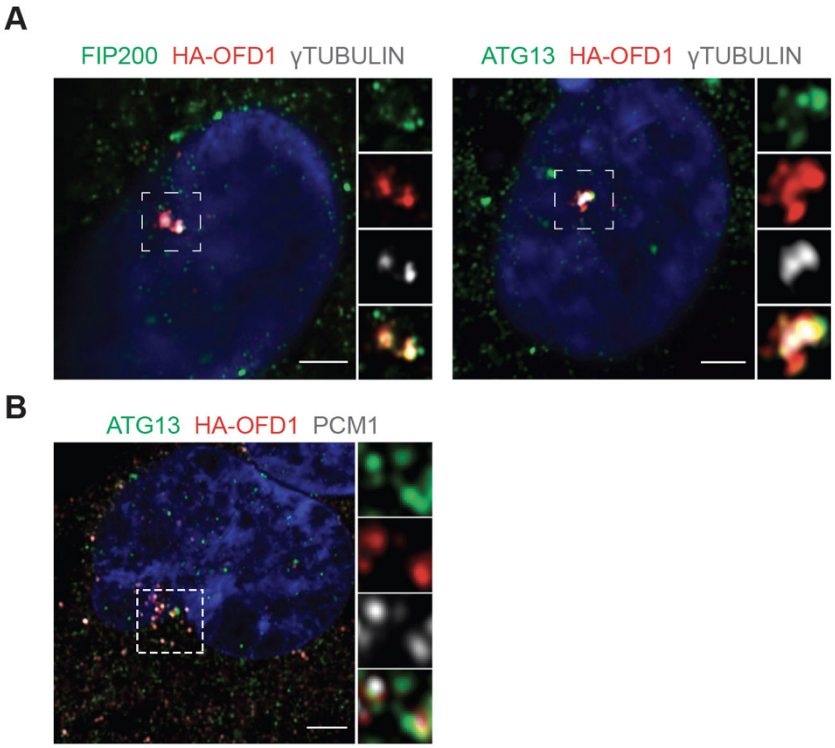

Figure 16. FIP200 and ATG13 localize at centrosome, ATG13 also at centriolar satellites. Airyscan confocal analysis of colocalization between FIP200/ATG13 and γTUBULIN and ATG13 with PCM1 in lentiviral delivered OFD1 in HK2 cells cultured in HBSS for 90min. The insets show higher magnification and single-color channels of the boxed areas. Green, FIP200 and ATG13; red, HA-OFD1; grey, γTUBULIN and PCM1; blue, Hoechst labels nuclei. Scale bar=3.5µm.

To this purpose, I used stable and doxycycline-inducible HK2 cell line generated by infection of HK2 cells with HA-tagged OFD1 wild-type gene cloned in a lentiviral vector. To induce OFD1 protein expression, the cells were treated with doxycycline for 36h and then analyzed. Triple IF staining for HA-OFD1 and endogenous γTUBULIN/PCM1 and FIP200/ATG13, revealed partial colocalization of both proteins at the centrosome, whereas only ATG13 seems to localize at centriolar satellites (Fig.16A, B).

Silencing of *ATG13* and *RB1CC1* (the gene codifying for FIP200) transcripts was performed to evaluate the specificity of the antibodies for the centrosomal signals (Fig. 17).

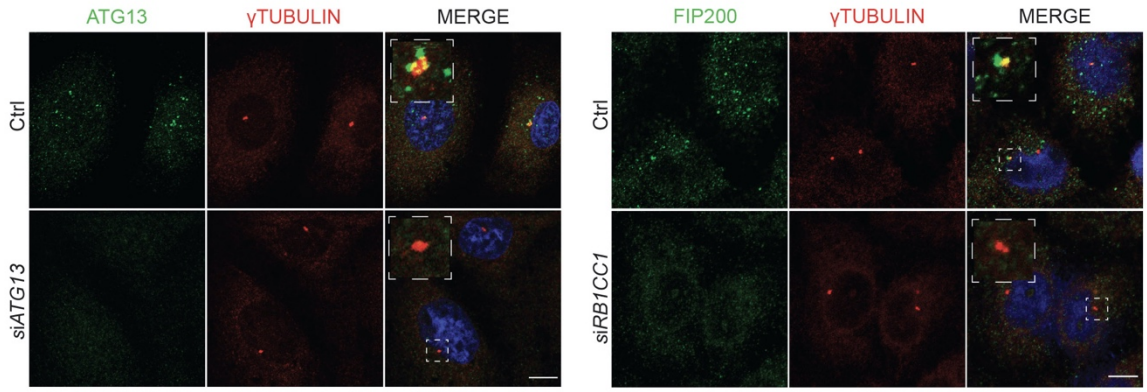

Figure 17. FIP200 and ATG13 antibodies specificity.
Representative confocal images of γTUBULIN and ATG13 (left) and FIP200 (right) puncta in wt and ATG13-silenced and RB1CC1 (FIP200)-silenced HK2 cells starved for 90min. Green, FIP200 and ATG13; red, γTUBULIN; blue, Hoechst labels nuclei. Scale bar=10µm.

The measurement of the amount of OFD1 protein overlapping with FIP200 or ATG13 spots revealed a higher percentage of OFD1 protein colocalizing with ATG13 compared to FIP200 in starved HK2 cells (Fig. 18A). Indeed, only few spots of OFD1 are shared by FIP200 and ATG13 (Fig. 18B), suggesting that the interaction with OFD1 is not dependent on the simultaneous existence of both proteins.

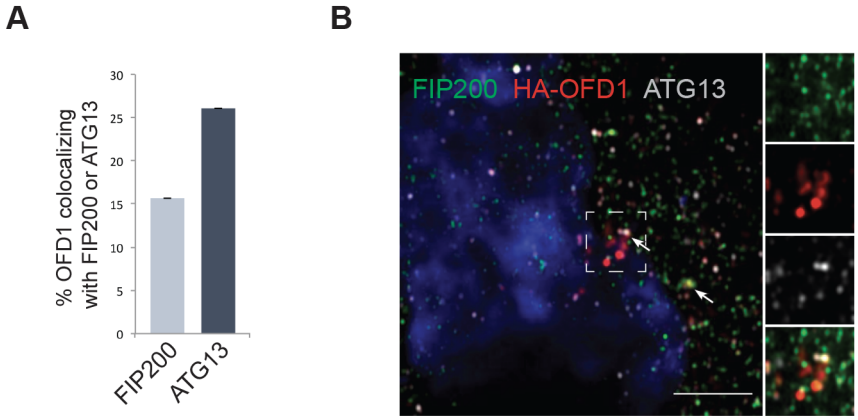

Figure 18. OFD1/ATG13/FIP200 colocalization.
A. Bar graphs show quantification of HA-OFD1/ATG13 and HA-OFD1/FIP200 colocalization, expressed as % of total OFD1 fluorescence (mean ± SEM). n= 3 independent experiments; n=55 cells for ATG13 and n=40 for FIP200 were analyzed. B. Representative image of airyscan confocal analysis of endogenous ATG13 and FIP200 colocalization with lentiviral delivered OFD1 in HK2 cells cultured in HBSS for 90min. Green, FIP200; red; HA-OFD1; grey, ATG13; blue, Hoechst for nuclei. The insets show higher magnification and single-color channels of the boxed areas. Scale bar=3.5µm.

2. OFD1 controls the ULK1 complex stability

To better define the nature and the significance of the interaction of OFD1 with core proteins of the ULK1 complex, I considered to analyze any change in protein expression of the ULK1 complex components in the absence of OFD1. Using CRISPR-Cas9 genome editing technology, a HK2 cell clone knock-out for *OFD1* (KO-*OFD1*), which does not express any level of protein due to a frameshift mutation leading to a premature stop codon was generated by a member of the laboratory (Fig. 19A-B). As expected, HK2 KO-*OFD1* cells are not able to form primary cilia (Fig.19C).

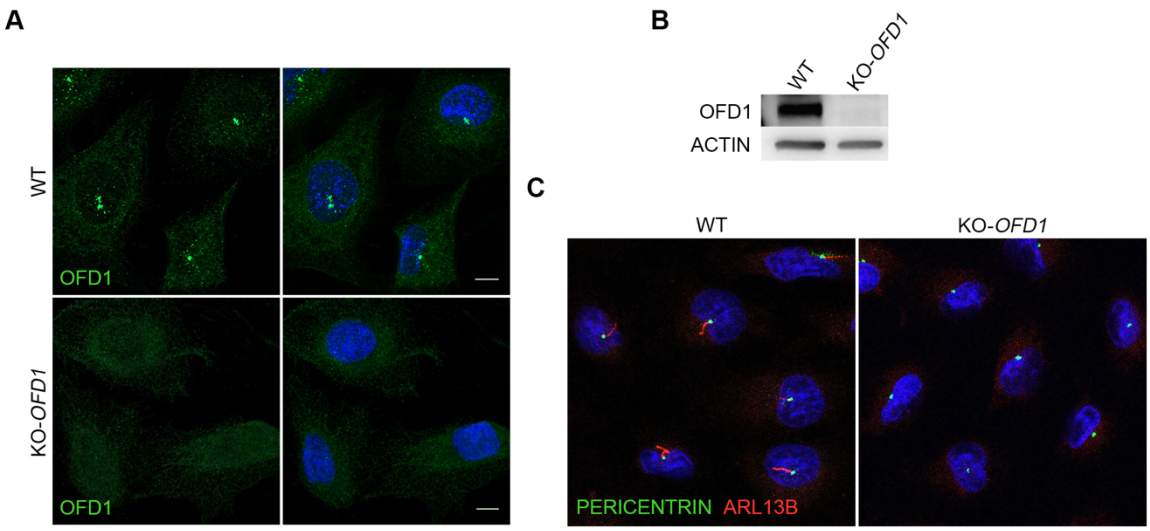

Figure 19. HK2 KO-*OFD1* are deficient for OFD1 and are not able to form cilia. A. Representative confocal images of OFD1 signal in HK2 wt and *KO-OFD1* cells. Green, OFD1; blue, Hoechst for nuclei. Scale bar=10µm. B. WB analysis of OFD1 protein level in HK2 wt and KO-*OFD1* cells. C. Representative confocal images of cilia labelled with ARL13B antibodies in HK2 wt and *KO-OFD1* cells after 24h of serum starvation. Green, PERICENTRIN; red, ARL13B.

Therefore, I checked for ULK1 complex protein levels at different time point of nutrient deprivation comparing them between wild-type (wt) and KO-*OFD1* cells. The analysis revealed a clear enhancement of protein levels for all ULK1 complex components in KO-*OFD1* cells compared with wt both in basal condition and after treatment with HBSS (Fig. 20A-B).

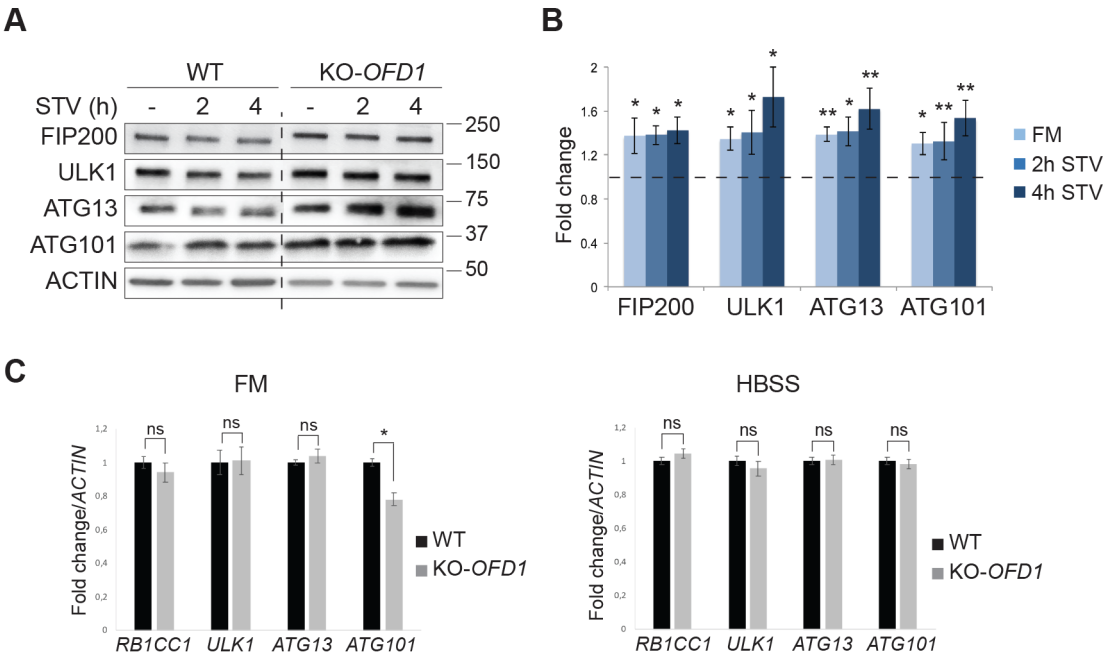

Figure 20. Loss of OFD1 increases ULK1 complex protein levels in absence of transcriptional changes.

A, B. Western blot analyses of FIP200, ULK1, ATG13 and ATG101 in HK2 wt and KO-*OFD1* cells assessed in fed (-) conditions or following 2 and 4h of starvation. ACTIN was used as loading control, The bands are at the same exposure, noncontiguous on the same gel, The blot is representative of n=5 independent experiments, Protein levels values, normalized versus ACTIN, are expressed as the fold increase compared with wt cells (represented by the dashed line). Mean ± SEM. One tailed Student's *t* was applied; *p≤0.05, **p≤0.01. C. qRT-PCR analysis of mRNA expression levels of *ULK1, RB1CC1, ATG13, ATG101* in HK2 wt and KO-*OFD1* cells assessed in FM or following 2h of STV. qRT-PCR expression analysis is expressed as fold change after normalization on ACTIN as reference gene, as mean ± SEM. FM=full medium; STV=HBSS starvation. Paired Student's *t* test was applied; *p≤0.05; ns=not significative.

To rule out that the enhanced protein expression is due to an upstream increase of mRNA levels, quantitative Real-Time PCR (RT-PCR) was performed in both rich and starved conditions. No significant differences were observed in *RB1CC1*, *ULK1*, *ATG13* and *ATG101* mRNA levels between wt and KO-*OFD1* cells (Fig. 20C), confirming that the increased expression levels in KO-*OFD1* does not occur at the transcriptional level. At this point, I wondered if the loss of the OFD1 protein could affect ULK1 complex proteins degradation.

Thus, I performed cycloheximide (CHX) chase assay at different point of treatment. CHX is widely used for this purpose, as cycloheximide inhibits peptide synthesis (Ennis and Lubin, 1964). CHX treatment caused a progressive decay of the levels

of all proteins of the ULK1 complex in HK2 wt cells, as expected; conversely a slower reduction of protein expression levels was observed in KO-*OFD1* cells (Fig. 21). All together these data suggest that in the absence of OFD1, the complex remain stabilized.

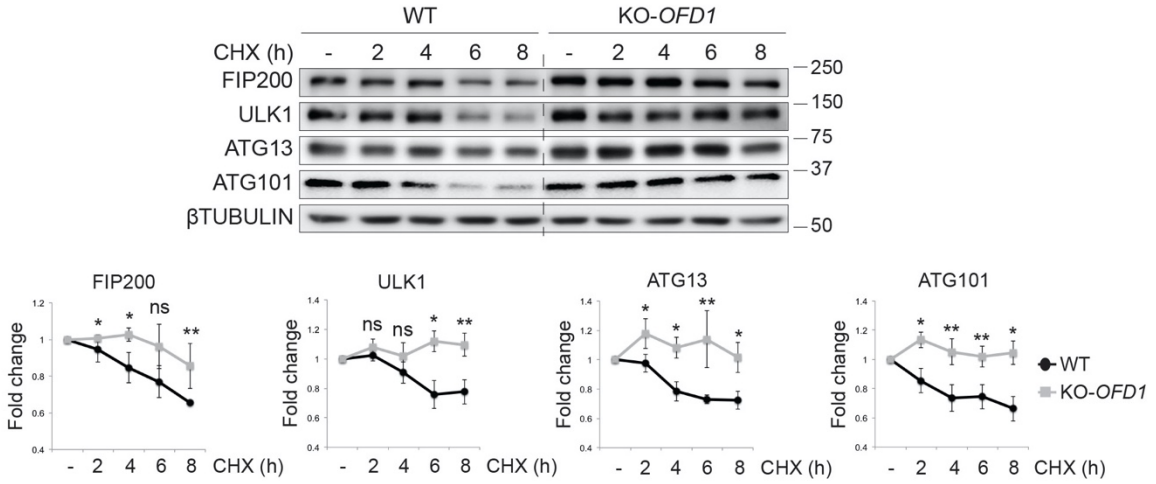

Figure 21. OFD1 contributes to ULK1 complex stabilization in HK2 cells.
HK2 wt and KO-*OFD1* cells were grown in complete medium, incubated with 50*μ*g/ml cycloheximide (CHX) and collected at the indicated time points. Immunoblots were probed with anti-FIP200, -ULK1, -ATG13 and -ATG101 antibodies. ßTUBULIN was used as loading control. n=4 independent experiments. Graphs on the bottom show densitometric analysis of time-dependent degradation of ßTUBULIN normalized protein levels of FIP200, ULK1, ATG13 and ATG101 versus untreated conditions (-) which were defined as 1.0 for each panel. Data are expressed as mean ± SEM. One tailed Student's *t* was applied; *p≤0.05, **p≤0.01. CHX=cycloheximide, ns=not significative.

Moreover, IF analysis and relative quantification of total number of ULK1 and ATG13 puncta exhibited an increase of the spots in HBSS treated KO-*OFD1* cells compared to wt, supporting previous Western-Blot (WB) analysis (Fig. 22).

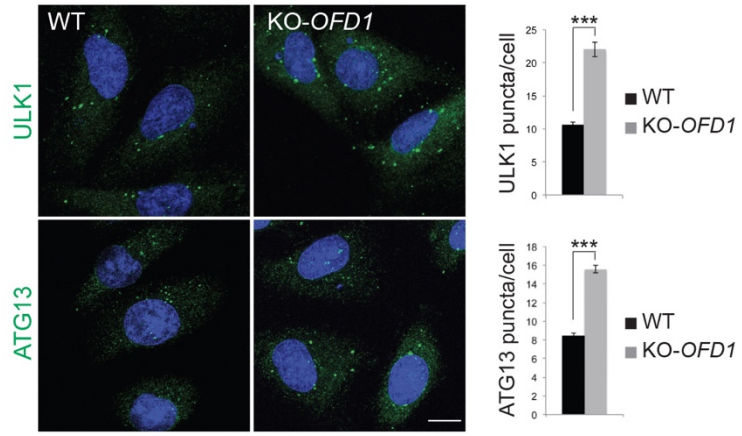

Figure 22. ULK1 and ATG13 puncta increase in KO-*OFD1* cells. Scanning confocal analysis of ULK1 and ATG13 puncta in HK2 wt and KO-*OFD1* cells cultured in HBSS for 90min. Green, ULK1 and ATG13; blue, Hoechst for nuclei. Scale bar=10µm. Graphs display quantization of ULK1 and ATG13 puncta/cell. Data are expressed as mean ± SEM. n=5 independent experiments, *n*≥ 200 cells for each antibody. The likelihood ratio test for Negative Binomial generalized linear models was applied. *** p≤0,001

On the same line, overexpression of 3xFLAG-OFD1 construct in KO-*OFD1* cells was able to reduce protein levels of ULK1 complex components compared to cells transfected with the empty vector alone (Fig. 23), demonstrating that OFD1 regulates the stability of ULK1 complex components by promoting their degradation.

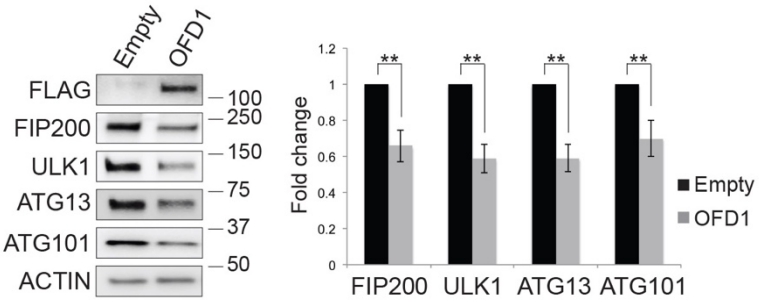

Figure 23. OFD1 overexpression in KO-*OFD1* cells reduces ULK1 complex protein levels. Western blot analysis of ULK1 complex components in KO-*OFD1* cells transiently transfected with the empty vector (Empty) or the 3xFLAG-OFD1 construct (OFD1) for 48h. Histograms show quantification of relative band intensities for FIP200, ULK1, ATG13, ATG101 normalized versus ACTIN. Data are expressed as mean ± SEM. n=5 independent experiments. One tailed Student's *t*-test was applied. **p≤0.01

The principal signal routes to protein degradation in mammalian cells are represented by the ubiquitin-proteasome degradative system and the

autophagosome-lysosome pathway. To understand how OFD1 could act on the control of degradation of the ULK1 complex, it was necessary to investigate about the involvement of OFD1 in these networks and discriminate which of the two systems is required for ULK1 complex degradation. A colleague in the lab spent some time and a considerable effort to clarify these aspects through different experimental strategies; indeed, he used several chemical approaches (SAR405, Baf-A1, and proteasome inhibitors MG132 and bortezomib) and genetic models (KO-*ATG9,* Saos-2 cells depleted for ATG9, a key regulator of the autophagic cascade) to confirm that ULK1 is mainly degraded by the proteasome as previously shown (C. C. Liu *et al.*, 2016; Nazio *et al.*, 2016); conversely, he demonstrated that ATG13 is not influenced by the proteasomal route but is targeted by autophagy-mediated degradation (Fig. 44 in Appendix).

Indeed, modulation of autophagy using compounds well known and commonly used to repress autophagy, namely SAR405, an ATP-competitive Vps34 inhibitor and Bafilomycin A1 (Baf-A1), an autophagosome-lysosome fusion inhibitor, were able to restore ATG13 protein level in overexpressing 3xFLAG-OFD1 HK2 cells (Fig. 24A-B). I also performed IF experiments that confirmed these findings. Indeed, HK2 cells transfected with the 3xFLAG-OFD1 construct and treated with HBSS to induce puncta assembling, display ATG13 spots which are consistently decreased compared to the control in all experiments, as previously shown by WB analysis (Fig. 24C). Conversely, in overexpressing HK2 cells treated with Baf-A1, and therefore when autophagy is blocked, no significant variation in the number of ATG13 puncta is found comparing Baf-A1-treated 3xFLAG-OFD1 overexpressing cells and controls, thus proving that OFD1 promotes ATG13 degradation through autophagy (Fig. 24C).

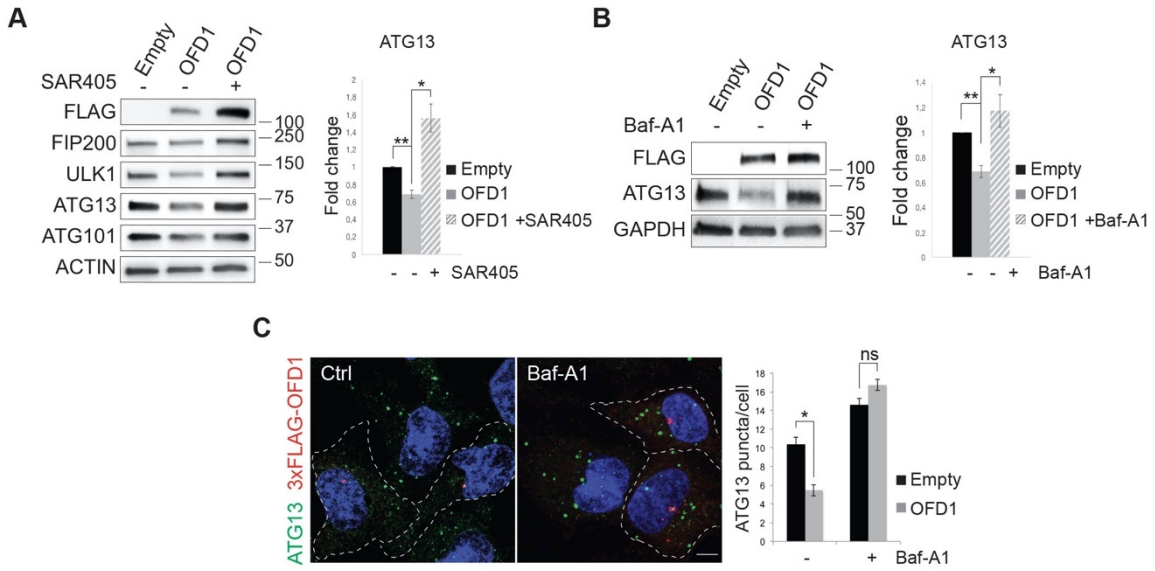

Figure 24. Autophagy inhibition in HK2 cells overexpressing OFD1 rescues ATG13 protein level.

A. Western blot of ULK1 complex components in KO-*OFD1* cells transfected with 3xFLAG-OFD1 (OFD1) or empty vector (Empty) and treated (+) or not (-) with SAR405 (10μM, 6h). ACTIN was used as loading control. ATG13 levels are expressed as fold increase compared with the empty vector (mean ± SEM); n=3 independent experiments. One tailed Student's *t*-test was applied; *p≤0.05, **p≤0.01. B. WB analysis of ATG13 in KO-*OFD1* cells transfected with 3xFLAG-OFD1 (OFD1) or empty vector (Empty) and treated (+) or not (-) with Baf-A1 (100nM, 2h). GAPDH was used as loading control. Protein levels values are expressed as fold increase (mean ± SEM) compared with the empty vector; n=3 independent experiments. One tailed Student's *t* was applied; *p≤0.05, **p≤0.01. C. Representative confocal images of co-staining of 3xFLAG-OFD1 with ATG13 in KO-*OFD1* cells incubated in starvation medium (HBSS), treated (+) or not (-) with Baf-A1(100nM, 90min). ATG13 puncta/cell are quantified on the right. Green, ATG13; red, 3x-FLAG-OFD1; blue, Hoechst to label nuclei. Scale bar=10μm. n=3 independent experiments, *n*≥ 100 cells. Data are expressed as mean ± SEM., the likelihood ratio test for Negative Binomial generalized linear models was applied. *p≤0.05. Baf-A1=bafilomycin, ns=not significative.

3. OFD1 interacts and colocalizes with LC3/GABARAP by a canonical LIR domain

Tang et al. illustrated in their study two basic finding linking OFD1 to autophagy: a), OFD1 is an autophagy substrate, and b), the OFD1 protein binds the mammalian homologs of yeast Atg8 (LC3/GABARAP proteins) in HEK293 cells (Tang *et al.*, 2013; Holdgaard *et al.*, 2019). These insights, together with all data described so far, suggested us that OFD1 might operate as an autophagy receptor for ATG13.

To validate this hypothesis, I performed Glutathione S-transferase (GST) pulldown assay and IF experiments to confirm OFD1/LC3B interaction in renal cells. In

HEK293 cells, the 3xFLAG-OFD1 protein was pulled-down by purified LC3B and GABARAP-L1 proteins linked to the Glutathione Sepharose 4B resin (Fig. 25A). In addition, GST-tagged LC3B purified proteins bearing specific mutations in the LC3B LIR domain were used to further prove the accuracy of the interaction. Indeed, my results illustrated in Fig 25 demonstrated that 3xFLAG-OFD1 is not able to bind GST-LC3B mutants lacking the N-terminal region (dN LC3 dG) and specifically mutated in the LC3B LIR binding pocket (LC3B F52A-V53A dG) (Fig. 25A). These mutations are known to affect the capability of LC3B to bind autophagic proteins (Grumati *et al.*, 2017).

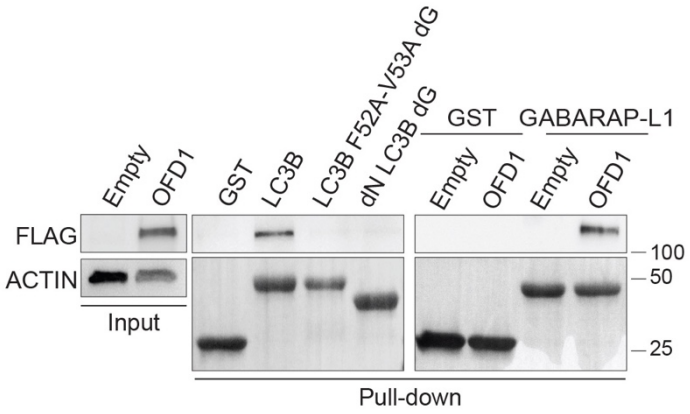

Figure 25. OFD1 interacts with LC3B and GABARAP-L1.
Cell lysates from empty vector (Empty) or 3xFLAG-OFD1 (OFD1) overexpressing HEK293 were added to beads with immobilized GST only, GST-LC3B, LC3B F52A-V53A and dN LC3 dG mutants, and with GST-GABARAP-L1 followed by WB. All panels display WB for FLAG, ACTIN was used as loading control.

As described before, one of the main features of autophagy receptors is represented by the presence in their protein sequences of a peculiar and determined region of interaction named LIR domain. A dedicated tool to search for LIR consensus sequences has been developed and made available to the scientific community thus potential LIR domains can be easily identified. Being just potential however, designated LIR motifs must be validated. Analysis of the OFD1 protein sequence (Refseq NP_003602) by using the iLIR Autophagy tool (https://ilir.warwick.ac.uk/) (Kalvari *et al.*, 2014), revealed the presence of six putative LIR domains widespread

along the OFD1 protein sequence (Fig. 26). Some of these putative LIRs fall within CC domains and are close to known OFDI patients' mutations.

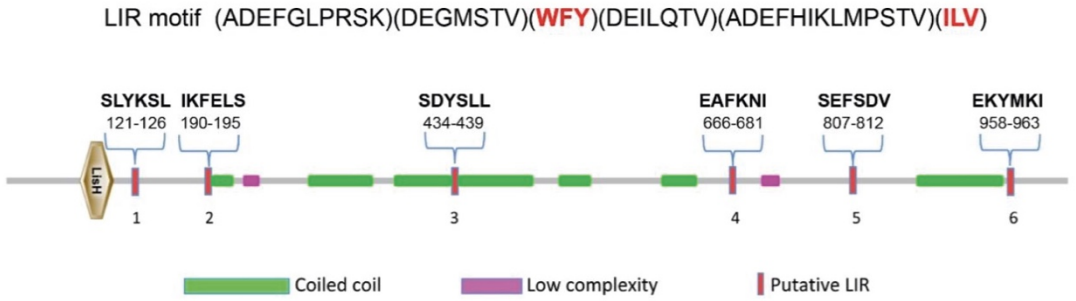

Figure 26. **Analysis of OFD1 protein reveals six putative LIR motifs.**
Schematic representation of domains architecture of OFD1 and putative LIRs. Green, coiled-coil (CC) domain; diamond, LisH domain; violet rectangle, low complexity region; red rectangle, LC3-interacting region (LIR). The amino acid sequence of the functional LIR motif is boxed.

To validate the real biological meaning of these potential LIRs, I performed alanine scanning mutagenesis on 3xFLAG-OFD1 constructs for all six putative LIR motifs and then tested them for binding with LC3B/GABARAP. Indeed, alanine scanning is a site-direct mutagenesis (SDM) which allows to create precise targeted alterations in double strand DNA plasmid to discriminate the contribution of a specific residue to the integrity and/or functionality of a protein of interest. The choice of alanine is due to its chemical features which allows to discriminate residue value without affecting protein conformational status (Lefèvre, Rémy and Masson, 1997). As stated above, in most cases LIR domains are characterized by a specific consensus region, represented by the following extended sequence (ADEFGLPRSK) (DEGMSTV) (**WFY**) (DEILQTV) (ADEFHIKLMPSTV) (**ILV**). Therefore, my approach consisted in the substitution into alanine of the two hydrophobic amino acids in positions 3 and 6 (in bold) within all OFD1 putative LIR domains (Fig.26). Previous reports demonstrated that these specific mutations are sufficient to ablate the interaction with Atg8 family proteins (Birgisdottir, Lamark and

Johansen, 2013). After the mutagenesis all constructs were sequence verified and then subjected to GST pull-down assays.

GST pulldown assay was performed in HEK293 cells overexpressing 3xFLAG-OFD1 constructs mutated in the amino acids core for each of the six putative LIR motif as described above (Fig. 27A, B). Analysis revealed that only one of the six putative LIRs is functional (EK**Y**MK**I** to EK**A**MK**A**, hereinafter OFD1ΔLIR). Indeed, 3xFLAG-OFD1 mutated in this LIR domain almost completely lost the ability to bind both GST-LC3B and GST-GABARAP-L1, confirming the effective biological function of the validated OFD1 LIR motif and its affinity for both LC3B and GABARAP-L1 (Fig. 27B). OFD1 LIR motif is located in the C-terminal region of the protein and further bioinformatics analysis and alignment of homologous proteins in *Homo sapiens*, *Mus musculus*, *Bos taurus, Gallus gallus, Takifugu rubripes*, displayed high conservation of this sequence across species (Fig. 27C).

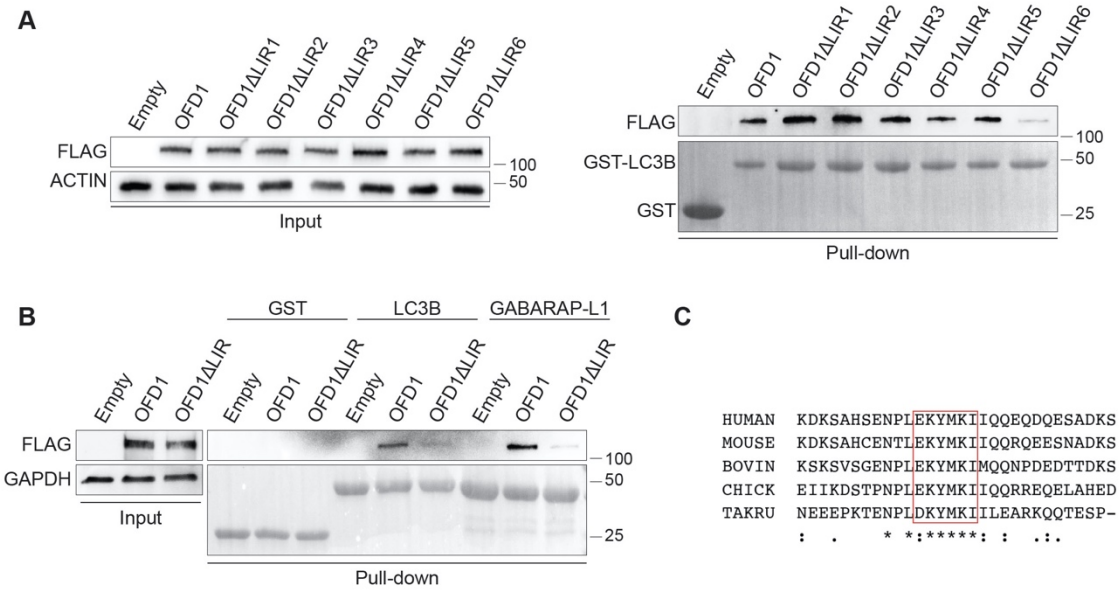

Figure 27. OFD1 binds LC3B/GABARAP-L1 through a canonical and evolutionarily conserved LIR motif.

A, B. The OFD1 protein displaying a mutated LIR motif among the six putative LIRs (OFD1ΔLIR6) almost completely lost the interaction with GST-LC3B and GST-GABARAP-L1 when over-expressed in HEK293 cells. All panels display WB for FLAG, GAPDH was used as loading control. C. Schematic representation of alignment of the LIR motif among species. The amino acid sequence of LIR motif is boxed; residues with full (*), strong (:) and weak (.) conservation are indicated.

In line with these data, IF analysis revealed that endogenous LC3B and GABARAP colocalize respectively with endogenous OFD1 and 3xFLAG-OFD1 in HK2 cells (Fig. 28A-B) and that, conversely, the 3xFLAG-OFD1ΔLIR construct lost the colocalization with both of them (Fig. 28C-D).

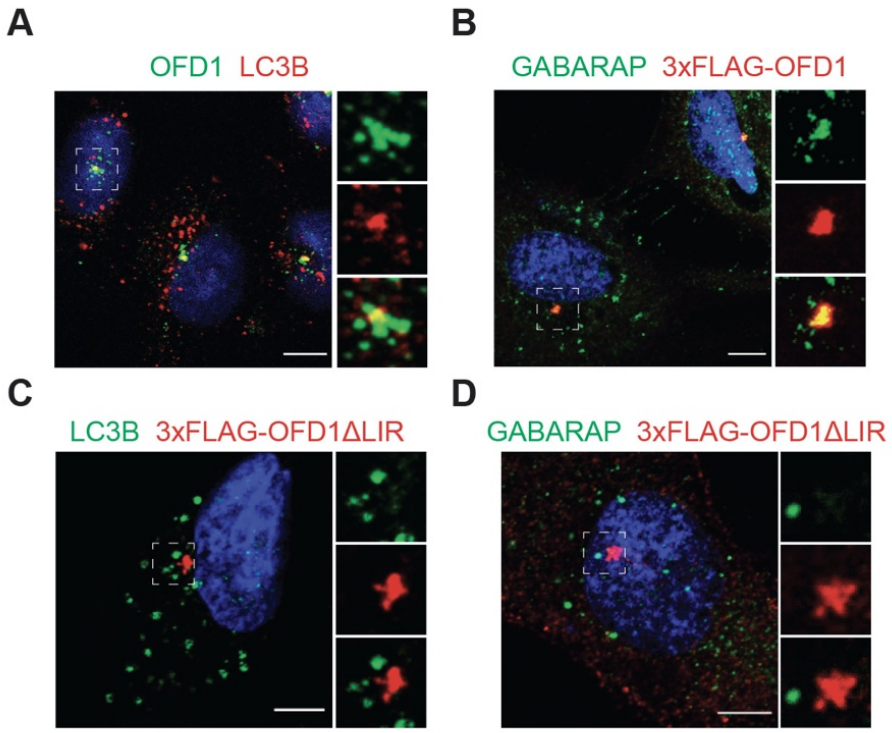

Figure 28. 3xFLAG-OFD1ΔLIR not colocalize with LC3B and GABARAP in HK2 cells.
A, B. Representative confocal images of endogenous OFD1 (green) co-staining with LC3B (red), and of 3xFLAG-OFD1 (red) with GABARAP (green) in HK2 cells (top). Scale bar=10µm. C,D. Representative confocal images of OFD1ΔLIR co-staining with LC3B (left) and GABARAP (right), displaying the lost co-localization of OFD1 with LC3B and GABARAP in HK2 cells (bottom); cells were starved with HBSS for 90 min. Green, LC3B and GABARAP; red, 3XFLAG OFD1ΔLIR; blue, Hoechst to label nuclei. Scale bar=3.5µm. n≥50 cells analyzed/sample. Insets show magnifications and single-color channels of selected (dotted) areas.

The specificity of the antibody recognizing GABARAP, which was not validated for IF, has been demonstrated in a Hela triple knock-out (TKO) cell line genetically engineered for inactivation of all members of the GABARAP subfamily which includes γ-amino-butyric acid receptor-associated protein (GABARAP), Glandular epithelial cell protein/GABARAP-like 1 (GEC1/GABARAPL1) and Golgi-associated

ATPase enhancer of 16 kDa/GABARAP-like 2 (GATE-16/GABARAPL2). The signal of the antibody against GABARAP is clearly identified in Hela wt cells, while is totally absent in Hela TKO cells (Fig. 29).

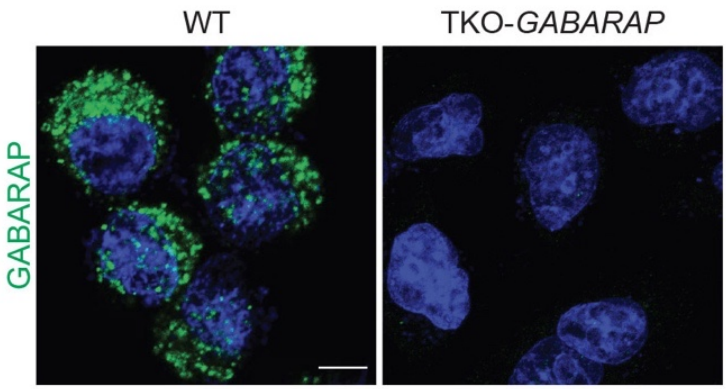

Figure 29. GABARAP antibody specificity.
Representative confocal images of GABARAP puncta in wt and GABARAP family-deficient (GABARAP, GABARAP-L1 and GABARAP-L2 triple knockout) HeLa cells starved for 90min. Green, GABARAP; blue, Hoechst labels nuclei. Scale bar=10µm.

4. OFD1 is a novel selective autophagy receptor for ATG13

4.1. OFD1 promotes ATG13 degradation through its functional LIR motif

At this point to confirm that OFD1 works as a selective autophagy receptor for ATG13, I carried out experiments to prove that in the absence of the identified LIR domain, the OFD1 protein is unable to bind LC3B/GABARAP-L1 and, then, to foster autophagic degradation of ATG13.

In HK2 cells, 3xFLAG-OFD1 overexpression reduces ATG13 protein levels and ATG13 puncta, as shown before. Conversely, transfection with 3xFLAG-OFD1ΔLIR fails to induce degradation of ATG13. Indeed, WB analysis demonstrates rescue of ATG13 protein levels in HK2 cells overexpressing OFD1ΔLIR (Fig. 30A). In the same way, quantification of ATG13 puncta in IF experiments on HK2 overexpressing OFD1ΔLIR clearly indicates an increased number of puncta as opposed to 3xFLAG-OFD1 and comparable to the empty vector (Fig. 30B). These

data demonstrate that OFD1-mediated ATG13 degradation is dependent on OFD1-LC3B/GABARAP-L1 binding through a functional LIR motif.

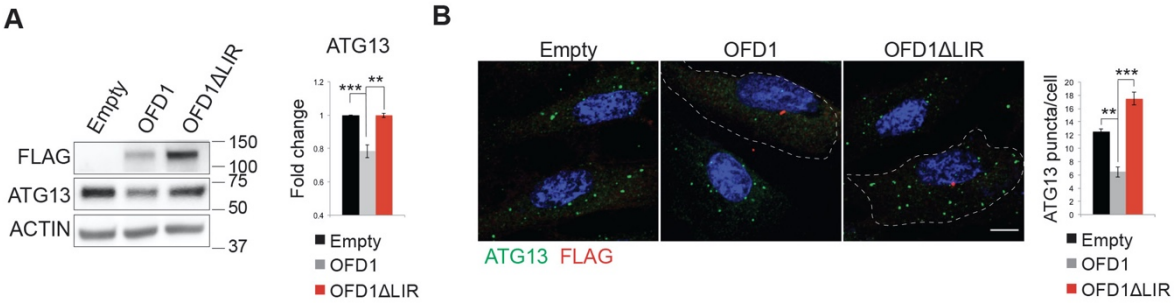

Figure 30. OFD1ΔLIR overexpression rescues ATG13 protein level and puncta.
Western blot of ATG13 in KO-*OFD1* cells transfected with 3xFLAG-OFD1 (OFD1) or 3xFLAG-OFD1ΔLIR (OFD1ΔLIR) or empty vector (Empty). ACTIN was used as loading control. ATG13 protein levels are expressed as fold increase compared with empty vector (mean ± SEM); n=3 independent experiments. One tailed Student's *t* was applied; **p≤0.01, ***p≤0.001. Representative confocal images of 3xFLAG-OFD1 (OFD1) and 3xFLAG-OFD1ΔLIR (OFD1ΔLIR) co-staining with ATG13 in KO-*OFD1* cells incubated in starvation medium (HBSS) for 90min. ATG13 puncta/cell are quantified on the right. Green, ATG13; red, 3xFLAG-OFD1 and 3xFLAG-OFD1ΔLIR; blue, Hoechst to label nuclei. Scale bar=10µm. Data are expressed as mean ± SEM. n=4 independent experiments, n≥100 cells. The likelihood ratio test for Negative Binomial generalized linear models was applied. **p≤0.01 and ***p≤0.001

Furthermore, to better define the role of OFD1 as a novel selective autophagy receptor for ATG13, I decided to better dissect the OFD1-ATG13 interaction.

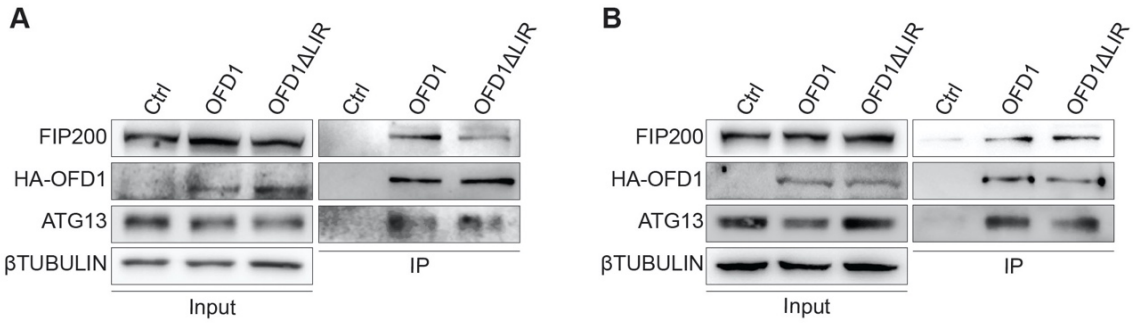

Figure 31. ATG13 binding with OFD1 is LIR-independent both in HK2 and in HEK293 cells.
Lysates from lentiviral delivered OFD1 wt or ΔLIR HK2 (A) or HEK293 cells (B) cultured in HBSS for 90min were immunoprecipitated with anti-HA-tagged resin and analyzed by WB; ßTUBULIN was used as loading control. IP=immunoprecipitation

First, I set up the condition ensure that the interaction between OFD1 and ATG13 is not facilitated by LC3B/GABARAP binding with OFD1 and, therefore, not strictly dependent on the presence of a functional LIR domain. To this purpose, I used a stable HK2 cell line expressing HA-tagged OFD1 wild-type and OFD1ΔLIR cloned in a doxycycline-inducible lentiviral vector as described before. I then used immobilized anti-HA affinity resin to immunoprecipitated HA-tagged OFD1 wt and ΔLIR and blotted for ATG13 and FIP200 antibodies to check for binding. As clearly shown in Fig. 31, the interaction with ATG13 and FIP200 was demonstrated in both clones, confirming that in the absence of the LIR domain, OFD1 is still able to bind ATG13/FIP200 and that this interaction is independent on LC3B/GABARAP binding. The same results were also obtained in a cell type different from HK2 (Fig. 31A). HEK293 cells were used to produce inducible HA-tagged cell lines expressing OFD1 wt or OFD1ΔLIR. As observed and earlier described for HK2 cells, also in HEK293 cells, ATG13 and FIP200 immunoprecipitated both with HA-OFD1 wt and OFD1ΔLIR, thus supporting the results observed in HK2 cells (Fig. 31B).

In addition, different fragments of the OFD1 protein were cloned in 3xFLAG-tagged constructs with the aim of identifying the portion of the protein responsible for ATG13 binding. The OFD1 protein was divided in three fragments which have already been described (Giorgio *et al.*, 2007) covering the entire aminoacidic sequence and correspond to the N-terminal (fragment A), central (fragment B) and C-terminal regions (fragment C) of the OFD1 protein (Fig. 32). In particular, fragment A (from aa 1 to 276) contains the LisH motif and the first of the six coiled-coil domains which contribute to OFD1 centriolar satellites localization (Romio *et al.*, 2004); fragment B (aa 277 to 663) holds CC from 2nd to 5th and is responsible for OFD1 oligomerization (Giorgio *et al.*, 2007); fragment C (aa 664 to 1012) carries only the last CC domain and the OFD1 LIR motif I described and characterized.

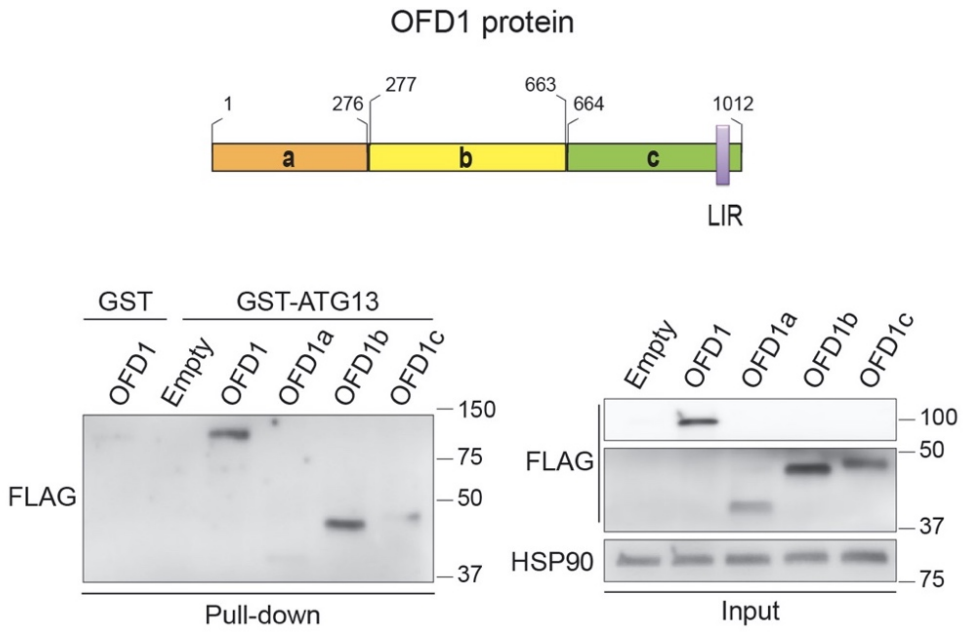

Figure 32. Recombinant GST-tagged ATG13 selectively binds OFD1 central region.
Top. Schematic representation of OFD1 protein sequence and indicated portion cloned (a, b, c) with relative range of amino acids. Left. Lysates from empty vector (Empty), 3xFLAG-OFD1(OFD1), 3xFLAG-OFD1a (OFD1a), 3xFLAG-OFD1b (OFD1b), 3xFLAG-OFD1c (OFD1c) overexpressing HEK293 cells were added to GST-ATG13; lysates from 3xFLAG-OFD1(OFD1) overexpressing HEK293 cells were added to GST as control. Right. WB of total lysates (input). All panels display WB for FLAG, HSP90 was used as loading control.

HEK293 cells were transfected to overexpress the 3xFLAG-OFD1 constructs and the A, B and C 3XFLAG-tagged fragments of the OFD1 protein. Cells lysates were then used to perform GST pull-down assay. Therefore, pull-down of GST-tagged ATG13 recombinant protein validates the interaction with 3xFLAG-OFD1 (Fig. 32), supporting previous co-IP experiments of OFD1 and ATG13 endogenous proteins. Moreover, the OFD1-B fragment was specifically pulled-down by GST-ATG13, suggesting that this portion of the protein, rich in coiled-coil domains and suitable for protein-protein interactions, is inclined to bind ATG13. Moreover, these data suggest that the LIR domain, localized in the fragment C, is not involved in the binding to ATG13 thus supporting previous co-IP experiments.

4.2. OFD1 and ATG13 are found in autophago-lysosome structures

As further evidence of the involvement of OFD1 as a selective receptor in autophagic degradation of ATG13, I performed immunofluorescence analysis evaluating the occurrence of autophagosome structures positive for both OFD1 and ATG13. To do that, a stably transfected HK2 cell line expressing GFP-LC3B which was obtained by single clone isolation through sorting of GFP positive cells was generated. The chosen clone has been selected for a mild expression of GFP-LC3B puncta after starvation, comparable to HK2 wild-type cells. In these cells, staining for endogenous OFD1 and ATG13 after treatment with HBSS to induce puncta formation, exhibits multiple structures simultaneously positive to GFP-LC3B, OFD1 and ATG13, thus supporting our hypothesis (Fig. 33A).

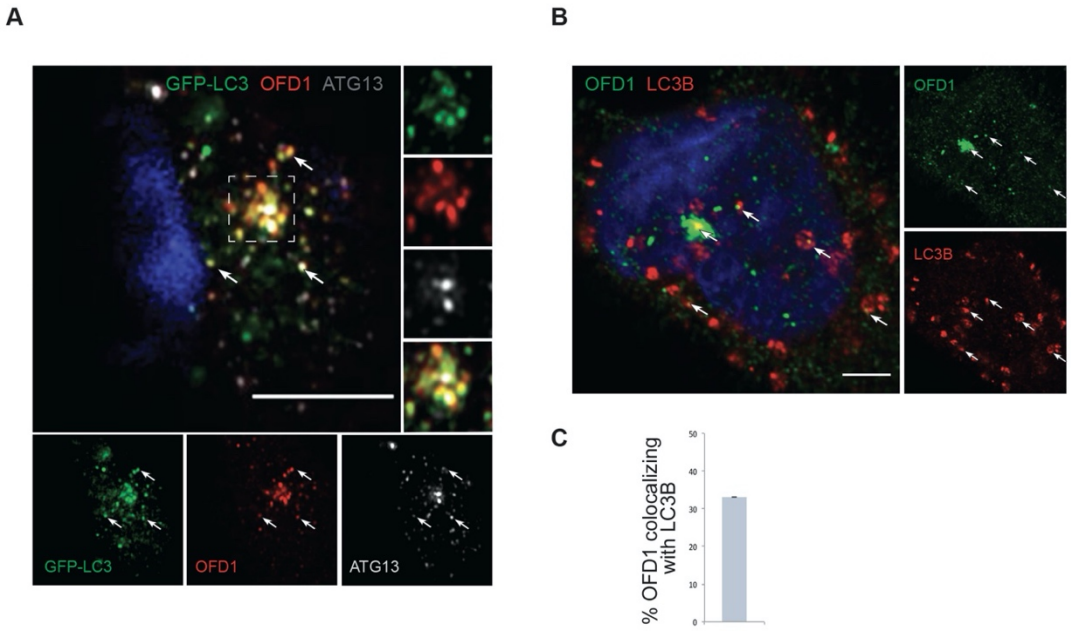

Figure 33. OFD1 and ATG13 colocalization occurs as multiple spots on autophagosome structures.

A. Airyscan confocal analysis of OFD1 (red) and ATG13 (grey) co-localization with GFP-LC3 (green) in HK2 cells (white arrows). Scale bars = 3.5 µm. The insets show higher magnification and single colour channels of the boxed area. B. Airyscan confocal analysis of endogenous OFD1 and LC3B colocalization (white arrows) in HK2 cells cultured in HBSS (90min). Green, OFD1; red, LC3B; blue, Hoechst for nuclei. Scale bar=5µm. C. Histograms show quantification of OFD1-LC3B colocalization, expressed as % of total OFD1 fluorescence colocalizing with LC3B (mean ± SEM). *n*= 3 independent experiments; *n*=40 cells analyzed.

Moreover, airyscan super-resolution microscopy analysis of OFD1-LC3B colocalization contributes to better define the occurrence of several OFD1 spots on autophagosomes structures (Fig. 33B). The quantification of colocalization expressed as % of total OFD1 fluorescent signal overlapping with LC3B, shown in Fig. 33C, established that almost 30% of the OFD1 protein colocalizes with LC3B.

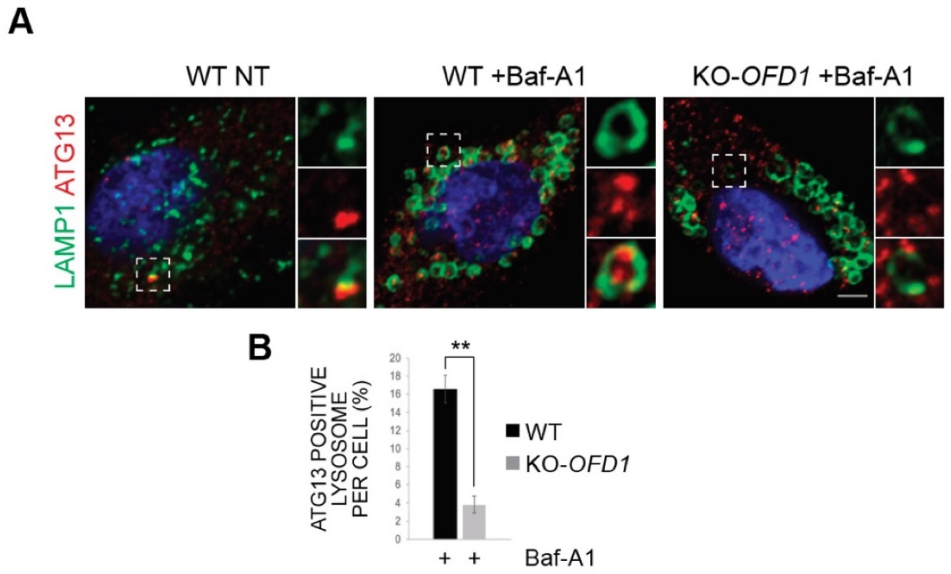

Figure 34. ATG13 fails to be found in lysosomal lumen in KO-*OFD1* cells.
A. Scanning confocal microscopy analysis of HK2 wt and KO-*OFD1* cells incubated in HBSS (8h), treated (+) or not (-) with Baf-A1(50nM, 8h). Green, LAMP1; red, ATG13; blue, Hoechst for nuclei. Scale bar=5µm. Insets show higher magnification and single colour channels of the boxed area. B. Bar graphs show quantification of lysosomes containing ATG13 expressed as % of total amount of LAMP1 per cell (mean ± SEM). n=38 WT cells, n=32 KO-*OFD1* cells counted; n=3 independent experiments. One tailed Student's *t* was applied; ***p≤0.001. NT=not treated, Baf-A1=bafilomycin

To complete the analysis, I looked for ATG13-positive spots colocalizing with LAMP1, which is a well-known marker of autolysosomal membranes. In HK2 wt starved cells, ATG13 groups into discrete puncta which are found on LAMP1-positive structures (Fig. 34A); after treatment with Baf-A1, extended to 8 hours to ensure complete inhibition of autolysosome acidification and autophagosome-lysosome fusion, ATG13 spots agglomerate into the lumen of swollen lysosomes,

confirming that the block of autophagy leads to a lack of ATG13 degradation (Fig. 34A).

Conversely, in KO-*OFD1* cells ATG13 puncta fail to accumulate into the lumen of lysosomes, whereas they are mainly gathered on lysosomal membranes, suggesting failure of appropriate control in ATG13 degradation by autophagy, which we believe is due to the absence of the OFD1 protein (Fig. 34A). Quantification of the phenomenon expressed as % of LAMP1-positive vesicles containing ATG13 scaled to the total content of lysosomes, confirmed the observations made by immunofluorescence (Fig. 34B).

4.3. OFD1 is degraded through autophagy

Selective autophagy receptors are known to be degraded together with their cargoes, we thus tested if OFD1 is degraded through autophagy. To this purpose, I performed time course experiments of starvation and Baf-A1 treatment to evaluate and identify any shift in the level of endogenous OFD1 protein. Western blot analysis revealed a progressive decrease in OFD1 protein levels that were rescued by autophagy inhibition due to Baf-A1 treatment (Fig. 35A). These results are in line with the hypothesis of OFD1 as selective autophagy receptor.

Moreover, in starved HK2 cells OFD1 shows colocalization with LAMP1 in multiple spots at the centrosome and widespread in the cell, while in cells treated with Baf-A1 OFD1 is found in the lumen of lysosomal vesicles like previously shown for ATG13 (Fig. 35B-C), suggesting the involvement of the autophagosomal-lysosomal system for OFD1 degradation.

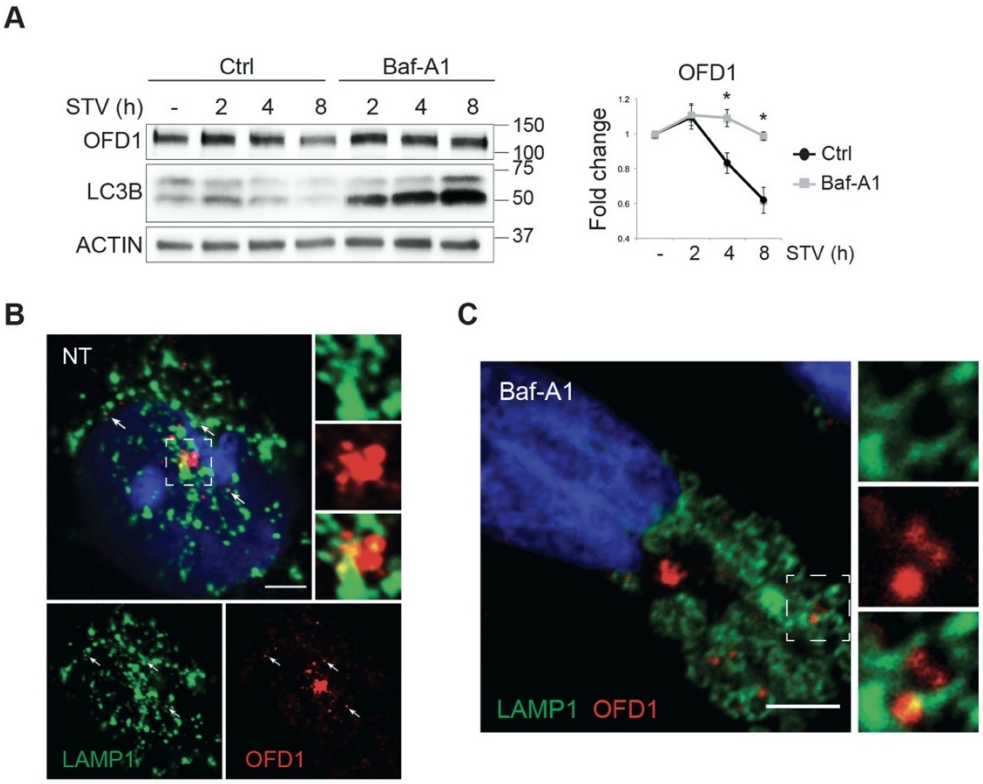

Figure 35. OFD1 is degraded through autophagy and is found in lysosomes.
A. HBSS starvation (STV) time course in wt HK2 cells displaying levels of the OFD1 protein detected by WB, Baf-A1 was added (100nM) and cells collected at the indicated time points. LC3B was used as control for Baf-A1 treatment, ACTIN was used as loading control. Graphs represent the densitometric analysis of time-dependent degradation of ACTIN-normalized OFD1 levels versus full medium condition (-), which was defined as 1.0. n=4 independent experiments. One tailed Student's *t* was applied; ***p≤0.001. B, C. Scanning confocal analysis of endogenous OFD1/LAMP1 colocalization in wt HK2 cells incubated in HBSS (8h), treated (C) or not (B) with Baf-A1(50nM, 8h), immunolabelled for OFD1 (red) and LAMP1 (green). Nuclei were stained with Hoechst. Scale bars =5µm. White arrows indicate the OFD1/LAMP1 colocalization in untreated cells. NT=not treated, Baf-A1=bafilomycin

Further experiments indicate that autophagy-mediated degradation of OFD1 is LIR dependent. Indeed, in HK2 cells transfected with 3xFLAG-OFD1 and OFD1ΔLIR constructs, western blot analysis detecting FLAG expression shows accumulation of OFD1 wt after treatment with Baf-A1 supporting previous data, while OFD1ΔLIR appears insensible to Baf-A1 treatment and does not accumulate (Fig. 36). Data shown up to this point support the role of OFD1 as a novel autophagy receptor which selectively recognizes ATG13 for degradation.

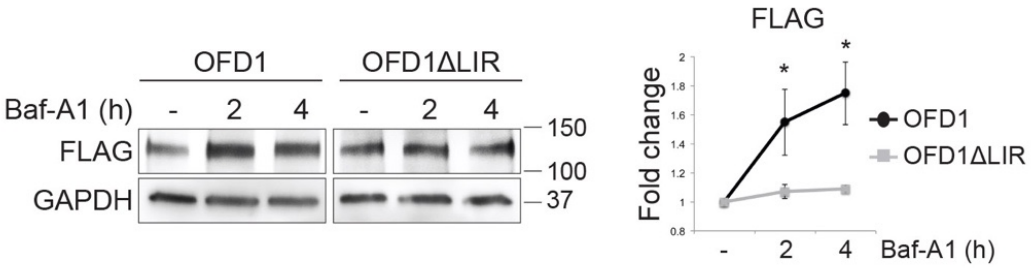

Figure 36. OFD1ΔLIR does not accumulate after Baf-A1 treatment.
Western blot analysis of FLAG levels in KO-*OFD1* cells transfected with 3xFLAG-OFD1 (OFD1) or 3xFLAG-OFD1ΔLIR (OFD1ΔLIR) and treated or not (-) with Baf-A1 (100nM). Cells were then collected at the indicated time points. Quantification of the relative band intensities of GAPDH-normalized FLAG levels versus untreated conditions (-) which was defined as 1.0 is shown on the right. n=3 independent experiments. Data are expressed as the mean ± SEM. One tailed Student's *t* test was applied. *p≤0.05. Baf-A1=bafilomycin

5. OFD1 is required for autophagy constrain

Given the crucial role of the ULK1 complex in starvation-induced autophagy, the next step was to clarify whether OFD1 plays a functional role in autophagy regulation. ULK1 kinase activity is essential for autophagy initiation; indeed, ULK1 regulates autophagy by phosphorylating itself, its binding partners and several downstream components of the autophagic machinery, such as ATG13 and VPS34 (Zachari and Ganley, 2017). To evaluate ULK1 kinase activity, the rate of phosphorylation of ULK1 direct target, ATG13 in Serine 318 and VPS34 in Serine 294 was analyzed. HK2 wt and KO-*OFD1* cells were transfected with GFP-ATG13 and FLAG-VPS34 constructs due to the low antibodies recognizing phosphorylated forms of the endogenous proteins, and then analyzed by WB. KO-*OFD1* cells showed increased phosphorylation levels of both proteins suggesting that the loss of OFD1 is associated with enhancement of ULK1 complex activity (Fig. 37A).

To better define the role of OFD1 on autophagy, I evaluated the formation of WIPI2 and LC3B-positive puncta in HBSS-starved HK2 cells, comparing wt to KO-*OFD1* cells. Indeed, WIPI2 and LC3B have been shown to be useful markers of early autophagosomes and phagophores formation and maturation, respectively, and it

has been also demonstrated that the number of autophagosomes correlate with the rate of autophagic activity running (Yoshii and Mizushima, 2017). Interestingly, I found a consistent increase of WIPI2/LC3B-positive puncta in KO-*OFD1* cells compared to controls, suggesting an enhancement of autophagosome biogenesis in *OFD1* depleted cells (Fig. 37B).

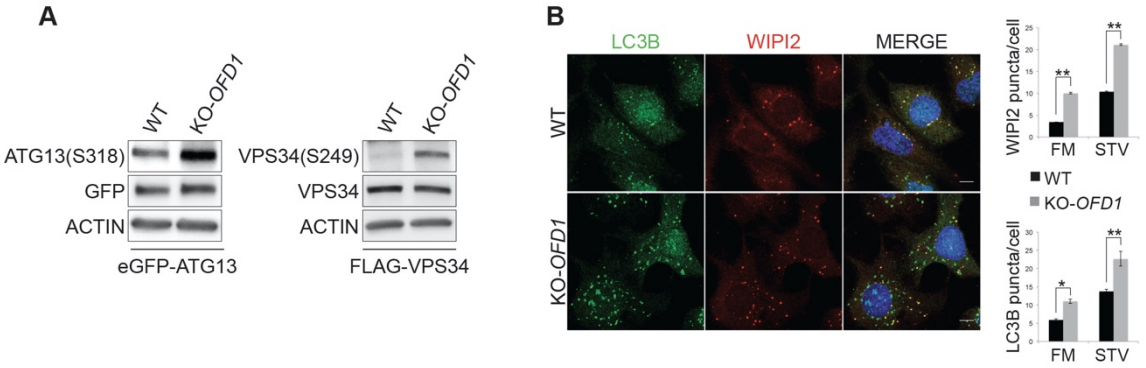

Figure 37. Loss of OFD1 enhanced ULK1 activity and increased autophagosome biogenesis. A. Representative blots of ATG13 (left) and VPS34 (right) phosphorylation levels in wt and KO-*OFD1* HK2 cells transiently expressing GFP-ATG13 and FLAG-VPS34, respectively, in FM. B. Representative confocal images of LC3B and WIPI2 puncta in wt and KO-*OFD1* cells after 90min of starvation with HBSS. Green, LC3B; red, WIPI2; blue, Hoechst to label nuclei. Scale bar=10µm. Histograms on the right show quantification of number of LC3B and WIPI2 puncta both in full medium (FM) and in starved condition (STV). Data are expressed as the mean ± SEM. n=5 independent experiments. ≥100 cells analyzed per sample. The likelihood ratio test for Negative Binomial generalized linear models was applied; *p≤0.05 and **p≤0.01. FM=full medium, STV=starvation, Baf-A1=bafilomycin

One of the most common and easy methods used to measure autophagy is through LC3B immunoblotting, rating LC3B-I to LC3B-II conversion (Mizushima and Yoshimori, 2007). Indeed, LC3B represents a good indicator of autophagosomes formation as LC3B-II correlates with the number of autophagosome structures. Since LC3B is degraded itself within autophago-lysosome, the right way to measure the amount of LC3B-II is by comparing the level of LC3B with and without treatment with lysosomal inhibitors. Therefore, I analyzed LC3B content by WB in HK2 cells (KO-*OFD1* and controls) after induction of autophagy, starving the cells for a short period, and blocking autophagy-mediated degradation using Baf-A1 treatment. KO-

OFD1 cells showed increased level of LC3B-II after treatment with Baf-A1, suggesting that the autophagy flux is enhanced compared with wt cells (Fig. 38A). The same results were obtained also in *Ofd1*-depleted mIMCD3 (mouse Inner Medullary Collecting Duct 3) cells, which are renal cells commonly used for primary cilia studies. Indeed, mIMCD3 cells silenced for the *Ofd1* gene, showed the same significant rise in autophagy observed in KO-*OFD1*, supporting the observation that the observed enhancement of autophagy is indeed a consequence of OFD1 loss (Fig. 38B).

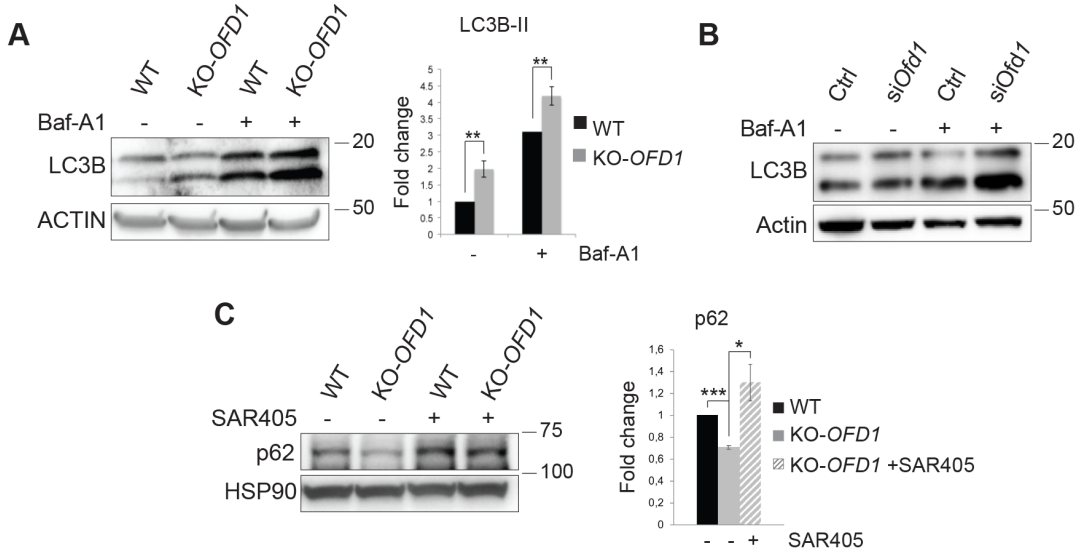

Figure 38. KO-*OFD1* cells show increased LC3-II protein levels and p62 degradation.
A. Wild-type and KO-*OFD1* HK2 cells were starved in HBSS with/without Baf-A1 (100nM, 2h) and total lysates were analyzed by immunoblotting using anti-OFD1, -LC3B (LC3B-I 18 kDa and LC3B-II 16 kDa) and -ACTIN antibodies. ACTIN-normalized LC3B-II levels are expressed as fold change versus untreated conditions (-) of wt cells. Data are expressed as the mean ± SEM. n=3 independent experiments. One tailed Student's *t* test was applied; **p≤0.01. B. WB analysis of LC3B protein levels in mIMCD3 transfected with siRNA against *OFD1.* 96h after transfection cells were starved with HBSS for 2h in presence of Baf-A1 (100nM). C. Western blot analysis of p62 in wt and KO-*OFD1* cells assessed following 2h of starvation and treated (+) or not treated (-) with SAR405 (10µM, 4h). The blot is representative of n=5 independent experiments. On the right, protein level values, normalized versus HSP90 (loading control), are expressed as fold increase compared with untreated wt cells (mean ± SEM). One tailed Student's *t* test was applied; *p≤0.05 and ***p≤0.001. Baf-A1=bafilomycin.

A well-known and widely used marker useful to monitor autophagy-mediated degradation is represented by p62/SQTM1. Autophagy induction leads to decreased levels of p62; conversely, p62 accumulates when autophagy is inhibited (Bjørkøy *et al.*, 2009). Decreased levels of p62 were observed in KO-*OFD1* starved cells due to the enhanced autophagic degradation, and, to further confirm our data, SAR405 treatment restored p62 levels (Fig. 38C).

As mentioned before, the main result of activation of autophagy consists in the formation of autophagosomes which undergo a necessary maturation process ending in the fusion with lysosomes. Then, lysosomes contribute to acidify the environment of fused autophagosomes providing the digestive enzymes to complete the removal of waste materials. The mRFP-eGFP tandem fluorescent-tagged LC3 (tfLC3) construct is frequently used to monitor autophagy. This system takes advantage of the different localization pattern of red (mRFP) and green (GFP) fluorescence of the autophagosomal and lysosomal compartments, respectively as lysosomal acidic and degradative conditions quench GFP-LC3 fluorescence while mRFP fluorescence persists in the same conditions (Kimura, Noda and Yoshimori, 2007). Therefore, mRFP-eGFP-LC3B is used as pH-sensitive reporter, highlighting autophagosomes as yellow puncta and autolysosomes (post lysosomal fusion) as red puncta.

To better investigate the autophagic flux in the absence of OFD1, HeLa cells were transiently transfected with mRFP-eGFP-LC3B construct comparing *OFD1*-silenced cells with controls.

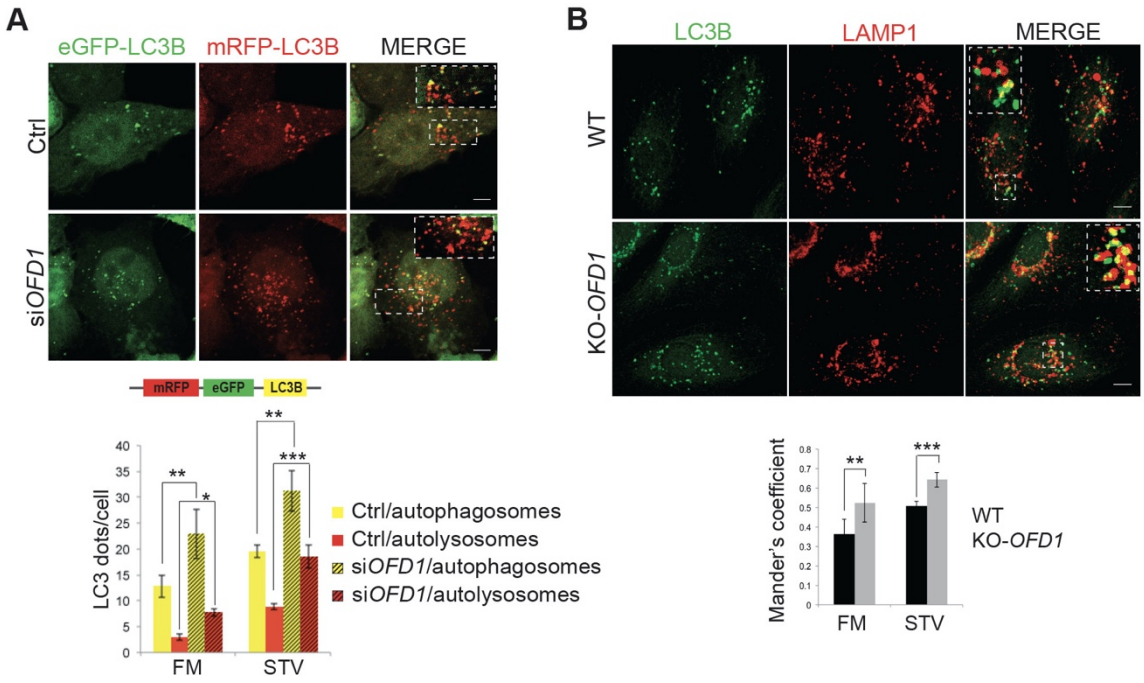

Figure 39. Loss of OFD1 enhances autophagic flux.
A. Representative confocal images of *OFD1* depleted (si*OFD1*) and control (Ctrl) HeLa cells transiently expressing mRFP–eGFP–LC3B after 90min of starvation with HBSS. Insets show colocalization in selected areas at higher magnification. Scale bar=10µm. The right panel shows the tandem structure of the mRFP-GFP-LC3B construct and the quantification of $RFP^{+}GFP^{+}$ and $RFP^{+}GFP^{-}$ puncta in si*OFD1*-depleted cells and control, cultured in full medium (FM) or kept in HBSS for 2h (STV). n≥150 cells/sample analyzed, *n*=5 independent experiments. The likelihood ratio test for Negative Binomial generalized linear models was applied; *p≤0.05, **p≤0.01 ***p≤0.001. B. Immunofluorescence analysis of LAMP1 (red) and LC3B (green) in wt and KO-*OFD1* cells following 90min of starvation in HBBS. Square dotted areas show colocalization at higher magnification. Scale bars=10µm. Histograms on the right show quantification of LAMP1-LC3B colocalization in fed (FM) or starved (STV) conditions expressed as mean ± SEM. n= 3 independent experiments; n=200 cells analyzed. One tailed Student's *t* test was applied; **p≤0.01 and ***p≤0.001. FM=full medium, STV=starvation, Baf-A1=bafilomycin

Cells were starved to induce the formation of puncta and LC3B was thus monitored by fluorescence microscopy (Fig. 39A). As showed in the graph, the analysis revealed that loss of OFD1 results in increased number of both yellow puncta (autophagosomes) and red puncta (autolysosomes) compared to controls, confirming that depletion of OFD1 increased the autophagic flux (Fig. 39A).

Moreover, KO-*OFD1* cells displayed increased percentage of colocalization between LC3B and LAMP1, used as marker of autophagosome and lysosome, respectively (Fig. 39B). These data support the hypothesis that the enhancement of

autophagy degradation activity due to the lack of control over ATG13 degradation is exerted by the OFD1 protein. The specificity of our findings was also supported by the observation that eGFP-OFD1 overexpression in HK2 cells induce a consistent decrease of autophagosomes biogenesis in wt cells.

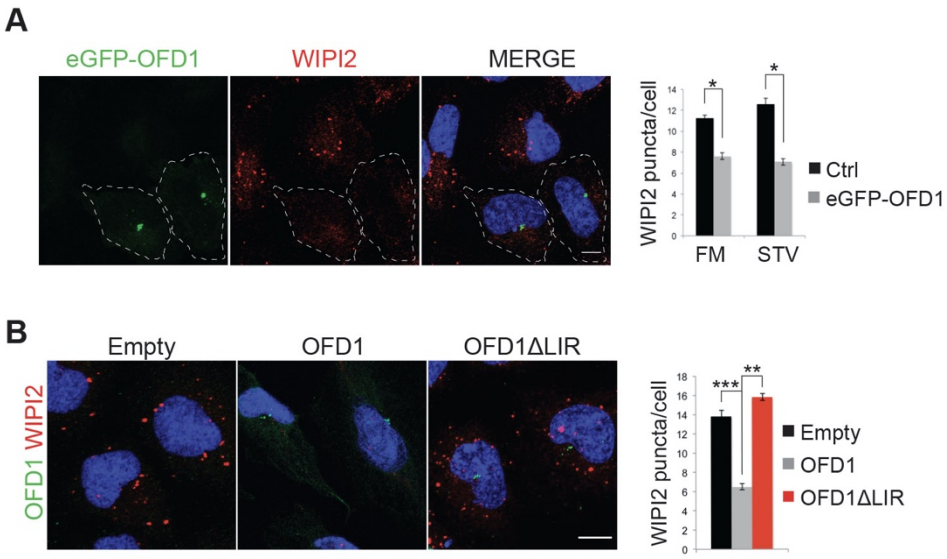

Figure 40. OFD1 controls autophagy in a LIR dependent manner. A. Representative confocal images of WIPI2 staining in wt HK2 cells transiently expressing eGFP-OFD1 after 90min of starvation with HBSS. Red, WIPI2; green, eGFP-OFD1; blue, Hoechst to label nuclei. Bar graphs show quantification of WIPI2 puncta in eGFP-OFD1 transfected cells compared to non-transfected cells used as control (Ctrl) both in full medium (FM) and in starved conditions (STV). Scale bar=10µm. n≥90 cells analyzed per sample, n=3 independent experiments. B. KO-*OFD1* cells transfected with the empty vector (Empty), 3xFLAG-OFD1 (OFD1) or 3xFLAG-OFD1ΔLIR (OFD1ΔLIR) were starved with HBSS for 90min and then processed by immunofluorescence to detect WIPI2 and OFD1 co-staining, and imaged. Red, WIPI2; green, OFD1; blue, Hoechst to label nuclei. Scale bars: 10µm. Quantification of WIPI2 puncta is shown on the right. n≥90 cells analyzed per sample, n=3 independent experiments. Data are expressed as mean ± SEM. The likelihood ratio test for Negative Binomial generalized linear models (A, B) were applied; *p≤0.05, **p≤0.01 and ***p≤0.001. FM=full medium, STV=starvation, Baf-A1=bafilomycin.

We observed a reduction of WIPI2 puncta in eGFP-OFD1 transfected cells compared to not transfected cells, demonstrating that OFD1 negatively regulates autophagosomes biogenesis (Fig. 40A). In addition, immunofluorescence analysis demonstrated that the *OFD1*ΔLIR mutant is not able to influence autophagosome

biogenesis, as demonstrated by quantification of WIPI2 puncta (Fig. 40B) further supporting our conclusion.

6. The role of OFD1 on autophagy modulation is mTOR-independent

mTOR is considered the master regulator of cellular metabolism and, consequently, is also a key element in the control of autophagy, acting as the major negative regulator of autophagy induction (Hosokawa, Hara, *et al.*, 2009).

Having said that we decided to monitor the phosphorylation status of mTOR targets to exclude that the enhancement of autophagy observed in HK2 KO-*OFD1* cells was not due to impairment of mTOR activity but was actually a consequence of OFD1 loss. HK2 wt and KO-*OFD1* cells were grown in full medium and then subjected to increasing intervals of HBSS starvation. WB analysis was then performed to check for phosphorylation levels of well-known direct targets of mTOR, as S6K1 on Thr389 (Romanelli, Dreisbach and Blenis, 2002), ULK1 on Ser575 (inhibitory phosphorylation) (Kim *et al.*, 2011) and S6 which is a target of S6K1 on Ser240, (Pende *et al.*, 2004) (Fig. 41A). Phosphorylation levels of all targets analyzed were comparable between wt and KO-*OFD1* cells, suggesting that the increased autophagy observed in the absence of OFD1 is not associated to reduced mTOR activity.

Evaluation of mTOR activation in response to nutrients gave the same results. Cells were starved with HBSS for a short time to induce autophagy, refeeded with complete medium for increasing intervals and then phosphorylation rates of mTOR targets were analyzed (Fig. 41B). In these conditions, the levels of phosphorylation, initially lower due to starvation, gradually increased both in wt and KO-*OFD1* cells.

These data confirmed that the increased autophagy observed in KO-*OFD1* cells is independent of mTOR signaling.

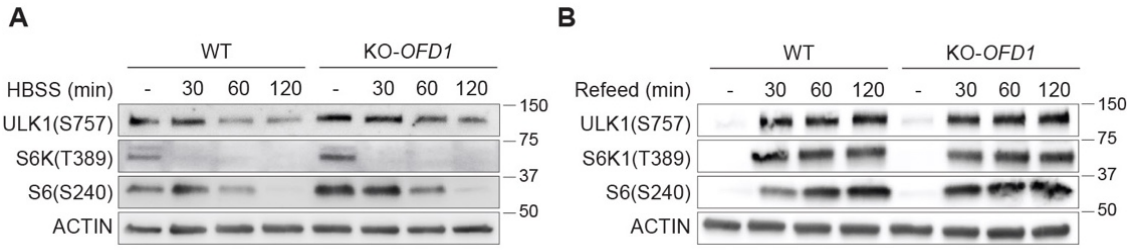

Figure 41. OFD1 controls autophagy independently from mTOR.
A. Western blot analysis of mTORC1 signaling upon nutrients deprivation in wt and KO-*OFD1* cells fed in full medium (-) and then starved in HBSS and collected at the indicated time points. Upon treatment, cell extracts were analyzed with the indicated antibodies. B. Western blot analysis of mTORC1 signaling upon nutrients stimulation in wt and KO-*OFD1* cells starved for 2h in HBSS (-) and then refed with complete medium and collected at the indicated time points. Upon treatment, cell extracts were analyzed with the indicated antibodies.

7. Autophagosomes biogenesis is enhanced in KO-OFD1 cells under cilia induction

As stated above, our cellular model KO-*OFD1* in HK2 cells shows absence of the OFD1 protein due to a premature stop codon which prevents assembling of a functional protein. Moreover, it has been already demonstrated that OFD1 loss leads to impaired ciliogenesis both *in vivo* (Ferrante *et al.*, 2006) and *in vitro* (Singla *et al.*, 2010), proving that OFD1 is necessary for proper cilia formation. Indeed, as expected, in HK2 KO-*OFD1* cells, ciliogenesis is impaired and no cilia are detectable in serum deprived conditions (Fig. 42A). Therefore, to assess whether, in ciliated conditions, autophagy is still enhanced in KO-*OFD1* cells, I performed IF experiments evaluating the number of WIPI2 puncta and comparing them between wt and KO-*OFD1* cells subjected to 24 hours of serum deprivation (Fig. 42A). Serum

starvation represents not only a widely used method to arrest cell cycle and induce cilia formation, but also a proven stimulus of autophagy induction.

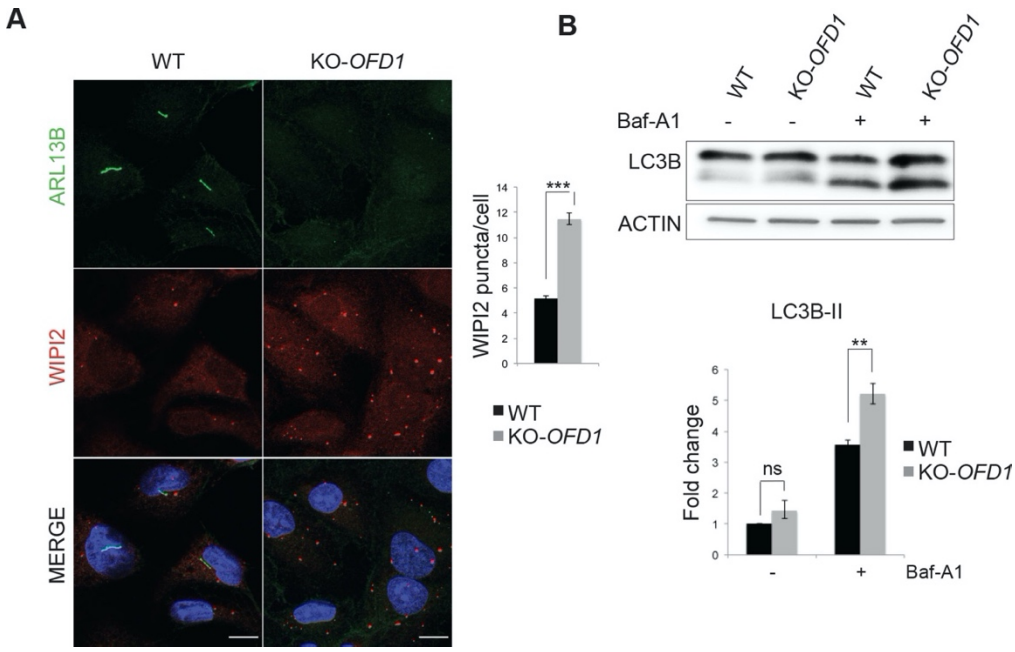

Figure 42. Autophagosome biogenesis increases in KO-*OFD1* cells in ciliated conditions.
A. Representative confocal images of primary cilia, marked by ARL13B, and of WIPI2 puncta in wt and KO-*OFD1* cells after 24h of serum starvation. Green, ARL13B; red, WIPI2; blue, Hoechst labels nuclei. Scale bar=10µm. Histograms on the right show quantification of WIPI2 puncta which is expresses as mean ± SEM. ≥300 cells analyzed per sample, n=5 independent experiments. The likelihood ratio test for Negative Binomial generalized linear models was applied; ***p≤0.001. B. Wild-type and KO-*OFD1* cells were serum starved for 24h and treated (+) or not treated (-) with Baf-A1 (100nM, 2h) and total lysates were analyzed by immunoblotting using anti-LC3B and -ACTIN antibodies. ACTIN was used a loading control. On the right, quantification of the relative amount of ACTIN-normalized LC3B-II is expressed as fold change versus the untreated condition (-) of wt cells which was defined as 1.0. Data are expressed as the mean values, error bars indicate the SEM. One tailed Student's *t*-test was applied. **p≤0.01. Baf-A1= bafilomycin, ns= not significative.

As shown in the graph in Fig 42, even under ciliated conditions WIPI2 puncta increased in KO-*OFD1* cells compared to wt as a consequence of enhanced autophagosome biogenesis.

Moreover, WB analysis of LC3B-II levels confirmed the enhancement of autophagy described in KO-OFD1 cells also in ciliated conditions (Fig. 42B). Cells were serum-starved and then treated with Baf-A1 to prevent autophagosome-lysosome fusion. The quantification of LC3B-II rate shows increased levels in Baf-A1 treated KO-

OFD1 cells compared to wt, demonstrating that autophagy is still increased under cilia induction stimuli.

8. Autophagy increased in lymphoblasts from OFD type I patients

So far, I demonstrated that loss of OFD1 has important effects on autophagy boosting autophagosome biogenesis and increasing the autophagic flux and that this is also true in biological conditions stimulating induction of ciliogenesis.

To confirm my observations, I analyzed autophagy in a cellular system physiologically linked to the OFD type I syndrome and not ciliated by definition. In particular, I used lymphoblastoid cell lines derived from OFD type I patients which carried frameshift mutations in the *OFD1* gene leading to a prematurely truncated protein. Lymphoblasts are immature white blood cells which in my opinion are physiologically unable to form cilia since they do not get in touch with each other. To the best of my knowledge blood cells cannot develop cilia and indeed, there are no reports describing the presence of primary cilia in human blood cells.

Lymphoblasts from several healthy controls and patients were collected and the autophagy was analyzed by western blot analysis both in steady state (FM) and in starved (STV) conditions. In addition, samples were also analysed with or without treatment with Baf-A1 to block LC3B degradation (Fig. 43A). Because of the high cell mortality rate due to HBSS starvation in these cells, I opted for short serum starvation to induce autophagy. The analysis illustrated in Fig. 43 confirmed the previous results further supporting that enhancement of autophagy is associated to OFD1 loss and further supporting that the role of OFD1 in autophagy is independent from cilia. Indeed, cells from OFD type I patients showed higher accumulation of LC3B-II levels compared to controls both in FM and STV conditions after Baf-A1

treatment (Fig. 43B). Moreover, OFDI patients lymphoblasts showed increased protein levels of components of the ULK1 complex, as ATG13 and ATG101 (Fig. 43C), suggesting that the role exerted by OFD1 in autophagy could be relevant in the pathogenesis of OFD type I syndrome.

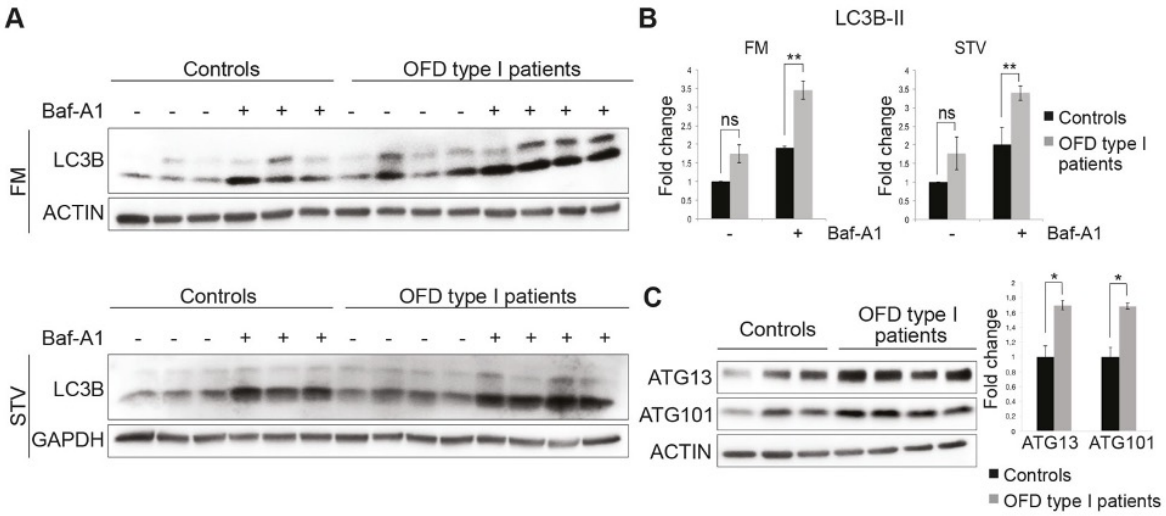

Figure 43. Lymphoblasts from OFD type I patients show increased autophagy.
A. Western blot of LC3B in lymphoblasts of OFD type I patients and controls, either untreated (-) or exposed to Baf-A1 (10nM, 2h) (+). Cells were cultured in complete medium (FM, top) or under serum starvation for 4h (STV, bottom). ACTIN and GAPDH were used as loading controls. B. Graphs show LC3B-II levels normalized on ACTIN and GAPDH, versus the untreated condition (-) of controls. C. Western blot of ATG13 and ATG101 proteins in serum starved lymphoblasts from controls and OFD type I patients. Protein levels relative to ACTIN (loading control) are expressed as fold change versus controls, represented by the dashed line. Data are expressed as mean values, error bars indicate SEM. One tailed Student's *t* test was applied (B and C); *p≤0.05, **p≤0.01.FM=full medium, STV=starvation, Baf-A1=bafilomycin, ns= not significative.

Discussion

Little is known on the molecular mechanisms underlying the cilia/autophagy interplay. Autophagy is known to be actively involved in cilia regulation and experimental evidence indicate that key regulators of ciliogenesis may be involved in critical steps of autophagy, not ruling out the possibility of a cilia independent effect. The primary cilium acts as a sensor of extracellular stimuli which are transduced into intracellular responses. Because of its functions, cilia may be used as sensory platform for autophagy induction and regulation and, conversely, it has already been shown that autophagy takes advantage of its degradation system to modulate cilia assembling or resorption.

Autophagy is a well-orchestrate and finely controlled mechanism; indeed, numerous protein complexes participate and influence the entire autophagic process. Each step of autophagy, from its induction to autophagosome maturation and lysosome fusion, has been extensively studied. Despite of that, not much is known about the mechanisms through which autophagy is turned off. Yu et al. defined autophagy shutdown as a self-regulated process and proposed a cyclic mechanism of self-limitation that reverse autophagy and restore lysosome vesicles content, preventing excessive autophagy and consequently cell death (Yu *et al.*, 2010). My thesis project focalizes on the discovery of a novel negative feedback regulation mechanism aimed at limiting autophagy and based on selective autophagy-mediated degradation of components of the ULK1 initiation complex that plays a critical role in the early phases of autophagy. The key player in this novel regulatory mechanism of autophagy is the centrosomal OFD1 protein responsible for a primary cilia-associated inherited disorder. My results demonstrate that OFD1 serves as an

autophagy receptor for ULK1 complex turnover by binding with LC3B and GABARAP-L1 through a canonical LIR motif.

OFD1 interacts with ATG13 and FIP200 which are both components of the ULK1 complex and in particular I demonstrated that the central portion of the OFD1 protein is responsible for the binding with ATG13. This region being rich in coiled coil domains, is particularly suitable for protein-protein interactions. I also demonstrated that OFD1 is able to modulate the ULK1 complex through regulation of the stability of its components. Indeed, loss of OFD1 determines increased levels of ULK1 complex proteins and puncta in HK2 cells and a slower decay of protein levels upon inhibition of protein synthesis. Conversely, overexpression of OFD1 promotes ULK1 complex degradation, which is rescued by pharmacological inhibition of autophagy, suggesting that autophagy is the degradation pathway implicated in the mechanism described. Depletion of components of the ULK1 complex leads to decreased stability of ULK1 kinase levels (Ganley *et al.*, 2009), and OFD1-mediated autophagic degradation of ATG13 could contribute to instability of the other components of the complex thus explaining the enhancement of ULK1 kinase activity in KO-*OFD1* cells.

As expected for an autophagy receptor, OFD1 is itself degraded by autophagy; furthermore, it was found in the swollen lumen of mature lysosome and to colocalize with autophagosome structures.

OFD1 is a basal body protein in confluent and mitotic quiescent cells and is known to be a key regulator of ciliogenesis (Ferrante *et al.*, 2006; Singla *et al.*, 2010; Tang *et al.*, 2013). The primary cilium is nucleated from centrioles of the centrosome which serves as the main microtubule organizing center. OFD1 is also a centrosomal protein and interact with some centriolar satellites proteins, such as PCM1 which has also been involved in autophagic processes. Although OFD1 and

PCM1 act on autophagy in different ways, they share the presence of a functional LIR motif to bind Atg8 proteins, supporting the knowledge that also the centrosome plays a role in the link between cilia and autophagy. Indeed, the centrosome has been presented as a control station for GABARAP-mediated autophagy since GABARAP stability and recruitment to centrosomes is controlled by PCM1 (Joachim *et al.*, 2017). Moreover, recent studies highlight an involvement of autophagy in selective degradation of centriolar satellites components as a mechanism to limit centrosome abnormalities and genomic instability, expanding the range of action of autophagy (Holdgaard *et al.*, 2019; Holdgaard, Cianfanelli and Cecconi, 2020).

As mentioned before the cilia/autophagy crosstalk is still poorly understood and novel players have yet to be identified. Besides the players an intriguing point is also in which cell compartment this interplay may take place. Autophagy so far has been mainly confined to the cytoplasm and cilia are a specialized structure of the cell membrane. The peri-ciliary area is indeed a good candidate to look at. The ciliary membrane has been proposed as a new nucleation site for autophagosomes formation. ATG proteins involved in initial steps of autophagy localize at the base of cilia and other ATG proteins are recruited to this location upon starvation (Pampliega *et al.*, 2013). From this perspective, the ciliary pocket may represent an attractive site for autophagosome assembling, since it may act as a platform for cilia-associated autophagic vescicular trafficking and allow the autophagic machinery and ciliary proteins to be compartmentalized in the same cellular district influencing each other.

Besides being involved in ciliogenesis, several reports demonstrated additional functions for the pleiotropic protein codified by the gene responsible for OFD type I syndrome (Morleo and Franco, 2020). The results generated by the work performed during my thesis add another piece to the puzzle of the function of the OFD1 protein.

Indeed I demonstrated yet an other activity not related to the control of primary cilia formation. However, as mentioned above OFD1 is not the only cilioprotein for which a role in autophagy has been shown. A variety of proteins localizing at cilia, involved in cilia assembling or maintanance, and/or associated to ciliopathies, share a direct functional role in autophagy (Fig 14). The control exerted from these proteins on autophagy is not strictly related to cilia and, frequently, they display a dual role in ciliogenesis and autophagy, according to specific culturing conditions allowing or not allowing cilia formation.

In this context, OFD1 represents a novel noncanonical autophagic player, which in subconfluent non ciliated conditions exerts a regulative role on autophagy constrain. As mentioned before, OFD1 is essential for cilia formation and indeed, KO-*OFD1* cells are not able to generate primary cilia. Although other studies demonstrated that loss of cilia results in decreased autophagy (Pampliega *et al.*, 2013), analysis of autophagosome biogenesis and autophagic flux in conditions promoting ciliogenesis in KO-*OFD1* cells reproduced the same autophagic phenotype observed in conditions that do not allow cilia formation (i.e. cycling and sub-confluent cells). These findings indicate that the control exerted by OFD1 on autophagy occurs independently from cilia. This observation was also confirmed by analysis of autophagy performed on OFD type I patients' lymphoblasts that grow in suspension and are never ciliated. Notably, the demonstration of increased autophagy in lymphoblasts of OFDI individuals suggest the possibility that autophagy may contribute to the pathogenetic mechanisms underlying the disease phenotype. Excessive autophagy associated to primary cilia loss has been also described in several tumor studies on pancreatic ductal adenocarcinoma (PDAC) cells (Seeley *et al.*, 2009) and models of human cholangiocarcinoma (CCA) (Peixoto *et al.*, 2020). Tumors are not observed in female OFD1 patients although they do

display clinical signs of increased cell proliferation such as aberrant oral frenulae. On the other hand, also the fact that the human OFD1 transcript escapes X-inactivation should be taken into account since it could modulate the phenotype and justify the absence of more severe clinical signs.

Since autophagy has been mainly proposed as a protective mechanism, the harmful effects of increased autophagy are not widely described in the scientific literature. Indeed, unrestrained autophagy can contribute to the development of pathological conditions (Antonioli *et al.*, 2017). For example, autophagy has been linked to tumor progression. Indeed, in cancer cells, enhanced autophagy helps to refuel the tumor of substrates for high-level metabolism besides promoting cell proliferation (White, 2015). One of the main clinical features of the OFD type I syndrome is represented by renal cystic disease which shares some traits with cancer, like higher cellular proliferation rate and altered metabolism (Seeger-Nukpezah *et al.*, 2015). Enhancement of autophagy may be responsible for metabolism changing and hyper-proliferation of cyst-lining cells, contributing to the progression of the renal disease. Interestingly, altered autophagy has also been described in other models of renal cystic disease namely Polycystic kidney disease (PKD) and Tuberous sclerosis complex (TSC) and von Hippel-Lindau (VHL) disease (Wang and Choi, 2014).

Cell death represents another possible consequence of excessive autophagy and, indeed, in some cases, autophagy may be considered as a new type of programmed cell death (Shi *et al.*, 2012). Talking about renal cystic disease, it has been demonstrated that increased apoptosis contributes to cystogenesis and determines progressive loss of normal nephrons (Goilav, 2011) and autophagy may contribute to this pathological process.

In line with this observation, colleagues in the laboratory where I trained demonstrated that autophagy is enhanced also in *in vivo* models of *Ofd1* mutants and in particular in a conditional model with kidney specific inactivation of the transcript. It was also demonstrated that this excessive autophagy contributes to the renal cystic phenotype as genetic inhibition of autophagy is able to reduce renal cysts formation and to partially preserve renal function in *Ofd1* mutant mice (EMBO J, under revision).

On the basis of these observations, although the clinical phenotype observed in OFD type I syndrome is probably mostly due to defective ciliogenesis, it cannot be ruled out that some of the clinical manifestation observed in this disorder may be due to altered autophagy or to a combination of the latter with cilia dysfunction.

In conclusion, the work performed during my PhD training allowed me to identify another player of the centrosome/cilia/autophagy network. Future studies will establish whether these findings have implications for the clinical signs observed in ciliopathies.

Materials & Methods

Cell culture and treatments

Human Kidney 2 (HK2), HEK293, HeLa and mIMCD3 cell lines were from the American Type Culture Collection (ATCC; http://www.atcc.org, Manassas, VA). HK2 cells were cultured in Dulbecco's Modified Eagle Medium/F12 (DMEM/F12, Gibco) supplemented with 10% FBS, 1mM l-glutamine, 1% antibiotics (penicillin/streptomycin) plus 1% insulin-transferrin-sodium selenite (Sigma I1884). HEK293 and HeLa cell lines were cultured in Dulbecco's Modified Eagle Medium (DMEM, Gibco) supplemented with 10% FBS, 1mM l-glutamine, and 1% antibiotics (penicillin/streptomycin). Lymphoblastoid cells were maintained in RPMI medium (Gibco 11875) supplemented with 15% FBS, 1mM glutamine, 1% antibiotics (penicillin/streptomycin and Amphotericin B). mIMCD3 cells were cultured in DMEM/F12 supplemented with 10% FBS, 1mM l-glutamine and 1% antibiotics (penicillin/streptomycin). To study mTOR activity, cells were cultured in amino acid–free RPMI 1640 medium (US Biological) supplemented with 10% dialyzed FBS (Invitrogen, Thermo Fisher Scientific) for 1h, then a complete RPMI 1640 medium (with amino acids) was added back to cells. Cells were maintained at 37°C with 5% CO_2. Cell lines were regularly tested negative for the presence of mycoplasma using the EZ-PCR Mycoplasma PCR Test Kit (Biological Industries). Cells were treated with 50μg/ml of CHX (SIGMA), 10μM of SAR405 (ApexBIO), 100nM of Baf-A1 (SIGMA), for the indicated time periods. For each treatment cells were plated the day before to perform the experiments at a final confluence of 70%. HK2 cells were grown to 100% density and brought to quiescence by serum starvation for 24 hours to induce ciliogenesis.

Cloning procedures, DNA mutagenesis and cell transfections

The full-length human OFD1, OFD1a (aa 1-276), OFD1b (aa 277-663), OFD1c (aa 664-1012), OFD1ΔLIR transcripts were tagged at the N-terminus with a 3xFLAG tag by cloning it into the CMV10 vector and the plasmids were sequence-verified. Mutations were generated via site-directed mutagenesis according to standard protocols. All cDNAs used are reported in Table 1. For transient expression, DNA plasmids were transfected with TransIT®-LT1 Transfection Reagent (Mirus) according to manufacturer's instructions.

RNAi

HeLa cells were transfected with 25nM of the ON-TARGETplusSMARTpool against *OFD1* (L-009300–00-0020; Thermo Scientific Dharmacon) using Interferin (Polyplus), following manufacturer's recommendations for 96h. Cells were then transfected with mRFP-eGFP-LC3 for 24h. HK2 cells were transfected with 25nM of the ON-TARGETplus siRNA SMARTpool against *ATG13* (L-020765-01-0005; Thermo Scientific Dharmacon) and *FIP200* (L-021117-00-0005; Thermo Scientific Dharmacon) using Lipofectamine RNAiMAX Transfection Reagent (Invitrogen), following manufacturer's recommendations for 72h. Cells were then collected and fixed for immunofluorescence staining and WB analysis.

Antibodies used for western blot, immunoprecipitation and immunofluorescence staining

The complete list of primary antibodies used is reported in Table 2. Secondary antibody HRP-conjugated was from Amersham ECL. For immunofluorescence staining, the following antibodies were used: Alexa Fluor Plus donkey anti-rabbit

488 (Life Technology; A32790; Ober-Olm, Germany), donkey anti-mouse 568 (Life Technology; A32766), donkey anti-rabbit or anti-mouse 647 (Life Technology; A32795 and A32787, respectively).

Immunofluorescence

Cells were grown on glass coverslips, fixed for 5 min in cold methanol and permeabilized in 0.05% (w/v) saponin, 0.5% (w/v) BSA, 50mM NH_4Cl, and 0.02% NaN_3 in PBS (blocking buffer) for 30min. Cells were incubated with primary antibodies either at 4°C ON or at room temperature for 2h and then washed three times with PBS and incubated with appropriate secondary antibodies for 1h at room temperature. DNA was stained with Hoechst (33342, Sigma). After three washings with PBS, slides were mounted on coverslips with Mowiol (Calbiochem). The experiments were repeated at least three times and representative images are shown.

Confocal fluorescence microscopy, image processing and colocalization analysis

Samples were examined under LSM800 High-resolution confocal laser-scanning microscope (Zeiss). Optical sections were obtained under a 63x oil-immersion objective at a definition of 1024 X 1024 pixels, adjusting the pinhole diameter to 1 Airy unit for each emission channel. Airyscan microscopy was performed using a LSM 880 (Zeiss) confocal microscope using a 63x Plan-Apochromat 1.4NA DIC oil immersion objective. Images were subjected to Airyscan processing performed with Zen Blue software. To perform quantitative image analysis, 10–15 randomly chosen fields that included 8-10 cells each were scanned, using the same setting parameters (i.e. laser power and detector amplification) below pixel saturation

between samples of interest and controls. Dots analysis was performed using ImageJ software on Z-Stacks images with a slice thickness of 0.5µm. Single channels from each image were converted into 8-bit grayscale images and thresholded in order to subtract background. Counting was performed either automatically or manually using the tool available at https://imagej.nih.gov/ij/docs/guide/146-19.html. The levels of colocalization of OFD1/LC3B, LAMP1/LC3B, HA-OFD1/ATG13 and HA-OFD1/FIP200 were calculated by acquiring confocal sections at the same laser power and photomultiplier gain. Images were processed using the ImageJ software. Single channels from each image were converted into 8-bit grayscale images and thresholded in order to subtract background. The ImageJ "JACoP" plugin was then used to quantify Manders' overlap coefficient. Values range from 0 (corresponding to non-overlapping images) to 1 (as 100% co-localization between both images) and express the ratio of the green channel intensities overlapping the red one for image.

Western blot

Cells and renal tissues were lysed in RIPA buffer containing protease inhibitors (Sigma-Aldrich), and phosphatase inhibitors (PhosSTOP, Roche). Protein lysates were resolved in SDS-PAGE 4–20% gradient gels (BioRad; Hercules, CA, USA) and transferred to polyvinylidene difluoride (PVDF) membranes (Immobilon-P, Merck Millipore). Membranes were blocked in TBS-Tween containing 5% Non-Fat Dry Milk (Cell Signaling Technology) and incubated ON at 4°C with the specific primary antibody. Western blot images were acquired using the UVITEC imaging system; immunoblot bands were quantified using ImageJ (Gels and Plot Lanes plug-in).

Co-Immunoprecipitation

HK2 cells were lysed in lysis buffer (50mM Tris-HCl, 1mM EDTA, 10mM MgCl2, 5mM EGTA, 0.5% Triton X-100, pH 7.28). An equal amount of each protein lysate was incubated ON at 4°C with 5µg of the indicated antibodies and IgG (Cell Signaling), followed by incubation with 50µl of Protein A/G PLUS-Agarose beads (Santa Cruz sc-2003) for 3h at 4°C. For HA-tagged clones, protein lysate was incubated ON at 4°C with immobilized anti-HA affinity resin (Pierce, Thermo Fisher Scientific). Beads were then washed in lysis buffer, resuspended in Laemmli buffer and boiled. Supernatants were loaded on SDS-PAGE.

GST pull-down

GST, LC3B-, dN LC3B dG-, LC3B F52A-V53A dG-, GABARAP-L1- and ATG13-GST were cloned, as GST fusion proteins, into pGEX-4T-1 (GE Healthcare; Little Chalfont, UK) and were expressed in *E. coli* BL21 (DE3) cells in LB medium. Expression was induced by addition of 0.5mM IPTG and cells were incubated at 37°C for 5h. Harvested cells were sonicated in lysis buffer (20mM Tris-HCl pH 7.5, 10mM EDTA, 5mM EGTA, 150mM NaCl) and GST fused proteins were immuno-precipitated using Glutathione Sepharose 4B beads (GE Healthcare) and used in GST pull down assays. HEK293 cells were transfected with 3xFLAG-OFD1, 3xFLAG-OFD1ΔLIR, OFD1a, OFD1b, OFD1c, and empty constructs as described above, and then lysed in lysis buffer (50mM HEPES, pH 7.5, 150mM NaCl, 1mM EDTA, 1mM EGTA, 1% Triton X-100, 10% glycerol, 25mM NaF). Lysates were cleared by centrifugation at 12000g for 10min and incubated with GST fusion protein-loaded beads ON at 4°C. Beads were then washed five times in lysis buffer, resuspended in Laemmli buffer and boiled. Supernatants were loaded on SDS-PAGE.

Quantitative RT-PCR

Total RNA extracted from HK2 cells and kidneys was isolated by using the RNeasy Mini Kit (Qiagen) according to manufacturer's instructions. RNA (1µg) was then reverse transcribed into cDNA by QuantiTect Reverse Transcription Kit (Qiagen) with random hexamers oligos. For quantitative real time PCR analysis (qRT-PCR), cDNAs were analyzed with Roche Light Cycler 480 system using a LigthCycler 480 SYBR Green I Master mix (Roche). The final concentration of primers was of 0.5µM. RT-minus controls confirmed the absence of genomic contamination. Quantification data were expressed as cycle threshold (Ct). Ct values were averaged for each in-plate technical triplicate and normalized as difference in Ct values (ΔCt) between each sample and the *ACTIN* gene, which was used as endogenous reference. ΔCt values were normalized with respect to ΔCt values of the control (ΔΔCt). The variation was reported as fold change (2-ΔΔCt). All results are shown as means ± SEM of at least 3 independent biological replicates. Primer sequences are reported in Table 3.

Generation of stable cell lines

KO-*OFD1* clone: HK2 cells were transfected with an all-in-one vector containing the sgRNA of interest (target site sequence: TTAGTCCAACATGTTTACCG with predicted no off-target sites), whose expression was driven by the U6 promoter, a recombinant form of Cas9 protein under the control of the CMV promoter and an mCherry reporter gene under the control of the SV40 promoter (Genecopoeia). Cells were transfected with Lipofectamine CRISPRMAX Cas9 Transfection Reagent (Invitrogen, Thermo Fisher Scientific) according to manufacturer's instructions. Forty-eight hours after transfection, putative positive clones were FACS sorted for mCherry expression using the BD FACS Aria flow cytometer. Sorted cells were kept

in culture until confluence and the GeneArt Genomic Cleavage Detection (GCD) Kit (Invitrogen, Thermo Fisher Scientific) was used to check editing efficiency; several clones were selected, and sequence verified.

HA-OFD1wt, HA-OFD1ΔLIR, HEK293-OFD1wt and HEK293-OFD1ΔLIR clones: Wild-type and LIR mutant OFD1 sequences were cloned into pDONR223 vector using the BP Clonase Reaction Kit (Invitrogen) and further recombined into the doxycycline inducible lentiviral GATEWAY destination vector HA-pLTD using In Fusion Cloning kit (Takara). Primers were designed following the indication available at https://www.takarabio.com/products/cloning/in-fusion-cloning. Stable and inducible cell lines were generated using the produced lentiviral plasmids. Virus were produced in HEK 293T cells and HK2/HEK293 cells were infected for 48hr before selection with puromycin.

GFP-LC3 clone: HK2 cells transient transfections with eGFP-LC3B were performed using TransIT®-LT1 Transfection Reagent. Forty-eight hours after transfection, cells were selected with HK2 medium containing 400 µg/ml hygromicin until the amount of resistant cell clones was observed. A concentration of 200 µg/ml hygromicin was used as maintenance dose. After selection, GFP-positive cells were sorted on FACS to obtain single cell clones.

Statistical analysis

In experiments requiring counts of ATG13, ULK1, LC3B and WIPI2 puncta the likelihood ratio test for Negative Binomial was applied. In all remaining experiments, statistical significance between two groups was evaluated by one tailed Student's *t*-test, $p<0.05$ was considered significant. Quantitative data are presented as the mean ± SEM (Standard Error of the Mean).

TABLE 1. Plasmids related to the experimental procedures.

Plasmid	Gene	Reference
pCMV10-3xFLAG Expression Vector	3xFLAG only	SIGMA (#E7658)
pCMV10-3xFLAG-OFD1	Human OFD1	(Giorgio et al., 2007)
pCMV10-3xFLAG-OFD1a	Human OFD1a (aa1-276)	This study
pCMV10-3xFLAG-OFD1b	Human OFD1b (aa277-663)	This study
pCMV10-3xFLAG-OFD1c	Human OFD1c (aa664-1012)	This study
pCMV10-3xFLAG-OFD1ΔLIR LIR mutated 2xAla	Human OFD1ΔLIR EKYMKI / EKAMKA	This study
pCDNA3.1-Myc-eGFP-OFD1	Human OFD1	This study
pGEX-4T1 alone	GST only	(Kirkin et al., 2009)
pGEX-4T1 GABARAP-L1 dG	Human GABARAP-L1 deletion of terminal glycine	(Kirkin et al., 2009)
pGEX-4T1 LC3B dG	Human LC3B deletion of terminal glycine	(Kirkin et al., 2009)
pGEX-4T1 dN LC3B dG	LC3B lacking N-terminus and deletion of terminal glycine	(Grumati et al., 2017)
pGEX-4T1 LC3B F52A-V53A dG	LC3B with mutated LIR binding pocket and deletion of terminal glycine	(Grumati et al., 2017)
pGEX-4T1 ATG13	Human ATG13	This study
pMXs-IP-eGFP-hATG13	Human ATG13	Addgene plasmid (#38181)
FLAG-VPS34	Human VPS34	(C. C. Liu et al., 2016)
mRFP-eGFP-LC3B	Human LC3B	(De Leo et al., 2016)
pCDNA3.1-eGFP-LC3B	Human LC3B	This study

TABLE 2. Antibodies related to the experimental procedures.

Antigen	Company	Catalog number	Application
ACTIN	SIGMA	A5316	WB

ARL13B	SANTA CRUZ BIOTECHNOLOGY	SC-515784	IF
ATG13	CELL SIGNALING	13273	WB; IP
ATG13	CELL SIGNALING	13468	IF
ATG101	CELL SIGNALING	13492	WB
BETA-TUBULIN	SIGMA	T4026	WB
GABARAP	CELL SIGNALING	11876	IF
GAMMA-TUBULIN	SIGMA	T6557	IF
FIP200	PROTEINTECH	17250-1-AP	WB; IF
FLAG	SIGMA	F1804	WB; IF
GAPDH	SANTA CRUZ BIOTECHNOLOGY	SC-515381	WB
GFP	ABCAM	AB290	WB; IP
HA	THERMOFISHER	26181	IF; IP; WB
HSP90	CST	4874	WB
LAMP1	DSHB	H4A3	IF
LC3B	NANOTOOLS	0231-100	IF
LC3B	NOVUS BIO	NB100-2220	WB; IF
OFD1	SIGMA	HPA031103	WB; IP; IF
P62	ABNOVA	H00008878	WB
p-ATG13 (S318)	ROCKLAND	600-401-C49	WB
p-S6 (S240)	CELL SIGNALING	2215	WB
p-S6K1 (T389)	CELL SIGNALING	9205	WB
p-ULK1 (S757)	CELL SIGNALING	6888	WB
p-VPS34 (S249)	CELL SIGNALING	13857	WB
ULK1	CELL SIGNALING	8054	WB; IF
WIPI2	BIORAD	MCA5780GA	IF

TABLE 3. Sequences of the primers related to the experimental procedures.

Primer	Sequence
hFIP200-FW	5'-GGATCTCAAACCAGGTGAGGG-3'

hFIP200-REV	5'-GTGCCTTTTTGGCTTGACAGT-3'
hULK1-FW	5'-CTGGTCCTCTTGCTTCCGTC-3'
hULK1-REV	5'-ACACCAGCCCAACAATTCC-3'
hATG13-FW	5'-GACCTTCTATCGGGAGTTTCAG-3'
hATG13-REV	5'-GGGTTTCCACAAAGGCATCAAAC-3'
hATG101-FW	5'-CCCAGGATGTT GACTGTGAC-3'
hATG101-REV	5'-ACATCTGCCCCAGCCCATCG-3'
hACTIN-FW	5'-AGAGCTACGAGCTGCCTGAC-3'
hACTIN-REV	5'-AGCACTGTGTTGGCGTACAG-3'

Contributions

Paolo Grumati generated HA-OFD1wt, HA-OFD1ΔLIR, HEK293-OFD1wt and HEK293-OFD1ΔLIR delivered lentiviral clones. Elvira Damiano generated the KO-OFD1 HK2 cells used in this thesis by CRISPR/Cas9 technology. Umberto Formisano performed HBSS and CHX assay, phosphorylation assay for ATG13 and

VPS34 illustrated in Fig. 20-21-37 and experiments in Appendix. Luigi Ferrante performed the RT PCR showed in Fig. 20. Fabrizia Carbone performed WB analysis of mTOR target illustrated in Fig. 41.

References

Abramowicz, I. *et al.* (2017) 'Oral-facial-digital syndrome type I cells exhibit impaired DNA repair; unanticipated consequences of defective OFD1 outside of the cilia network', *Human molecular genetics*. doi: 10.1093/hmg/ddw364.

Alemu, E. A. *et al.* (2012) 'ATG8 family proteins act as scaffolds for assembly of the ULK complex: Sequence requirements for LC3-interacting region (LIR) motifs', *Journal of Biological Chemistry*. doi: 10.1074/jbc.M112.378109.

Antonioli, M. *et al.* (2017) 'Emerging Mechanisms in Initiating and Terminating Autophagy', *Trends in Biochemical Sciences*. doi: 10.1016/j.tibs.2016.09.008.

Arquint, C., Gabryjonczyk, A. M. and Nigg, E. A. (2014) 'Centrosomes as signalling centres', *Philosophical Transactions of the Royal Society B: Biological Sciences*. doi: 10.1098/rstb.2013.0464.

Axe, E. L. *et al.* (2008) 'Autophagosome formation from membrane compartments enriched in phosphatidylinositol 3-phosphate and dynamically connected to the endoplasmic reticulum', *Journal of Cell Biology*. doi: 10.1083/jcb.200803137.

Bangs, F. and Anderson, K. V. (2017) 'Primary cilia and Mammalian Hedgehog signaling', *Cold Spring Harbor Perspectives in Biology*. doi: 10.1101/cshperspect.a028175.

Bao, Z. and Huang, W. (2017) 'Thioridazine promotes primary ciliogenesis in lung cancer cells through enhancing cell autophagy', *International Journal of Clinical and Experimental Medicine*.

Barbelanne, M. and Tsang, W. Y. (2014) 'Molecular and cellular basis of autosomal recessive primary microcephaly', *BioMed Research International*. doi: 10.1155/2014/547986.

Barker, A. R., Thomas, R. and Dawe, H. R. (2014) 'Meckel-Gruber syndrome and the role of primary cilia in kidney, skeleton, and central nervous system development', *Organogenesis*. doi: 10.4161/org.27375.

Di Bartolomeo, S. *et al.* (2010) 'The dynamic interaction of AMBRA1 with the dynein motor complex regulates mammalian autophagy', *Journal of Cell Biology*. doi: 10.1083/jcb.201002100.

Bernabé-Rubio, M. and Alonso, M. A. (2017) 'Routes and machinery of primary cilium biogenesis', *Cellular and Molecular Life Sciences*. doi: 10.1007/s00018-017-2570-5.

Birgisdottir, Å. B., Lamark, T. and Johansen, T. (2013) 'The LIR motif - crucial for selective autophagy', *Journal of Cell Science*. doi: 10.1242/jcs.126128.

Bjørkøy, G. *et al.* (2009) 'Chapter 12 Monitoring Autophagic Degradation of p62/SQSTM1', *Methods in Enzymology*. doi: 10.1016/S0076-6879(08)03612-4.

Boehlke, C. *et al.* (2010) 'Primary cilia regulate mTORC1 activity and cell size through Lkb1', *Nature Cell Biology*. doi: 10.1038/ncb2117.

Brown, J. M. and Witman, G. B. (2014) 'Cilia and diseases', *BioScience*. doi: 10.1093/biosci/biu174.

Bruel, A. L. *et al.* (2017) 'Fifteen years of research on oral-facial-digital syndromes: From 1 to 16 causal genes', *Journal of Medical Genetics*. doi: 10.1136/jmedgenet-2016-104436.

Cardenas-Rodriguez, M. and Badano, J. L. (2009) 'Ciliary biology: Understanding the cellular and genetic basis of human ciliopathies', *American Journal of Medical Genetics, Part C: Seminars in Medical Genetics*. doi: 10.1002/ajmg.c.30227.

Christensen, S. T. *et al.* (2013) 'Analysis of primary cilia in directional cell migration in fibroblasts', in *Methods in Enzymology*. doi: 10.1016/B978-0-12-397944-5.00003-1.

Clement, C. A. *et al.* (2009) 'The primary cilium coordinates early cardiogenesis and hedgehog signaling in cardiomyocyte differentiation', *Journal of Cell Science*. doi: 10.1242/jcs.049676.

Clement, D. L. *et al.* (2013) 'PDGFRα signaling in the primary cilium regulates NHE1-dependent fibroblast migration via coordinated differential activity of MEK1/2-ERK1/2-p90RSK and AKT signaling pathways', *Journal of Cell Science*. doi: 10.1242/jcs.116426.

Coene, K. L. M. *et al.* (2009) 'OFD1 Is Mutated in X-Linked Joubert Syndrome and Interacts with LCA5-Encoded Lebercilin', *American Journal of Human Genetics*. doi: 10.1016/j.ajhg.2009.09.002.

De Conciliis, L. *et al.* (1998) 'Characterization of Cxorf5 (71-7A), a novel human

cDNA mapping to Xp22 and encoding a protein containing coiled-coil α-helical domains', *Genomics*. doi: 10.1006/geno.1998.5348.

Cookson, M. R. (2012) 'Parkinsonism due to mutations in PINK1, Parkin, and DJ-1 and oxidative stress and mitochondrial pathways', *Cold Spring Harbor Perspectives in Medicine*. doi: 10.1101/cshperspect.a009415.

Cornec-Le Gall, E., Alam, A. and Perrone, R. D. (2019) 'Autosomal dominant polycystic kidney disease', *The Lancet*. doi: 10.1016/S0140-6736(18)32782-X.

D'Angelo, A. and Franco, B. (2009) 'The dynamic cilium in human diseases', *PathoGenetics*. doi: 10.1186/1755-8417-2-3.

Dikic, I. and Elazar, Z. (2018) 'Mechanism and medical implications of mammalian autophagy', *Nature Reviews Molecular Cell Biology*. doi: 10.1038/s41580-018-0003-4.

Ding, W. X. and Yin, X. M. (2012) 'Mitophagy: Mechanisms, pathophysiological roles, and analysis', *Biological Chemistry*. doi: 10.1515/hsz-2012-0119.

Dirksen, E. R. (1991) 'Centriole and basal body formation during ciliogenesis revisited', *Biology of the Cell*. doi: 10.1016/0248-4900(91)90075-X.

Doherty, D. (2009) 'Joubert Syndrome: Insights Into Brain Development, Cilium Biology, and Complex Disease', *Seminars in Pediatric Neurology*. doi: 10.1016/j.spen.2009.06.002.

Dooley, H. C. *et al.* (2014) 'WIPI2 Links LC3 Conjugation with PI3P, Autophagosome Formation, and Pathogen Clearance by Recruiting Atg12-5-16L1', *Molecular Cell*. doi: 10.1016/j.molcel.2014.05.021.

Doyon, Y. and Côté, J. (2004) 'The highly conserved and multifunctional NuA4 HAT complex', *Current Opinion in Genetics and Development*. doi: 10.1016/j.gde.2004.02.009.

Dunlop, E. A. *et al.* (2014) 'FLCN, a novel autophagy component, interacts with

GABARAP and is regulated by ULK1 phosphorylation', *Autophagy*. doi: 10.4161/auto.29640.

Egan, D. F. *et al.* (2011) 'Phosphorylation of ULK1 (hATG1) by AMP-activated protein kinase connects energy sensing to mitophagy', *Science*. doi: 10.1126/science.1196371.

Emes, R. D. (2001) 'A new sequence motif linking lissencephaly, Treacher Collins and oral-facial-digital type 1 syndromes, microtubule dynamics and cell migration', *Human Molecular Genetics*. doi: 10.1093/hmg/10.24.2813.

Ennis, H. L. and Lubin, M. (1964) 'Cycloheximide: Aspects of inhibition of protein synthesis in mammalian cells', *Science*. doi: 10.1126/science.146.3650.1474.

Feng, Y. and Klionsky, D. J. (2017) 'Autophagic membrane delivery through ATG9', *Cell Research*. doi: 10.1038/cr.2017.4.

Ferrante, M. I. *et al.* (2001) 'Identification of the gene for oral-facial-digital type 1 syndrome', *American Journal of Human Genetics*. doi: 10.1086/318802.

Ferrante, M. I. *et al.* (2003) 'Characterization of the OFD1/Ofd1 genes on the human and mouse sex chromosomes and exclusion of Ofd1 for the Xpl mouse mutant', *Genomics*. doi: 10.1016/S0888-7543(03)00091-0.

Ferrante, M. I. *et al.* (2006) 'Oral-facial-digital type I protein is required for primary cilia formation and left-right axis specification', *Nature Genetics*. doi: 10.1038/ng1684.

Follit, J. A. *et al.* (2006) 'The intraflagellar transport protein IFT20 is associated with the Golgi complex and is required for cilia assembly', *Molecular Biology of the Cell*. doi: 10.1091/mbc.E06-02-0133.

Franco, B. and Ballabio, A. (2006) 'X-inactivation and human disease: X-linked dominant male-lethal disorders', *Current Opinion in Genetics and Development*. doi: 10.1016/j.gde.2006.04.012.

Franco, B. and Thauvin-Robinet, C. (2016) 'Update on oral-facial-digital syndromes (OFDS)', *Cilia*. doi: 10.1186/s13630-016-0034-4.

Gan, B. *et al.* (2006) 'Role of FIP200 in cardiac and liver development and its regulation of TNFα and TSC-mTOR signaling pathways', *Journal of Cell Biology*. doi: 10.1083/jcb.200604129.

Ganley, I. G. *et al.* (2009) 'ULK1·ATG13·FIP200 complex mediates mTOR signaling and is essential for autophagy', *Journal of Biological Chemistry*. doi: 10.1074/jbc.M900573200.

Gao, C. *et al.* (2010) 'Autophagy negatively regulates Wnt signalling by promoting Dishevelled degradation', *Nature Cell Biology*. doi: 10.1038/ncb2082.

Giorgio, G. *et al.* (2007) 'Functional characterization of the OFD1 protein reveals a nuclear localization and physical interaction with subunits of a chromatin remodeling complex', *Molecular Biology of the Cell*. doi: 10.1091/mbc.E07-03-0198.

Girardet, L. *et al.* (2019) 'Primary cilia: biosensors of the male reproductive tract', *Andrology*. doi: 10.1111/andr.12650.

Del Giudice, E. *et al.* (2014) 'CNS involvement in OFD1 syndrome: A clinical, molecular, and neuroimaging study', *Orphanet Journal of Rare Diseases*. doi: 10.1186/1750-1172-9-74.

Goilav, B. (2011) 'Apoptosis in polycystic kidney disease', *Biochimica et Biophysica Acta - Molecular Basis of Disease*. doi: 10.1016/j.bbadis.2011.01.006.

Gonçalves, J. and Pelletier, L. (2017) 'The ciliary transition zone: Finding the pieces and assembling the gate', *Molecules and Cells*. doi: 10.14348/molcells.2017.0054.

Gong, C. *et al.* (2013) 'Beclin 1 and autophagy are required for the tumorigenicity of breast cancer stem-like/progenitor cells', *Oncogene*. doi: 10.1038/onc.2012.252.

Grumati, P. *et al.* (2017) ‘Full length RTN3 regulates turnover of tubular endoplasmic reticulum via selective autophagy’, *eLife*. doi: 10.7554/eLife.25555.

Gundersen, G. G. and Bulinski, J. C. (1986) ‘Distribution of tyrosinated and nontyrosinated α-tubulin during mitosis’, *Journal of Cell Biology*. doi: 10.1083/jcb.102.3.1118.

Hamasaki, M. *et al.* (2013) ‘Autophagosomes form at ER-mitochondria contact sites’, *Nature*. doi: 10.1038/nature11910.

Hasegawa, J. *et al.* (2016) ‘ Autophagosome–lysosome fusion in neurons requires INPP 5E, a protein associated with Joubert syndrome ’, *The EMBO Journal*. doi: 10.15252/embj.201593148.

Hildebrandt, F., Attanasio, M. and Otto, E. (2009) ‘Nephronophthisis: Disease mechanisms of a ciliopathy’, *Journal of the American Society of Nephrology*. doi: 10.1681/ASN.2008050456.

Holdgaard, S. G. *et al.* (2019) ‘Selective autophagy maintains centrosome integrity and accurate mitosis by turnover of centriolar satellites’, *Nature Communications*. doi: 10.1038/s41467-019-12094-9.

Holdgaard, S. G., Cianfanelli, V. and Cecconi, F. (2020) ‘Cloud hunting: doryphagy, a form of selective autophagy that degrades centriolar satellites’, *Autophagy*. doi: 10.1080/15548627.2019.1703356.

Horani, A. and Ferkol, T. W. (2016) ‘Primary ciliary dyskinesia and associated sensory ciliopathies’, *Expert Review of Respiratory Medicine*. doi: 10.1586/17476348.2016.1165612.

Hosokawa, N., Sasaki, T., *et al.* (2009) ‘Atg101, a novel mammalian autophagy protein interacting with Atg13’, *Autophagy*. doi: 10.4161/auto.5.7.9296.

Hosokawa, N., Hara, T., *et al.* (2009) ‘Nutrient-dependent mTORCl association with the ULK1-Atg13-FIP200 complex required for autophagy’, *Molecular Biology*

of the Cell. doi: 10.1091/mbc.E08-12-1248.

Huangfu, D. *et al.* (2003) 'Hedgehog signalling in the mouse requires intraflagellar transport proteins', *Nature*. doi: 10.1038/nature02061.

Iaconis, D. *et al.* (2017) 'The centrosomal OFD1 protein interacts with the translation machinery and regulates the synthesis of specific targets', *Scientific Reports*. doi: 10.1038/s41598-017-01156-x.

Ichimura, Y. *et al.* (2000) 'A ubiquitin-like system mediates protein lipidation', *Nature*. doi: 10.1038/35044114.

Irigoin, F. and L. Badano, J. (2011) 'Keeping the Balance Between Proliferation and Differentiation:The Primary Cilium', *Current Genomics*. doi: 10.2174/138920211795860134.

Isakson, P., Holland, P. and Simonsen, A. (2013) 'The role of ALFY in selective autophagy', *Cell Death and Differentiation*. doi: 10.1038/cdd.2012.66.

Itakura, E. *et al.* (2008) 'Beclin 1 forms two distinct phosphatidylinositol 3-kinase complexes with mammalian Atg14 and UVRAG', *Molecular Biology of the Cell*. doi: 10.1091/mbc.E08-01-0080.

Jaber, N. and Zong, W. X. (2013) 'Class III PI3K Vps34: Essential roles in autophagy, endocytosis, and heart and liver function', *Annals of the New York Academy of Sciences*. doi: 10.1111/nyas.12026.

Jackson, P. K. (2018) 'EZH2 Inactivates Primary Cilia to Activate Wnt and Drive Melanoma', *Cancer Cell*. doi: 10.1016/j.ccell.2018.06.011.

Jacomin, A. C. *et al.* (2016) 'iLIR database: A web resource for LIR motif-containing proteins in eukaryotes', *Autophagy*. doi: 10.1080/15548627.2016.1207016.

Jang, J. *et al.* (2016) 'Primary Cilium-Autophagy-Nrf2 (PAN) Axis Activation Commits Human Embryonic Stem Cells to a Neuroectoderm Fate', *Cell*. doi:

10.1016/j.cell.2016.02.014.

Janke, C. and Kneussel, M. (2010) 'Tubulin post-translational modifications: Encoding functions on the neuronal microtubule cytoskeleton', *Trends in Neurosciences*. doi: 10.1016/j.tins.2010.05.001.

Jerman, S. *et al.* (2014) 'OFD1 and flotillins are integral components of a ciliary signaling protein complex organized by polycystins in renal epithelia and odontoblasts', *PLoS ONE*. doi: 10.1371/journal.pone.0106330.

Joachim, J. *et al.* (2017) 'Centriolar Satellites Control GABARAP Ubiquitination and GABARAP-Mediated Autophagy', *Current Biology*. doi: 10.1016/j.cub.2017.06.021.

Jung, C. H. *et al.* (2009) 'ULK-Atg13-FIP200 complexes mediate mTOR signaling to the autophagy machinery', *Molecular Biology of the Cell*. doi: 10.1091/mbc.E08-12-1249.

Kaizuka, T. and Mizushima, N. (2016) 'Atg13 Is Essential for Autophagy and Cardiac Development in Mice', *Molecular and Cellular Biology*. doi: 10.1128/mcb.01005-15.

Kaliszewski, M., Knott, A. B. and Bossy-Wetzel, E. (2015) 'Primary cilia and autophagic dysfunction in Huntington's disease', *Cell Death and Differentiation*. doi: 10.1038/cdd.2015.80.

Kalvari, I. *et al.* (2014) 'iLIR: A web resource for prediction of Atg8-family interacting proteins', *Autophagy*. doi: 10.4161/auto.28260.

Karanasios, E. *et al.* (2013) 'Dynamic association of the ULK1 complex with omegasomes during autophagy induction', *Journal of Cell Science*. doi: 10.1242/jcs.132415.

Karantza-Wadsworth, V. *et al.* (2007) 'Autophagy mitigates metabolic stress and genome damage in mammary tumorigenesis', *Genes and Development*. doi:

10.1101/gad.1565707.

Keeling, J., Tsiokas, L. and Maskey, D. (2016) 'Cellular Mechanisms of Ciliary Length Control', *Cells*. doi: 10.3390/cells5010006.

Kim, E. S. *et al.* (2015) 'Inhibition of autophagy suppresses sertraline-mediated primary ciliogenesis in retinal pigment epithelium cells', *PLoS ONE*. doi: 10.1371/journal.pone.0118190.

Kim, J. *et al.* (2011) 'AMPK and mTOR regulate autophagy through direct phosphorylation of Ulk1', *Nature Cell Biology*. doi: 10.1038/ncb2152.

Kim, Y. M. *et al.* (2015) 'MTORC1 phosphorylates UVRAG to negatively regulate autophagosome and endosome maturation', *Molecular Cell*. doi: 10.1016/j.molcel.2014.11.013.

Kimura, S., Noda, T. and Yoshimori, T. (2007) 'Dissection of the autophagosome maturation process by a novel reporter protein, tandem fluorescent-tagged LC3', *Autophagy*. doi: 10.4161/auto.4451.

Kirkin, V. *et al.* (2009) 'A Role for NBR1 in Autophagosomal Degradation of Ubiquitinated Substrates', *Molecular Cell*. doi: 10.1016/j.molcel.2009.01.020.

Kobayashi, T. and Dynlacht, B. D. (2011) 'Regulating the transition from centriole to basal body', *Journal of Cell Biology*. doi: 10.1083/jcb.201101005.

Koenekoop, R. K. (2004) 'An overview of leber congenital amaurosis: A model to understand human retinal development', *Survey of Ophthalmology*. doi: 10.1016/j.survophthal.2004.04.003.

Komatsu, M. *et al.* (2005) 'Impairment of starvation-induced and constitutive autophagy in Atg7-deficient mice', *Journal of Cell Biology*. doi: 10.1083/jcb.200412022.

Konno, A., Setou, M. and Ikegami, K. (2012) 'Ciliary and Flagellar Structure and Function-Their Regulations by Posttranslational Modifications of Axonemal

Tubulin', in *International Review of Cell and Molecular Biology*. doi: 10.1016/B978-0-12-394305-7.00003-3.

Lechtreck, K. F. (2015) 'IFT-Cargo Interactions and Protein Transport in Cilia', *Trends in Biochemical Sciences*. doi: 10.1016/j.tibs.2015.09.003.

Lee, E. J. and Tournier, C. (2011) 'The requirement of uncoordinated 51-like kinase 1 (ULK1) and ULK2 in the regulation of autophagy', *Autophagy*. doi: 10.4161/auto.7.7.15450.

Lee, J. E. *et al.* (2012) 'CEP41 is mutated in Joubert syndrome and is required for tubulin glutamylation at the cilium', *Nature Genetics*. doi: 10.1038/ng.1078.

Lee, J. E. and Gleeson, J. G. (2011) 'A systems-biology approach to understanding the ciliopathy disorders', *Genome Medicine*. doi: 10.1186/gm275.

Lee, K. L. *et al.* (2015) 'The primary cilium functions as a mechanical and calcium signaling nexus', *Cilia*. doi: 10.1186/s13630-015-0016-y.

Lee, Y. K. and Lee, J. A. (2016) 'Role of the mammalian ATG8/LC3 family in autophagy: Differential and compensatory roles in the spatiotemporal regulation of autophagy', *BMB Reports*. doi: 10.5483/BMBRep.2016.49.8.081.

Lefèvre, F., Rémy, M. H. and Masson, J. M. (1997) 'Alanine-stretch scanning mutagenesis: A simple and efficient method to probe protein structure and function', *Nucleic Acids Research*. doi: 10.1093/nar/25.2.447.

De Leo, M. G. *et al.* (2016) 'Autophagosome-lysosome fusion triggers a lysosomal response mediated by TLR9 and controlled by OCRL', *Nature Cell Biology*. doi: 10.1038/ncb3386.

Liang, Y. *et al.* (2016) 'Mechanism of ciliary disassembly', *Cellular and Molecular Life Sciences*. doi: 10.1007/s00018-016-2148-7.

Liu, C. C. *et al.* (2016) 'Cul3-KLHL20 Ubiquitin Ligase Governs the Turnover of ULK1 and VPS34 Complexes to Control Autophagy Termination', *Molecular Cell*.

doi: 10.1016/j.molcel.2015.11.001.

Liu, W. J. *et al.* (2016) 'p62 links the autophagy pathway and the ubiqutin-proteasome system upon ubiquitinated protein degradation', *Cellular and Molecular Biology Letters*. doi: 10.1186/s11658-016-0031-z.

Liu, Y. and Levine, B. (2015) 'Autosis and autophagic cell death: The dark side of autophagy', *Cell Death and Differentiation*. doi: 10.1038/cdd.2014.143.

Lopes, C. A. M. *et al.* (2011) 'Centriolar satellites are assembly points for proteins implicated in human ciliopathies, including oral-facial-digital syndrome 1', *Journal of Cell Science*. doi: 10.1242/jcs.077156.

Lyons, R. A., Saridogan, E. and Djahanbakhch, O. (2006) 'The reproductive significance of human Fallopian tube cilia', *Human Reproduction Update*. doi: 10.1093/humupd/dml012.

Marina, M. and Franco, B. (2009) 'The molecular basis of oral-facial-digital syndrome, type 1', *American Journal of Medical Genetics, Part C: Seminars in Medical Genetics*. doi: 10.1002/ajmg.c.30224.

Mathew, R., Karantza-Wadsworth, V. and White, E. (2007) 'Role of autophagy in cancer', *Nature Reviews Cancer*. doi: 10.1038/nrc2254.

Matsunaga, K. *et al.* (2010) 'Autophagy requires endoplasmic reticulum targeting of the PI3-kinase complex via Atg14L', *Journal of Cell Biology*. doi: 10.1083/jcb.200911141.

Mirvis, M., Stearns, T. and Nelson, W. J. (2018) 'Cilium structure, assembly, and disassembly regulated by the cytoskeleton', *Biochemical Journal*. doi: 10.1042/BCJ20170453.

Mizushima, N. (2007) 'Autophagy: Process and function', *Genes and Development*. doi: 10.1101/gad.1599207.

Mizushima, N. *et al.* (2008) 'Autophagy fights disease through cellular self-

digestion', *Nature*. doi: 10.1038/nature06639.

Mizushima, N. (2010) 'The role of the Atg1/ULK1 complex in autophagy regulation', *Current Opinion in Cell Biology*. doi: 10.1016/j.ceb.2009.12.004.

Mizushima, N. and Yoshimori, T. (2007) 'How to interpret LC3 immunoblotting', *Autophagy*. doi: 10.4161/auto.4600.

Moreau, K., Luo, S. and Rubinsztein, D. C. (2010) 'Cytoprotective roles for autophagy', *Current Opinion in Cell Biology*. doi: 10.1016/j.ceb.2009.12.002.

Morleo and Franco (2019) 'The Autophagy-Cilia Axis: An Intricate Relationship', *Cells*. doi: 10.3390/cells8080905.

Morleo, M. and Franco, B. (2008) 'Dosage compensation of the mammalian X chromosome influences the phenotypic variability of X-linked dominant male-lethal disorders', *Journal of Medical Genetics*. doi: 10.1136/jmg.2008.058305.

Morleo, M. and Franco, B. (2020) 'OFD Type I syndrome: lessons learned from a rare ciliopathy', *Biochemical Society Transactions*. doi: 10.1042/bst20191029.

von Muhlinen, N. *et al.* (2012) 'LC3C, Bound Selectively by a Noncanonical LIR Motif in NDP52, Is Required for Antibacterial Autophagy', *Molecular Cell*. doi: 10.1016/j.molcel.2012.08.024.

Von Muhlinen, N. *et al.* (2010) 'NDP52, a novel autophagy receptor for ubiquitin-decorated cytosolic bacteria', *Autophagy*. doi: 10.4161/auto.6.2.11118.

Nakatogawa, H. (2013) 'Two ubiquitin-like conjugation systems that mediate membrane formation during autophagy', *Essays in Biochemistry*. doi: 10.1042/BSE0550039.

Nauli, S. M. *et al.* (2003) 'Polycystins 1 and 2 mediate mechanosensation in the primary cilium of kidney cells', *Nature Genetics*. doi: 10.1038/ng1076.

Nazio, F. *et al.* (2013) 'MTOR inhibits autophagy by controlling ULK1 ubiquitylation, self-association and function through AMBRA1 and TRAF6', *Nature*

Cell Biology. doi: 10.1038/ncb2708.

Nazio, F. *et al.* (2016) 'Fine-tuning of ULK1 mRNA and protein levels is required for autophagy oscillation', *Journal of Cell Biology*. doi: 10.1083/jcb.201605089.

Nigg, E. A. and Stearns, T. (2011) 'The centrosome cycle: Centriole biogenesis, duplication and inherent asymmetries', *Nature Cell Biology*. doi: 10.1038/ncb2345.

Ohashi, Y., Tremel, S. and Williams, R. L. (2019) 'VPS34 complexes from a structural perspective', *Journal of Lipid Research*. doi: 10.1194/jlr.R089490.

Ohsumi, Y. and Mizushima, N. (2004) 'Two ubiquitin-like conjugation systems essential for autophagy', *Seminars in Cell and Developmental Biology*. doi: 10.1016/j.semcdb.2003.12.004.

Orhon, I. *et al.* (2015) 'Autophagy and regulation of cilia function and assembly', *Cell Death and Differentiation*. doi: 10.1038/cdd.2014.171.

Orhon, I. *et al.* (2016) 'Primary-cilium-dependent autophagy controls epithelial cell volume in response to fluid flow', *Nature Cell Biology*. doi: 10.1038/ncb3360.

Pampliega, O. *et al.* (2013) 'Functional interaction between autophagy and ciliogenesis', *Nature*. doi: 10.1038/nature12639.

Pampliega, O. and Cuervo, A. M. (2016) 'Autophagy and primary cilia: Dual interplay', *Current Opinion in Cell Biology*. doi: 10.1016/j.ceb.2016.01.008.

Pattison, J. S., Osinska, H. and Robbins, J. (2011) 'Atg7 induces basal autophagy and rescues autophagic deficiency in CryABR120G cardiomyocytes', *Circulation Research*. doi: 10.1161/CIRCRESAHA.110.237339.

Pedersen, L. B. *et al.* (2012) 'The ciliary cytoskeleton', *Comprehensive Physiology*. doi: 10.1002/cphy.c110043.

Peixoto, E. *et al.* (2020) 'HDAC6-dependent ciliophagy is involved in ciliary loss and cholangiocarcinoma growth in human cells and murine models', *American Journal of Physiology - Gastrointestinal and Liver Physiology*. doi:

10.1152/ajpgi.00033.2020.

Pende, M. *et al.* (2004) 'S6K1−/−/S6K2−/− Mice Exhibit Perinatal Lethality and Rapamycin-Sensitive 5′-Terminal Oligopyrimidine mRNA Translation and Reveal a Mitogen-Activated Protein Kinase-Dependent S6 Kinase Pathway', *Molecular and Cellular Biology*. doi: 10.1128/mcb.24.8.3112-3124.2004.

Piperno, G., LeDizet, M. and Chang, X. J. (1987) 'Microtubules containing acetylated alpha-tubulin in mammalian cells in culture.', *The Journal of cell biology*. doi: 10.1083/jcb.104.2.289.

Plotnikova, O. V., Pugacheva, E. N. and Golemis, E. A. (2009) 'Primary cilia and the cell cycle.', *Methods in cell biology*. doi: 10.1016/S0091-679X(08)94007-3.

Prattichizzo, C. *et al.* (2008) 'Mutational spectrum of the oral-facial-digital type I syndrome: A study on a large collection of patients', *Human Mutation*. doi: 10.1002/humu.20792.

Prodromou, N. V. *et al.* (2012) 'Heat shock induces rapid resorption of primary cilia', *Journal of Cell Science*. doi: 10.1242/jcs.100545.

Quarmby, L. M. and Parker, J. D. K. (2005) 'Cilia and the cell cycle?', *Journal of Cell Biology*. doi: 10.1083/jcb.200503053.

Ravikumar, B. (2002) 'Aggregate-prone proteins with polyglutamine and polyalanine expansions are degraded by autophagy', *Human Molecular Genetics*. doi: 10.1093/hmg/11.9.1107.

Reiter, J. F. and Leroux, M. R. (2017) 'Genes and molecular pathways underpinning ciliopathies', *Nature Reviews Molecular Cell Biology*. doi: 10.1038/nrm.2017.60.

Rogov, V. V *et al.* (2017) 'Structural and functional analysis of the GABARAP interaction motif (GIM)', *EMBO reports*. doi: 10.15252/embr.201643587.

Rohatgi, R. and Snell, W. J. (2010) 'The ciliary membrane', *Current Opinion in Cell*

Biology. doi: 10.1016/j.ceb.2010.03.010.

Romanelli, A., Dreisbach, V. C. and Blenis, J. (2002) 'Characterization of phosphatidylinositol 3-kinase-dependent phosphorylation of the hydrophobic motif site Thr389 in p70 S6 kinase 1', *Journal of Biological Chemistry*. doi: 10.1074/jbc.M205168200.

Romio, L. *et al.* (2004) 'OFD1 is a centrosomal/basal body protein expressed during mesenchymal-epithelial transition in human nephrogenesis', *Journal of the American Society of Nephrology*. doi: 10.1097/01.ASN.0000140220.46477.5C.

Rui, Y. N. *et al.* (2015) 'Huntingtin functions as a scaffold for selective macroautophagy', *Nature Cell Biology*. doi: 10.1038/ncb3101.

Russell, R. C. *et al.* (2013) 'ULK1 induces autophagy by phosphorylating Beclin-1 and activating VPS34 lipid kinase', *Nature Cell Biology*. doi: 10.1038/ncb2757.

Ryan, M. J. *et al.* (1994) 'HK-2: An immortalized proximal tubule epithelial cell line from normal adult human kidney', *Kidney International*. doi: 10.1038/ki.1994.6.

Sankaran, D. G., Stemm-Wolf, A. J. and Pearson, C. G. (2019) 'CEP135 isoform dysregulation promotes centrosome amplification in breast cancer cells', *Molecular Biology of the Cell*. doi: 10.1091/mbc.E18-10-0674.

Satir, P. and Christensen, S. T. (2007) 'Overview of Structure and Function of Mammalian Cilia', *Annual Review of Physiology*. doi: 10.1146/annurev.physiol.69.040705.141236.

Satir, P., Pedersen, L. B. and Christensen, S. T. (2010) 'The primary cilium at a glance', *Journal of Cell Science*. doi: 10.1242/jcs.050377.

Sawamoto, K. *et al.* (2006) 'New neurons follow the flow of cerebrospinal fluid in the adult brain', *Science*. doi: 10.1126/science.1119133.

Scholey, J. M. (2008) 'Intraflagellar transport motors in cilia: Moving along the cell's antenna', *Journal of Cell Biology*. doi: 10.1083/jcb.200709133.

Seeger-Nukpezah, T. *et al.* (2015) 'The hallmarks of cancer: Relevance to the pathogenesis of polycystic kidney disease', *Nature Reviews Nephrology*. doi: 10.1038/nrneph.2015.46.

Seeley, E. S. *et al.* (2009) 'Pancreatic cancer and precursor pancreatic intraepithelial neoplasia lesions are devoid of primary cilia', *Cancer Research*. doi: 10.1158/0008-5472.CAN-08-1290.

Shi, R. *et al.* (2012) 'Excessive Autophagy Contributes to Neuron Death in Cerebral Ischemia', *CNS Neuroscience and Therapeutics*. doi: 10.1111/j.1755-5949.2012.00295.x.

Singla, V. *et al.* (2010) 'Ofd1, a Human Disease Gene, Regulates the Length and Distal Structure of Centrioles', *Developmental Cell*. doi: 10.1016/j.devcel.2009.12.022.

Singla, V. and Reiter, J. F. (2006) 'The primary cilium as the cell's antenna: Signaling at a sensory organelle', *Science*. doi: 10.1126/science.1124534.

SOROKIN, S. (1962) 'Centrioles and the formation of rudimentary cilia by fibroblasts and smooth muscle cells.', *The Journal of cell biology*. doi: 10.1083/jcb.15.2.363.

Sorokin, S. P. (1968) 'Centriole formation and ciliogenesis.', *Aspen Emphysema Conference*.

Stoetzel, C. *et al.* (2016) 'A mutation in VPS15 (PIK3R4) causes a ciliopathy and affects IFT20 release from the cis-Golgi', *Nature Communications*. doi: 10.1038/ncomms13586.

Struchtrup, A. *et al.* (2018) 'The ciliary protein RPGRIP1L governs autophagy independently of its proteasome-regulating function at the ciliary base in mouse embryonic fibroblasts', *Autophagy*. doi: 10.1080/15548627.2018.1429874.

Takahashi, Y. *et al.* (2018) 'An autophagy assay reveals the ESCRT-III component

CHMP2A as a regulator of phagophore closure', *Nature Communications*. doi: 10.1038/s41467-018-05254-w.

Tang, Z. *et al.* (2013) 'Autophagy promotes primary ciliogenesis by removing OFD1 from centriolar satellites', *Nature*. doi: 10.1038/nature12606.

Tanida, I. (2011) 'Autophagosome formation and molecular mechanism of autophagy', *Antioxidants and Redox Signaling*. doi: 10.1089/ars.2010.3482.

Thauvin-Robinet, C. *et al.* (2013) 'OFD1 mutations in males: Phenotypic spectrum and ciliary basal body docking impairment', *Clinical Genetics*. doi: 10.1111/cge.12013.

Toprak, O. *et al.* (2006) 'Oral-facial-digital syndrome type 1, Caroli's disease and cystic renal disease', *Nephrology Dialysis Transplantation*. doi: 10.1093/ndt/gfk013.

Tsang, S. H., Aycinena, A. R. P. and Sharma, T. (2018) 'Ciliopathy: Bardet-Biedl syndrome', in *Advances in Experimental Medicine and Biology*. doi: 10.1007/978-3-319-95046-4_33.

Tsun, Z. Y. *et al.* (2013) 'The folliculin tumor suppressor is a GAP for the RagC/D GTPases that signal amino acid levels to mTORC1', *Molecular Cell*. doi: 10.1016/j.molcel.2013.09.016.

Wang, S. *et al.* (2015) 'Reciprocal regulation of cilia and autophagy via the MTOR and proteasome pathways', *Autophagy*. doi: 10.1080/15548627.2015.1023983.

Wang, Z. and Choi, M. E. (2014) 'Autophagy in kidney health and disease', *Antioxidants and Redox Signaling*. doi: 10.1089/ars.2013.5363.

Wanner, A., Salathe, M. and O'Riordan, T. G. (1996) 'Mucociliary clearance in the airways', *American Journal of Respiratory and Critical Care Medicine*. doi: 10.1164/ajrccm.154.6.8970383.

Ward, C. J. *et al.* (2003) 'Cellular and subcellular localization of the ARPKD

protein; fibrocystin is expressed on primary cilia', *Human Molecular Genetics*. doi: 10.1093/hmg/ddg274.

Watanabe, Y. *et al.* (2016) 'Autophagy controls centrosome number by degrading Cep63', *Nature Communications*. doi: 10.1038/ncomms13508.

Wesselborg, S. and Stork, B. (2015) 'Autophagy signal transduction by ATG proteins: From hierarchies to networks', *Cellular and Molecular Life Sciences*. doi: 10.1007/s00018-015-2034-8.

White, E. (2015) 'The role for autophagy in cancer', *Journal of Clinical Investigation*. doi: 10.1172/JCI73941.

Wong, E. and Cuervo, A. M. (2010) 'Autophagy gone awry in neurodegenerative diseases', *Nature Neuroscience*. doi: 10.1038/nn.2575.

Xie, Z. and Klionsky, D. J. (2007) 'Autophagosome formation: Core machinery and adaptations', *Nature Cell Biology*. doi: 10.1038/ncb1007-1102.

Xu, Q. *et al.* (2016) 'Silibinin negatively contributes to primary cilia length via autophagy regulated by histone deacetylase 6 in confluent mouse embryo fibroblast 3T3-L1 cells', *Molecular and Cellular Biochemistry*. doi: 10.1007/s11010-016-2766-2.

Yamamoto, H. *et al.* (2012) 'Atg9 vesicles are an important membrane source during early steps of autophagosome formation', *Journal of Cell Biology*. doi: 10.1083/jcb.201202061.

Ye, H. *et al.* (2017) 'The regulatory 1α subunit of protein kinase a modulates renal cystogenesis', *American Journal of Physiology - Renal Physiology*. doi: 10.1152/ajprenal.00119.2017.

Yoshii, S. R. and Mizushima, N. (2017) 'Monitoring and measuring autophagy', *International Journal of Molecular Sciences*. doi: 10.3390/ijms18091865.

Yu, L. *et al.* (2010) 'Autophagy termination and lysosome reformation regulated by

mTOR', *Nature*. doi: 10.1038/nature09076.Autophagy.

Zachari, M. and Ganley, I. G. (2017) 'The mammalian ULK1 complex and autophagy initiation', *Essays in Biochemistry*. doi: 10.1042/EBC20170021.

Zaffagnini, G. and Martens, S. (2016) 'Mechanisms of Selective Autophagy', *Journal of Molecular Biology*. doi: 10.1016/j.jmb.2016.02.004.

Zhang, C. *et al.* (2020) 'Distinct Roles of TRAPPC8 and TRAPPC12 in Ciliogenesis via Their Interactions With OFD1', *Frontiers in Cell and Developmental Biology*. doi: 10.3389/fcell.2020.00148.

Appendix

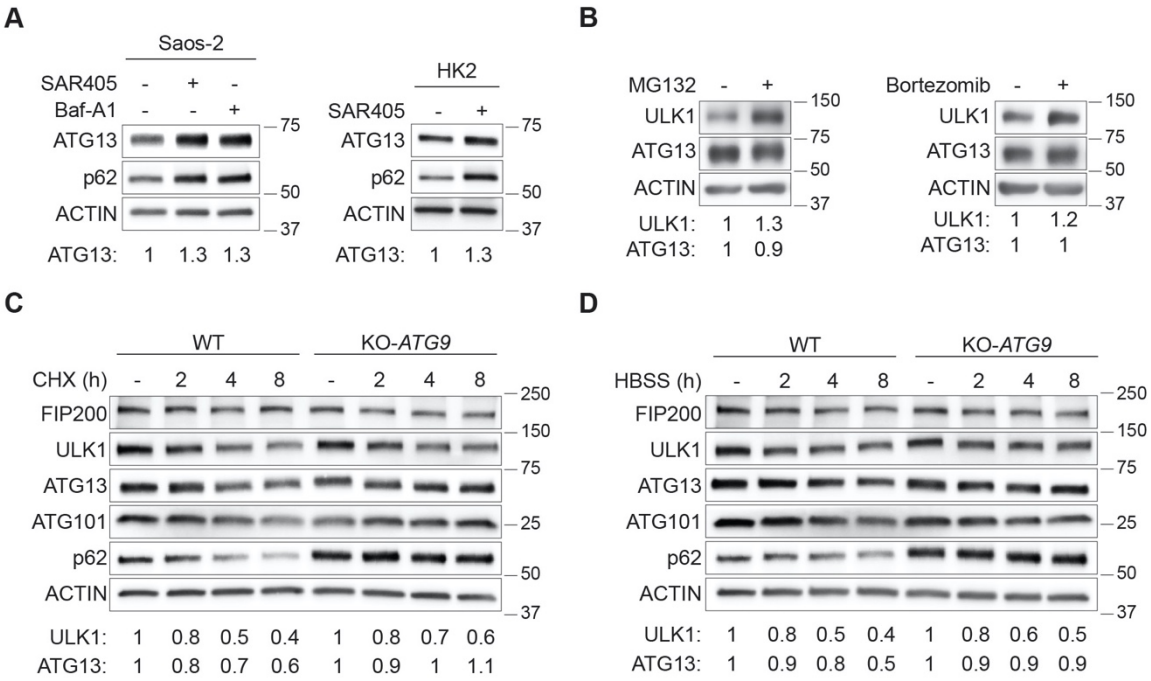

Figure 44. ATG13 is degraded through autophagy. A. Western blot of ATG13 and p62 in human osteosarcoma (Saos-2, left panel) and HK2 (right panel) cells treated (+) or not (-) with SAR405 (10μM, 6h) or Baf-A1 (100nM, 6h). Quantification of ATG13 protein levels, normalized versus ACTIN (loading control), is expressed as fold change compared with untreated conditions (-). Baf-A1=bafilomycin. B. Western blot of ULK1 and ATG13 levels in HK2 cells treated (+) or not (-) with MG132 (10μM, 2h, left panel) or Bortezomib (100nM, 2h, right panel). Quantification of protein levels normalized versus ACTIN (loading control) is expressed as fold change compared with untreated conditions (-). C. Representative blot of the indicated proteins in wt and KO-*ATG9* (ATG9 is a key regulator of the autophagic cascade) Saos-2 cells which were incubated with 50μg/ml cycloheximide (CHX) and collected at the indicated time points. Quantification of ATG13 and ULK1 protein levels, normalized versus ACTIN (loading control), is expressed as fold change compared with untreated conditions (-). D. Representative blot of time course evaluating levels of the indicated proteins in wt and KO-*ATG9* Saos-2 cells during starvation (HBSS treatment) and collected at the indicated time points. Quantification of ATG13 protein levels, normalized versus ACTIN (loading control), reported under the blot is expressed as fold change compared with full medium condition (-) and is referred to the blots shown in the figure. The images display representative blots of three independent experiments and the quantification refers to the experiment shown in the figure.